TEST TECHNOLOGY TECHNICAL COUNCIL (TTTC) OF THE IEEE COMPUTER SOCIETY
EDUCATION AND SCIENCE, YOUTH AND SPORT MINISTRY OF UKRAINE

KHARKOV NATIONAL UNIVERSITY
OF RADIOELECTRONICS

ISSN 1563-0064

RADIOELECTRONICS & INFORMATICS

Scientific and Technical Journal **Founded in 1997**

№ 1 (60) 2013 **Published 4 times a year**

Certificate of the State Registration КВ № 12097-968 ПР 14.12.2006

Address of journal edition: Ukraine, 61166, Kharkiv, Lenin avenu, 14, KNURE, Design Automation Department, room 321, ph. (0572) 70-21-326, d-r Hahanov V.I.
E-mail: ri@kture.kharkov.ua; hahanov@kture.kharkov.ua,
http://www.ewdtest.com/ri/

CONTENTS

An Efficient Algorithm for the Ellipse Packing Problem

A. Pankratov, T. Romanova and I. Subota
Department of Mathematical Modeling and Optimal Design, Institute for Mechanical Engineering Problems, the National Academy of Sciences of Ukraine, Ukraine

***Abstract* – The paper considers the problem of packing a given collection of ellipses into a rectangular container of minimal area. Our ellipses can be continuous rotated and translated. A class of radical-free quasi-phi-functions is introduced for an analytical description of non-overlapping and containment constraints for ellipses. We formulate the packing problem in the form of a nonlinear programming problem and develop an efficient solution algorithm. The algorithm allows us to reduce computational cost of our problem. We present computational results that compare with those published elsewhere recently.**

***Index Terms* – packing, ellipses, continuous rotations, quasi-phi-functions, nonlinear optimization, solution algorithm.**

I. INTRODUCTION

The literature on two dimensional packing problems is large and it is not possible to comprehensively review here. It is common for cutting and packing papers to indicate the problem type according to the typology presented in [1]. At present, the interest in finding effective solutions for packing problems is growing rapidly. This is due to a large and growing number of applications and an extreme complexity of methods used to handle many of them [2]. In this paper, we deal with the optimal ellipse packing problem, which is a part of operational research and computational geometry. It has multiple applications in modern biology, mineralogy, medicine, materials science, nanotechnology, as well as in the chemical industry, power engineering, logistics etc.

One way to tackle the packing problem for ellipses is to approximate the latter with line segments [3]. There is a short list of publications which deal with arc shapes without polygonal approximations. Packing problems with irregular objects of fixed orientation, whose frontier can be described by a sequence of line- and arc-segments, are tackled in [4] using the no-fit polygon.

Manuscript received December 12, 2013

A. V. Pankratov is a senior scientist associate at the Department of Mathematical Modeling and Optimal Design, A.M. Podgorny Institute of Mechanical Engineering of the National Academy of Sciences of Ukraine.
T. E. Romanova is a leading scientist at the Department of Mathematical Modeling and Optimal Design, A.M. Podgorny Institute of Mechanical Engineering of the National Academy of Sciences of Ukraine. Corresponding author, e-mail: tarom27@yahoo.com
I. A. Subota is an aspirant of the Department of Mathematical Modeling and Optimal Design, A.M. Podgorny Institute of Mechanical Engineering of the National Academy of Sciences of Ukraine.

That paper extends the heuristic orbital sliding method of calculating no-fit polygons to enable it to handle arcs and then shows the resultant no-fit polygons being utilised successfully on the two-dimensional irregular packing problem.

The other way is to use the existing phi-functions for arc objects, described in [5, 6]. However, the complexity of such a solution would depend on the number of lines/arcs used to approximate the ellipses. In any case, this approach would only give an approximate solution.

Our approach, which is based on quasi-phi-functions, is capable of handling precise ellipses (without any approximations) and thus finding an exact local optimal solution. The only other method of that sort was developed very recently by Josef Kallrath and Steffen Rebennack; see [7]. The paper is entirely devoted to the problem of cutting ellipses from a rectangular plate of minimal area. Incidentally, it offers a good overview of related publications. For a small number of ellipses they are able to compute a globally optimal solution subject to the finite arithmetic of global solvers at hand. However, for more than 14 ellipses none of the nonlinear programming (NLP) solvers available in GAMS can even compute a locally optimal solution. Therefore, the authors of [7] develop polylithic approaches, in which the ellipses are added sequentially in a strip-packing fashion to the rectangle restricted in width but unrestricted in length. The rectangle's area is minimized at each step in a greedy fashion. The sequence in which they add ellipses is random; this adds some GRASP flavor to the approach. The polylithic algorithms allow the authors to compute good solutions for up to 100 ellipses. A number of examples are presented in the paper.

In order to compare the performance of the two methods, we applied our algorithm to some instances of the ellipse packing problem as used in [7].

The paper is organized as follows: In Section 2 we formulate the optimal ellipse packing problem and give a short review of related works. In Section 3 we propose a mathematical model as a continuous nonlinear programming problem by means of quasi-phi-functions. In Section 4 we develop a new efficient solution algorithm to search for local optimal solutions. In Section 5 we provide our computational results for several instances studied in [7], and finish with some concluding remarks in Section 6.

II. PROBLEM FORMULATION

We consider here a packing problem in the following setting**.** Let Ω denote a rectangular domain of length l and width w. Both of these dimensions may be variable, or one may be fixed and the other variable. Suppose a set of ellipses E_i, $i \in \{1,2,...,n\} = I_n$, is given to be placed in Ω without overlaps. Each ellipse E_i is defined by its semi-axes a_i and b_i, whose values are fixed. With each ellipse E_i we associate its eigen coordinate system whose origin coincides with the center of the ellipse and the coordinate axes are aligned with the ellipse's axes. In that system the ellipse is described by parametric equations $x = a\cos t$, $y = b\sin t$, $0 \le t \le 2\pi$. We also use a fixed coordinate system attached to the container Ω. The position of ellipse E_i in the fixed coordinates is specified by the coordinates (x_i, y_i) of its center and the rotation angle θ_i.

Ellipse packing problem. Place the set of ellipses E_i, $i \in I_n$, within a rectangular container $\Omega = \{(x,y) \in R^2 : 0 \le x \le l, 0 \le y \le w\}$ of minimal area.

III. MATHEMATICAL MODEL

First we assemble a complete set of variables for our optimization problem. The vector $u \in R^\sigma$ of all our variables can be described as follows: $u = (l, w, u_1, u_2, ..., u_n, \tau)$, where (l, w) denote the variable length and width of the container Ω and $u_i = (x_i, y_i, \theta_i)$ is the vector of placement parameters for the ellipse E_i, $i \in I_n$. Lastly, τ denotes the vector of additional variables, defined as follows: $\tau = (t_{ij}^1, t_{ij}^2, j > i \in I_n, t_{i1}, t_{i2}, i \in I_n)$, where t_{ij}^1, t_{ij}^2 are additional variables for the pair of ellipses E_i and E_j, and t_{i1}, t_{i2} are additional variables for each ellipse E_i. Here R^σ denotes the σ-dimensional Euclidean space, where $\sigma = 2 + 3n + n(n-1) + 2n = n^2 + 4n + 2$ is the number of the problem variables.

A mathematical model of the ellipse packing problem may now be stated in the form:

$$\min_{u \in W \subset R^\sigma} F(u), \tag{1}$$

$$W = \{u \in R^\sigma : \Phi_{ij}^{'} \ge 0, \Phi_i^{'} \ge 0, j > i \in I_n\}, \tag{2}$$

where $F(u) = l \cdot w$, $\Phi_{ij}^{'}$ is a quasi-phi-function defined for the pair of ellipses E_i and E_j (to hold the *non-overlapping* constraint),

$$\Phi_{ij}'(u_i, u_j, u_{ij}^{'}) = \min\{\chi(\theta_i, \theta_j, u_{ij}^{'}), \chi^+(u_i, u_j, u_{ij}^{'}), \chi^-(u_i, u_j, u_{ij}^{'})\},$$

$u_{ij}^{'} = (t_{ij}^1, t_{ij}^2)$, $\chi = -\left\langle N_{ij}^1, N_{ij}^2 \right\rangle = -\alpha_{ij}^{'1}\alpha_{ij}^{'2} - \beta_{ij}^{'1}\beta_{ij}^{'2}$,

$\alpha_{ij}^{'1} = \alpha_{ij}^1 \cos\theta_i + \beta_{ij}^1 \sin\theta_i$, $\beta_{ij}^{'1} = -\alpha_{ij}^1 \sin\theta_i + \beta_{ij}^1 \cos\theta_i$,

$\alpha_{ij}^1 = \dfrac{\cos t_{ij}^1}{a_i}$, $\beta_{ij}^1 = \dfrac{\sin t_{ij}^1}{b_i}$,

$\alpha_{ij}^{'2} = \alpha_{ij}^2 \cos\theta_j + \beta_{ij}^2 \sin\theta_j$, $\beta_{ij}^{'2} = -\alpha_{ij}^2 \sin\theta_j + \beta_{ij}^2 \cos\theta_j$,

$\alpha_{ij}^2 = \dfrac{\cos t_{ij}^2}{a_j}$, $\beta_{ij}^2 = \dfrac{\sin t_{ij}^2}{b_j}$,

$\chi^+ = \alpha_{ij}^{'1}(x_{ij}^{2+} - x_i) + \beta_{ij}^{'1}(y_{ij}^{2+} - y_i) - 1$,

$\chi^- = \alpha_{ij}^{'1}(x_{ij}^{2-} - x_i) + \beta_{ij}^{'1}(y_{ij}^{2-} - y_i) - 1$,

$(x_{ij}^{2+}, y_{ij}^{2+}) = (x_{ij}^{'2}, y_{ij}^{'2}) + \eta(-\beta_{ij}^{'2}, \alpha_{ij}^{'2})$,

$(x_{ij}^{2-}, y_{ij}^{2-}) = (x_{ij}^{'2}, y_{ij}^{'2},) - \eta(-\beta_{ij}^{'2}, \alpha_{ij}^{'2})$, $\eta = (a_j)^2$,

$(x_{ij}^{'2}, y_{ij}^{'2}) = v_j + M(\theta_j) \cdot (x_{ij}^2, y_{ij}^2)$,

$(x_{ij}^2, y_{ij}^2) = (a_j \cos t_{ij}^2, b_j \sin t_{ij}^2)$, $M(\theta_j)$ denotes the standard rotation matrix, $v_j = (x_j, y_j)$ is a translation vector of ellipse E_j; $\Phi_i^{'}$ is a quasi-phi-function defined for the ellipse E_i and the object $\Omega^* = R^2 \setminus \operatorname{int}\Omega$ (to hold the *containment* constraint),

$$\Phi_i^{'}(u) = \min\{\varphi_{i11}(p_1), \varphi_{i11}(p_2), \varphi_{i12}(p_3), \varphi_{i12}(p_4), \varphi_{i21}(p_2), \varphi_{i21}(p_3), \varphi_{i22}(p_1), \varphi_{i22}(p_4)\},$$

$u = (x_i, y_i, \theta_i, t_{i1}, t_{i2}) \in R^5$, $p_1 = (0,0)$, $p_2 = (l,0)$, $p_3 = (l,w)$, $p_4 = (0,w)$, $\varphi_{ik1} = A_{ik}x + B_{ik}y + C_{ik} - 1$, $\varphi_{ik2} = -A_{ik}x - B_{ik}y - C_{ik} - 1$, $A_{ik} = \alpha_{ik} \cdot \cos\theta_i + \beta_{ik} \cdot \sin\theta_i$,

$B_{ik} = -\alpha_{ik} \cdot \sin\theta_i + \beta_{ik} \cdot \cos\theta_i$, $\alpha_{ik} = \dfrac{\cos t_{ik}}{a_i}$, $\beta_{ik} = \dfrac{\sin t_{ik}}{b_i}$,

$C_{ik} = -A_{ik}x_i - B_{ik}y_i$, $k = 1,2$.

Our constrained optimization problem (1)-(2) is NP-hard nonlinear programming problem [8]. The solution space *W* has a complicated structure: it is, in general, a disconnected set, each connected component of *W* is multiconnected, the frontier of *W* is made of nonlinear surfaces containing valleys, ravines. A matrix of the inequality system which specifies *W* is strongly sparse and has a block structure.

IV. SOLUTION STRATEGY

Our solution strategy consists of three major stages:

1) First we generate a number of starting points from the feasible region of the problem (1)-(2). We employ the special starting point algorithm based on homothetic transformation of ellipses using a modification of the optimization procedure developed in [9] for a circular packing problem.

2) Then starting from each point obtained at Step 1 we search for a local minimum of the objective function

$F(u)$ of problem (1)-(2). We employ special the Local Optimization Procedure (LOP) for ellipse packing problem (1)-(2).

3) Lastly, we choose the best local minimum from those found at Step 2. This is our best approximation to the global solution of the problem (1)-(2).

An essential part of our local optimization scheme (Step 2) is the LOP procedure that reduces the dimension of the problem and runtime. It is due to this reduction that our strategy can process large sets of non-identical ellipses. The reduction scheme used by our LOP algorithm is described below. The actual search for a local minimum is performed by a standard IPOPT algorithm [10], which is available at an open access noncommercial software depository (https://projects.coin-or.org/Ipopt) .

Let $u^{(0)} \in W$ be one of feasible starting points. The main idea of the subsequent LOP algorithm is as follows.

First we circumscribe a circle C_i of radius a_i around each ellipse E_i, $i = 1,2,...,n$. Then for each circle C_i we construct an "individual" rectangular container $\Omega_i \supset C_i \supset E_i$ with equal half-sides of length $a_i + \varepsilon$, $i = 1,2,...,n$, so that C_i, E_i and Ω_i have the same center (x_i^0, y_i^0) subject to the sides of Ω_i being parallel to those of Ω. Here ε is a fixed constant. Further we fix the position of each individual container Ω_i and let the local optimization algorithm move the corresponding ellipse E_i only within the container Ω_i. It is clear that if two individual containers Ω_i and Ω_j do not have common interior points (i.e. $\Phi^{\Omega_i\Omega_j} \geq 0$), then we do not need to check the non-overlapping constraint for the corresponding pair of ellipses E_i and E_j. The idea allows us to extract subregions of our feasible region W of the problem (1)-(2) at each step of our optimization procedure as follows.

We create an inequality system of additional constraints on the translation vector v_i of each ellipse E_i in the form: $\Phi^{C_i\Omega_{1i}^*} \geq 0$, $i \in I_n$, where

$$\Phi^{C_i\Omega_{1i}^*} = \min\{-x_i + x_i^0 + \varepsilon, -y_i + y_i^0 + \varepsilon, x_i - x_i^0 + \varepsilon, y_i - y_i^0 + \varepsilon\},$$

is the phi-function for the circle C_i and $\Omega_{1i}^* = R^2 \setminus \operatorname{int}\Omega_{1i}$.

Then we form a new region defined by

$$W_1 = \{u \in R^{\sigma-\sigma_1} : \Phi_{ij}^{'} \geq 0, (i,j) \in \Xi_1, \Phi_i^{'} \geq 0, \Phi^{C_i\Omega_{1i}^*} \geq 0, i \in I_n\},$$

where $\Xi_1 = \{(i,j) : \Phi^{\Omega_{1i}\Omega_{1j}} < 0, i > j \in I_n\}$.

Then our algorithm searches for a point of local minimum $u_{w_1}^*$ of the subproblem $\min_{u_{w_1} \in W_1 \subset R^{\sigma-\sigma_1}} F(u_{w_1})$. When the point $u_{w_1}^*$ is found, it is used to construct a starting point $u^{(1)}$ for the second iteration of our optimization procedure (note that the σ_1 previously deleted additional variables τ_1 have to be redefined by a special procedure, assuming $\lambda^0 = 1$). At that iteration we again identify all the pairs of ellipses with non-overlapping individual containers, form the corresponding subregion W_2 (analogously to W_1) and let our algorithm search for a local minimum $u_{w_2}^* \in W_2$. The resulting local minimum $u_{w_2}^*$ is used to construct a starting point $u^{(2)}$ for the third iteration, etc.

We stop our iterative procedure when $F(u_{w_k}^*) = F(u_{w_{k+1}}^*)$, where $u_{w_k}^*$ is a point of local minimum of the problem

$$\min_{u_{w_k} \in W_k \subset R^{\sigma-\sigma_k}} F(u_{w_k}),$$

$$W_k = \{u \in R^{\sigma-\sigma_k} : \Phi_{ij}^{'} \geq 0, (i,j) \in \Xi_k, \Phi_i^{'} \geq 0, \Phi^{C_i\Omega_{ki}^*} \geq 0, i \in I_n\},$$

$$\Xi_k = \{(i,j) : \Phi^{\Omega_{ki}\Omega_{kj}} < 0, i > j \in I_n\}.$$

We claim that the point $u^* = u^{(k)*} = (u_{w_k}^*, \tau_k) \in R^\sigma$ is a point of local minimum of the problem (1)-(2), where $u_{w_k}^* \in R^{\sigma-\sigma_k}$ is the last point of our iterative procedure and $\tau_k \in R^{\sigma_k}$ is a vector of the previously deleted additional variables (the variables can be redefined by the special procedure). The assertion comes from the fact that any arrangement of each pair of ellipses E_i and E_j subject to $(i,j) \in \Xi \setminus \Xi_k$ guarantees that there always exists a vector τ_k of additional variables such that $\Phi_{ij}^{'} \geq 0, (i,j) \in \Xi \setminus \Xi_k$ at the point $u^{(k)*}$. Here $\Xi = \{(i,j), i > j = 1,2,...,n\}$. Therefore the values of additional variables of the vector τ_k have no effect on the value of our objective function, i.e $F(u_{w_k}^*) = F(u^{(k)*})$. That is why, indeed, we do not need to redefine the deleted additional variables of the vector τ_k at the last step of our algorithm.

V. COMPUTATIONAL RESULTS

Here we present a number of examples to demonstrate the high efficiency of our algorithm. We have run our experiments on an AMD Athlon 64 X2 5200+ computer, and for local optimisation we used the IPOPT code (https://projects.coin-or.org/Ipopt). We present instances taken from the recent paper [7]. We set a runtime limit for

each example to search for at least 10 local minima. We also use $\varepsilon = \sum_{i=1}^{n} b_i / n$ in our computational experiments.

We applied our method to some instances used in paper [7] and compare our optimal solutions to theirs.

We set runtime for the group of instances: up to 20 objects - time limit 2 hours, up to 50 - time limit 5 hours, 100 objects - time limit 12 hours.

Table 1 lists some examples presented in [7]. For each the example the minimal area of the container found by our method is smaller than the best solution reported in [7]. The improvement is not so big (1% to 2%) for smaller sets of ellipses, but it becomes significant (8% to 9%) for larger sets of ellipses. It should be noted that for examples TC02a, TC02b, TC03a, TC03b, TC04a and TC04b presented in the paper our method found the same results.

TABLE 1
COMPARISON OF OUR RESULTS TO THOSE IN [7]

Name	our result	the best result from [7]	Improvement (%)
TC05a	25.0206	25.29557	1.0990
TC05b	30.84870	31.28873	1.4264
TC06	25.47173	25.51043	0.1520
TC11	57.1783	57.24034	0.1085
TC14	24.25099	24.84634	2.4550
TC20	66.13647	67.83459	2.5676
TC30	95.36535	103.45212	8.4798
TC50	154.470487	166.91505	8.0563
TC100	297.73798	322.64663	8.3660

The local-optimal packing of 100 ellipses (for instance TC100 from [7]) into a rectangular container of area $F(u^*) = 297.738$ is shown in Figure 1.

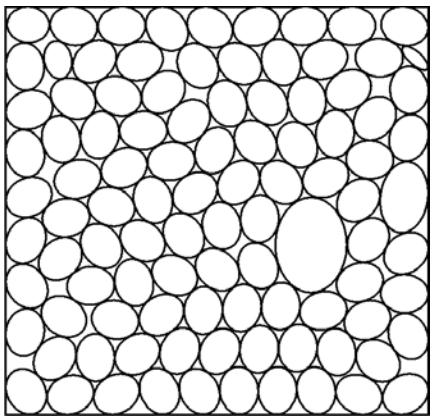

Fig. 1 The local-optimal packing of 100 ellipses

VI. CONCLUSIONS

The algorithm allows us to reduce computational cost of our problem. While there are $O(n^2)$ pairs of ellipses in the container, our algorithm may in most cases only actively controls $O(n)$ pairs of ellipses (this depends on the sizes of ellipses and the value of ε), because for each ellipse only its nearest neighbors have to be monitored. Thus our LOP algorithm allows us to reduce the problem (1)-(2) with $O(n^2)$ inequalities and a $O(n^2)$-dimensional solution space W to a sequence of sub-problems, each with $O(n)$ inequalities and a $O(n)$-dimensional solution subspace W_k. This reduction is of a paramount importance, since we deal with non-linear optimization problems.

REFERENCE

[1] Wascher, G., Hauner, H. and Schumann, H., (2007) An improved typology of cutting and packing problems, European Journal of Operational Research, Volume 183, Issue 3, 16, pp. 1109-1130.

[2] Bennell, J.A., Oliveira J.F, (2009) A tutorial in irregular shape packing problem, Journal of the Operational Research Society, 60:s93-s105 .

[3] Feng, Y., Han, K., and Owen, D. An Advancing Front Packing of Polygons, Ellipses and Spheres// Discrete Element Methods – 2002 – pp. 93-98.

[4] Burke, E.K., Hellier, R., Kendall, G., Whitwell, G., (2010) Irregular packing using the line and arc no-fit polygon. Operations Research. 58(4), 948-970

[5] Chernov N, Stoyan Y, Romanova T., (2010) Mathematical model and efficient algorithms for object packing problem. Computational Geometry: Theory and Applications 43(5): 535-553.

[6] Chernov, N., Stoyan, Y., Romanova, T., Pankratov, A., (2012) Phi-Functions for 2D Objects Formed by Line Segments and Circular Arcs. Advances in Operations Research, 26. doi:10.1155/2012/346358.

[7] Josef Kallrath and Steffen Rebennack, (2013) Cutting Ellipses from Area-Minimizing Rectangles" Journal of Global Optimization, DOI10.1007/s10898-013-0125-3

[8] Chazelle, B., Edelsbrunner, H., Guibas, L.J., (1989) The complexity of cutting complexes. Discrete & Computational Geometry. 4(2), 139-81

[9] Yu. Stoyan, G. Yaskov, (2013) Packing unequal circles into a strip of minimal length with a jump algorithm, Optimization Letters, DOI: 10.1007/s11590-013-0646-1.

[10] Wachter, A., Biegler, L. T., (2006) On the implementation of an interior-point filter line-search algorithm for large-scale nonlinear programming. Mathematical Programming.106, 1, 25-57

Alexander V. Pankratov received Doctor of Technical Sciences degree in Mathematical Modeling and Computational Methods (2013) from A.M. Podgorny Institute of Mechanical Engineering of the National Academy of Sciences of Ukraine (Kharkov). From 2012 he is a senior scientist associate at the Department of Mathematical Modeling and Optimal Design, A.M. Podgorny Institute of Mechanical Engineering of the National Academy of Sciences of Ukraine. His current research interests include mathematical modeling, operational research, computational geometry, optimization, packing and cutting.

Tatiana E. Romanova received Doctor of Technical Sciences degree in Mathematical Modeling and Computational Methods (2003) from V.M. Glushkov Institute of Cybernetics of the National Academy of Sciences of Ukraine (Kiev). She received the Professor title (2005) from the Department of Applied Mathematic of Kharkov National University of Radioelectronics (Kharkov). From 2013 she is a leading scientist at the Department of Mathematical Modeling and Optimal Design, A.M. Podgorny Institute of Mechanical Engineering of the National Academy of Sciences of Ukraine. Her current research interests include mathematical modeling, operational research, computational geometry, optimization, packing and cutting.

Iryna A. Subota received the M.Sc. (2011) from Kharkov National University of Radioelectronics. From 2011 she is an aspirant of the Department of Mathematical Modeling and Optimal Design, A.M. Podgorny Institute of Mechanical Engineering of the National Academy of Sciences of Ukraine. Her current research interests include mathematical modeling, operational research, computational geometry, optimization, packing and cutting.

K band Antennas Conjugated with a Metal Waveguide

Maksym Khruslov, *Member, IEEE*

***Abstract*—Two planar spiral antennas conjugated with the standard metal waveguide and operating in the millimeter range are proposed. The first antenna has the bandwidth of 6.12GHz and second 5.93GHz. The axial ration of both antennas does not exceed -3dB in the frequency band 32.4 – 37 GHz. The elevation angle of peak directivity close the zenith for single planar spiral antenna, is oriented and at θ=20^0 for the double planar spiral antenna. The radiation pattern shape is practically the same within the operational frequency band for both antennas. The nature of axial ratio changing is explained from the analysis of near-field distributions at two orthogonal polarizations. The proposed antennas can be used for different practical applications in the millimeter range.**

***Index Terms*—spiral antenna, millimeter range, impedance transformer, near-field distribution, axial ratio**

I. Introduction

THE different types of planar spiral antennas are usually excited by a co-axial feed line with various balun circuits [1-4]. Moving towards the higher frequencies the radiating area of the spiral antenna is reduced. However, the disadvantages of such designs include the fact that in the millimeter range they will have the great losses due to the long feed path. The original planar single-arm fractional spiral antenna with the aforementioned exciting method was reported in [5]. A simple antenna design and the good expected performance seem to be very attractive for its millimeter wave applications by taking into account a possibility to be easily integrated with RF components or MMICs on the same printed circuit board. For good matching of feeding 50-Ohm coaxial cable with the antenna in the wide frequency band the different approaches are used [4, 5]. At the same time, the variety of practical applications of planar spiral antennas sometimes has specific requirements to the feeding or receiving networks, in particular, when the antenna should be loaded with the standard waveguide [6].

In this article, we present the two types of antennas with circular polarization and different radiation patterns: first antenna produce the radiation pattern with maximum radiation close to the zenith, and second antenna with omnidirectional radiation pattern (minima radiation to the zenith) for the wireless applications in the millimeter range.

Manuscript received December 21, 2013.

Khruslov M.M. is with the Usikov Institute for Radiophysics and Electronics of the National Academy of Sciences of Ukraine, 12 Ak. Proskura St., Kharkov, 61085, Ukraine, tel. +38 (057) 7203594, fax. +38 (057) 3152105 (e-mail: ireburan@yahoo.com)..

II. Antenna Design

Figure 1 shows the antennas geometry. Both spiral antennas 1 are printed on the low losses dielectric substrate 2. First planar spiral (called single planar spiral) (Fig 1a) is described by two equations (1):

$$x(t)=ae^{bt}\cos(t) \qquad y(t)=ae^{bt}\sin(t) \qquad (1)$$

Second planar spiral (called double planar spiral) is consist of two spirals noted above (Fig. 1b). Parameters a and b are changed in the simulation process in such limits: $0.0005<a_1<0.0015$, $0.1<b_1=<0.2$; $0.001<a_2<0.002$, $0.1<b_2<0.25$, $0<t<2\pi$.

Planar spiral is located on the output aperture of the conical wave impedance transformer 3, which is similar to that described in [7] (Fig. 1c). It is a truncated hollow metal cone filled with a low-loss dielectric. The spiral antenna is excited by a co-axial line and coupled with the standard rectangular waveguide by means of the coaxial-to-waveguide transition 4. In this case the adjustment of the coupling coefficient is implemented by a shorting piston 5. In simulations the height H_2 of the cone, the diameters D_1 of the cone, and the relative dielectric permittivity of the transformer filling ε_t are varied within the following limits: $4mm<H_2<16mm$; $6mm<D_1<16mm$; $1.07<\varepsilon_t<3.8$. Cross-section of the smaller cone base has the diameter D_2 and corresponds to the cross-section of the feeding coaxial cable.

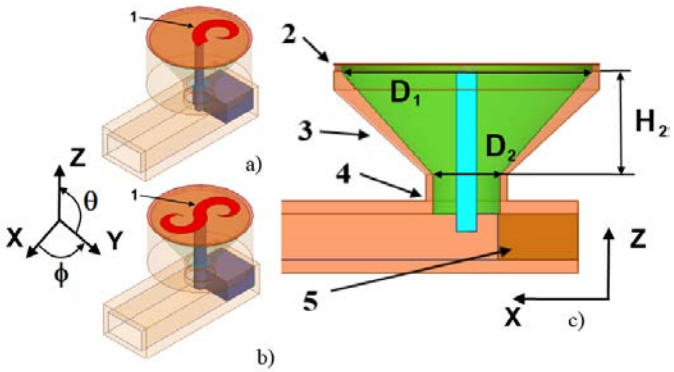

Fig. 1. Geometry of the proposed antennas: single planar spiral (a); double planar spiral (b); antenna with waveguide (c)

III. RESULTS AND DISCUSSIONS

In simulations the antenna characteristics such as: input reflection coefficient S_{11}, radiation patterns, axial ratio, and near-field distributions were studied. As can be seen from the Figure 2a, for first antenna the -10dB return loss bandwidth ranges from 31 to 37.5 GHz excluding the frequency band 32<f<34GHz. Two bandwidth for the double planar spiral antenna is observed 30.05-31.8 GHz and 32.46-36.64 GHz (Fig. 2b).

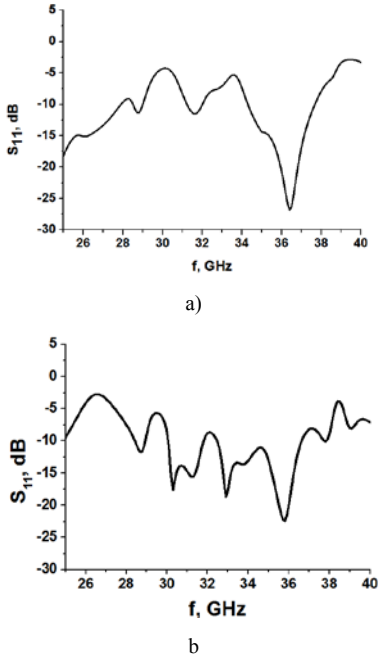

Fig. 2. Simulated return loss of two antennas: single planar spiral antenna (a) double planar spiral antenna (b)

The simulated radiation patterns of single spiral antenna for two basic planes are virtually the same within the operational frequency band. At that, the elevation angle of peak directivity is oriented close the zenith and slightly changed within the working band. For example, the radiation pattern at 35GHz is shown in the Figure 3a. The beamwidths for both basic plane are $\Delta\theta=29^0$. For the double planar spiral antenna the elevation angle of peak directivity is oriented at $\theta_{max}=\pm22^0$ and $\theta_{max}=\pm25^0$ for two basic planes (Fig 3b).

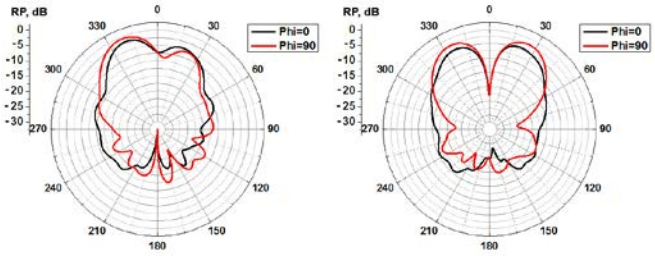

Fig. 3. Simulated radiation patterns at the frequency f=35GHz for two antennas: single planar spiral antenna (a), double planar spiral antenna

Following from simulations the axial ratio is less than 3dB in the frequency band 34.2<f<37GHz for both antennas (Fig. 4).

The influence of edge effects as well as impedance matching of the antenna input with the feeding line on the antenna performance can be studied by applying near-field technology [8]. Therefore, in order to explain the axial ratio behavior within the operational frequency band the simulations of near-field distributions for both orthogonal components have been carried out. The similar near-field distributions on both orthogonal components and the location of areas with the high intensity of the electromagnetic field close the spiral arm guarantee the circular polarization of the antenna radiation. Indeed, in the frequency band 34.2<f<37GHz the near-fields have the spatial distributions shown as the pictures are presented in the Figure 4.

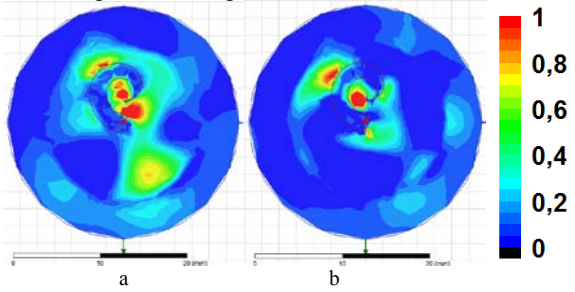

Fig. 4. Near-field distributions on the Ex (a) and Ey (b) components for single planar spiral antenna at f=35GHz

We are noted, that maxsima intensity of the near field distributions for both components of electromagnetic fields and for total field is situated on the spiral surface (Fig. 5).

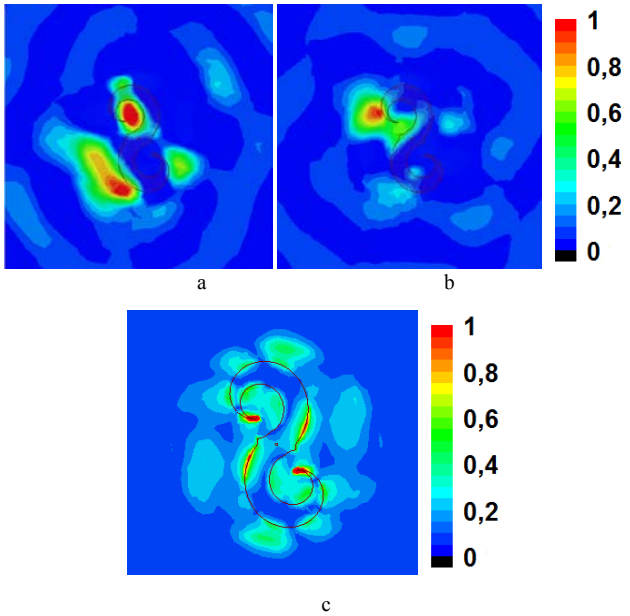

Fig. 5. Near-field distributions on the Ex (a) and Ey (b) components and E–total (c), for double planar spiral antenna f=35GHz

IV. Experimental Results

Both antenna prototypes were manufactured and tested. In Fig. 6 the antennas are presented.

Fig.6 Two antenna prototypes: single planar spiral antenna (a); double (b)

Input reflection coefficient S_{11}, radiation patterns, axial ratio were measured. In the case of single planar spiral antenna the -10dB return loss bandwidth ranges from 32.88GHz to 39GHz (Fig. 7a). The maximum efficiency is observed at the f=35.2GHz (-27dB). In case of double planar spiral antenna the -10dB return loss bandwidth ranges is f=31.37GHz ÷ f=36.6GHz, the maximum efficiency is observed at the f=34.9GHz (-49dB)

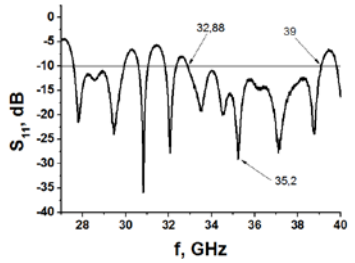

a

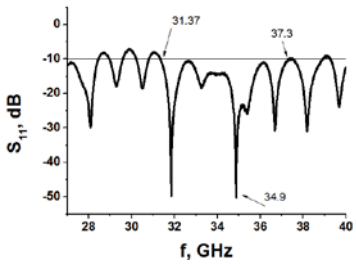

b

Fig. 7 Measured return loss of two antennas: single planar spiral antenna (a) double planar spiral antenna (b)

In case of single planar spiral antenna the monobeam radiation pattern is observed in all working frequency band. The radiation pattern at the f = 35.2GHz for the both of measured components (E_x and E_y) characterized by one beam slightly shifted from the zenith direction (Fig. 8a). Here the axial ratio is changed from 9dB at f=27GHz where polarization is linear to 3dB in operating frequency band f=32GHz ÷ f=38.8GHz (Fig. 9a). Qualitative agreement between the experimental near-field (Fig. 10) and simulation results (Fig. 4) confirm the presence of circular polarization of the under test antenna.

The elevation angle of peak directivity for double planar spiral antenna is oriented at $\theta_{max}=\pm 20^0$ for E_x and E_y components (Fig. 8b). The circular polarization have to observe within working frequency band, but in experiment the axial ration less than 3dB from 32.4 – 37.1GHz (Fig. 9b).

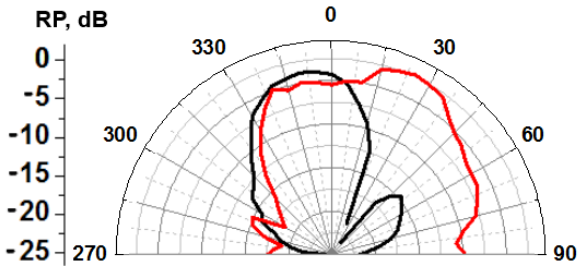

a

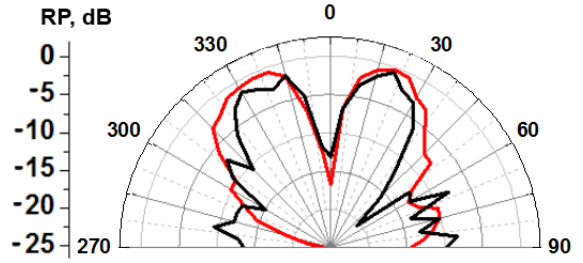

b

Fig. 8. Measured radiation patterns of two antennas for E_x and E_y components; single planar spiral antenna f=35.2GHz (a) and double planar spiral antenna f=34.9GHz (b)

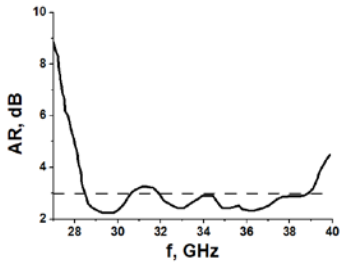

a

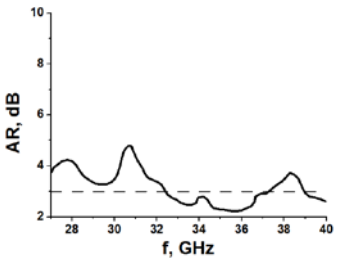

b

Fig. 9. Experimental axial ration of the single spiral antenna (a), double spiral antenna (b)

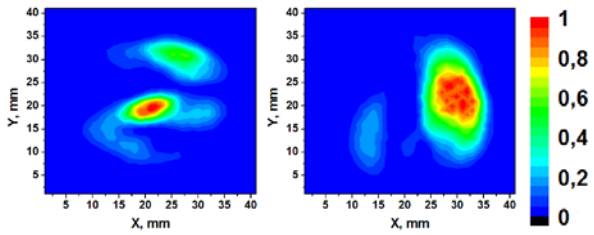

a b

Fig. 10. Measured near-field distributions on the Ex (a) and Ey (b) components for single planar spiral antenna f=35.2GHz

Near field distribution for the double spiral antenna were measured by waveguide probe in the plane XY, when the vector E of the probe was in the plane Y = X (Fig. 11a) and Y =-X (Fig. 11b). The obtained pattern in the near field zone exhibit substantially uniform distribution of intensity (Fig. 11). Distribution data confirm the numerical simulation result (Fig. 5). Presented distributions confirm the veracity of the experimental axial ratio. The obtained distributions show that the double spiral antenna has a circular polarization.

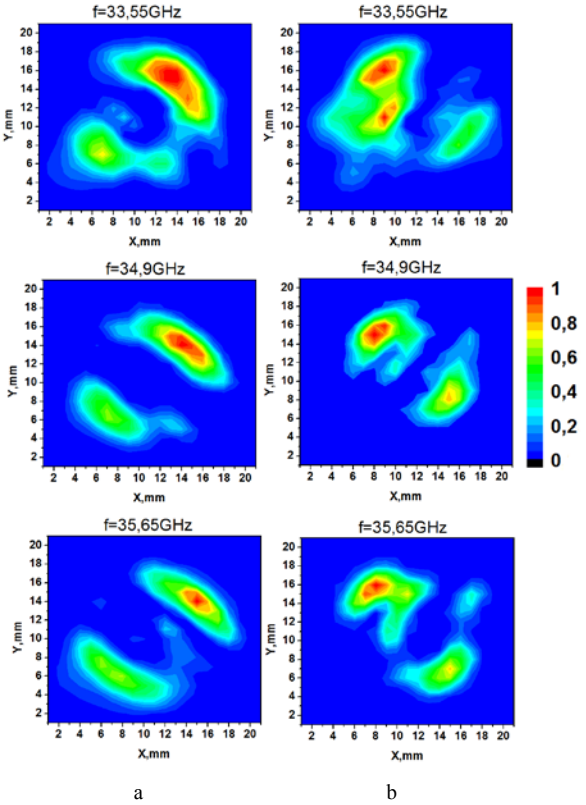

a b

Fig. 11. Measured vector E near-field distributions in the plane Y = X (a) and in the plane Y = –X (b) components for double planar spiral antenna

V. CONCLUSIONS

Two planar spiral antennas conjugated with the standard metal waveguide and operating in the millimeter range have been proposed. Following the results of simulations, the optimal physical and geometric parameters of both antennas have been determined. The prototypes have been manufactured and tested. As the result, the measured return loss coefficients point out the -10dB impedance bandwidth of 6.12GHz and 5.93GHz for the single and double planar spiral antennas respectively.

The radiation pattern of the single spiral antenna is characterized by the wide lobe with the elevation angle of peak directivity near the antenna axis. For the double spiral antenna we obtained the omnidirectional radiation pattern in the azimuth plane with the elevation angle of peak directivity oriented at $\theta_{max}=\pm 20^0$ and with the minimum intensity in the antenna axis.

The axial ration does not exceed -3dB in the frequency band f=32GHz ÷ 38.8GHz for the single spiral antenna and f=32.4GHZ ÷ 37.1GHz for the double spiral antenna. The different values of the axial ration and the nature of their changing in the impedance bandwidth of both antennas become apparent following the analysis of measured near-field distributions.

The proposed antenna can be used for different practical applications in the millimeter range.

REFERENCES

[1] L. Schreider, X. Begaud, M. Soiron, and B. Perpere, “Archimedean microstrip spiral antenna loaded by chip resistors inside substrate”, IEEE Antennas and Propagation Society [Digests of International Symposium, Monterey, California, USA, pp. 1066–1069, 2004.

[2] W. Lopez, E.R. Rowe, and W.S.T. Ghorbani, “A planar dual-arm equiangular spiral antenna”, IEEE Trans Antennas Propag., vol. 58, pp. 1775–1779, 2010.

[3] Eubanks, T.W., Kai Chang. A Compact Parallel-Plane Perpendicular-Current Feed for a Modified Equiangular Spiral Antenna. AP Trans., Vol. 58, Issue 7, pp. 2193-2202, July 2010.

[4] Sang Heun Lee, Jaebok Lee, Young Joong. Wideband thick-arm spiral antenna for ingestible capsules. Microwave and Optical Technology Letters, Vol. 53, Issue 3, pp. 529–532, March 2011.

[5]] Kuo-Fong Hung and Yi-Cheng Lin. Simulation of Single-Arm Fractional Spiral Antennas for Millimeter Wave Applications. Proc. of Antennas and Propagation Society International Symposium 2006, IEEE, Albuquerque, NM, 9-14 July 2006, pp. 3697-3700.

[6] Roman Chernobrovkin, Christophe Granet, Vladimir Khaikin, and Nina Popenko. Compact Efficient Feed-Horn at 30-38 GHz for a Multi-beam Radio Telescope. – J Infrared Milli Terahz Waves DOI10.1007/s10762-010-9652-x , Springer, May 2010, - 12pages.

[7] R. Chernobrovkin, I. Ivanchenko, V.Pischikov, and N. Popenko, “UWB equiangular spiral antenna for 7.5–40GHz”, Microwave and Optical Technology Letters, vol. 54, No. 9, pp. 2190–2194, 2012

Maksym Khruslov was born in Kharkov, Ukraine, in 1982. He received the M.S. degree in radiophysics and electronics from Karazin Kharkov National University (Ukraine) in 2004. Since 2004, he works in the Institute for Radiophysics and Electronics of the National Academy of Sciences of Ukraine, Kharkov, Ukraine. He received the Ph.D degrees in Radiophysics in 2012. From 2013 he is a Researcher with the Department of Radio-Spectroscopy in the IRE NASU. with the Radiospectroscopy Department. His research interest includes the near-field technology, computational modeling of microwave antennas. Mr. Maksym Khruslov is a Member of IEEE, and a Member of EuMa.

Matrix-Model for Diagnosing SoC HDL-Code

Vladimir Hahanov, *Senior Member, IEEE* , Eugeniya Litvinova, *Member, IEEE,*
Vladimir Obrizan, Igor Yemelyanov

Abstract — **This article describes technology for diagnosis SoC HDL-models, based on transaction graph. Diagnosis method is focused to decrease the time of fault detection and memory for storage of diagnosis matrix by means of forming ternary relations between test, monitor, and functional component. The following problems are solved: creation of digital system model in the form of transaction graph and multi-tree of fault detection tables, as well as ternary matrices for activating functional components of the selected set of monitors by using test patterns; development of a method for analysis the activation matrix to detect the faulty blocks with given depth and synthesis logic functions for subsequent embedded hardware fault diagnosis.**

I. TAB-MODEL FOR DIAGNOSIS FAULTY SOC COMPONENTS

The goal is creation TAB-matrix model (Tests – Assertions – Blocks functional) model and diagnosis method to decrease the time of testing and memory for storage by means of forming ternary relations (test – monitor – functional component) in a single table.

The problems are: 1) development of digital system HDL-model in the form of a transaction graph for diagnosing functional blocks by using assertion set [1-6,15]; 2) development method for analyzing TAB-matrix to detect minimal set of fault blocks [4-7,13]; 3) Synthesis of logic functions for embedded fault diagnosis procedure [8-11,14].

Model for testing a digital system HDL-code is represented by the following xor-relation between the parameters <test – functionality – faulty blocks B*>:

$$T \oplus B \oplus B^* = 0;$$

$$B^* = T \oplus B = \{T \times A\} \oplus B,$$

which transformed relationship of the components in the TAB-matrix:

$$M = \{\{T \times A\} \times \{B\}\}, M_{ij} = (T \times A)_i \oplus B_j.$$

Here, the coordinate of the matrix is equal to 1, if the pair test–monitor $(T \times A)_i$ detects or activates some faults of the functional block $B_j \in B$.

An analytical model for verification by using a temporal assertion (additional observation statements or lines) is focused to achieve the specified diagnosis depth and presented as follows:

$$\Omega = f(G, A, B, S, T),$$

$$G = (A * B) \times S; S = f(T, B);$$

$$A = \{A_1, A_2, ..., A_i, ..., A_h\};$$

$$B = \{B_1, B_2, ..., B_i, ..., B_n\};$$

$$S = \{S_1, S_2, ..., S_i, ..., S_m\};$$

$$T = \{T_1, T_2, ..., T_i, ..., T_k\}.$$

Here $G = (A * B) \times S$ is functionality, represented by Code-Flow Transaction (CFT) Graph (Fig. 1); $S = \{S_1, S_2, ..., S_i, ..., S_m\}$ are nodes represented by software variables states when simulating test segments (patterns). Otherwise the graph can be considered as an ABC-graph – Assertion Based Coverage Graph. Each state $S_i = \{S_{i1}, S_{i2}, ..., S_{ij}, ..., S_{ip}\}$ is determined by the values of design essential variables (Boolean, registers, memory). The oriented graph arcs are represented by a set of software blocks:

$$B = \{B_1, B_2, ..., B_i, ..., B_n\}; \bigcup_{i=1}^{n} B_i = B; B_i \bigcap_{i \neq j} B_j = \varnothing.$$

The assertion $A_i \in A = \{A_1, A_2, ..., A_i, ..., A_n\}$ can be inserted to the end of each block B_i – a sequence of code statements which determines the state of the graph node $S_i = f(T, B_i)$ depending on the test pattern $T = \{T_1, T_2, ..., T_i, ..., T_k\}$. The monitor, uniting an assertions of incoming arcs $A(S_i) = A_{i1} \vee A_{i2} \vee ... \vee A_{ij} \vee ... \vee A_{iq}$ can be put on each node.

Manuscript received March 14, 2013.

Vladimir Hahanov is with Kharkov National University of Radioelectronics, Ukraine, 61166, Kharkov, Lenin Prosp., 14, room 321 (corresponding author to provide phone: (057)7021326; fax: (057)7021326; e-mail: hahanov@ kture.kharkov.ua).

Eugeniya Litvinova is with Kharkov National University of Radioelectronics, Ukraine, 61166, Kharkov, Lenin Prosp., 14, room 380 (phone: (057)7021421; fax: (057)7021421; e-mail: kiu@ kture.kharkov.ua).

Volodymyr Obrizan is with Kharkov National University of Radio Electronics, Ukraine, 61166, Kharkov, Lenin Prosp., 14, room 319 (e-mail: volodymyr.obrizan@gmail.com).

Igor Yemelyanov is with Kharkov National University of Radioelectronics, Ukraine, 61166, Kharkov, Lenin Prosp., 14, room 319 (phone: (057)7021326; fax: (057)7021326; e-mail: iyemelyanov@itdelight.com).

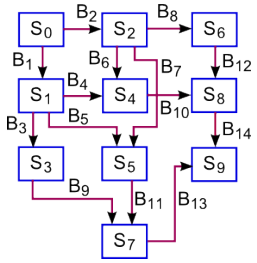

$$B = (B_1B_3B_9 \vee (B_2B_7 \vee B_1B_5)B_{11})B_{13} \vee$$
$$\vee ((B_1B_4 \vee B_2B_6)B_{10} \vee B_2B_8B_{12})B_{14} =$$
$$= B_1B_3B_9B_{13} \vee B_2B_7B_{11}B_{13} \vee B_1B_5B_{11}B_{13} \vee$$
$$\vee B_1B_4B_{10}B_{14} \vee B_2B_6B_{10}B_{14} \vee B_2B_8B_{12}B_{14}.$$

Figure 1. Example of ABC-graph for HDL-code

The model of HDL-code, represented in the form of ABC-graph, describes not only software structure, but also test segments of the functional coverage, generated by using software blocks, incoming to the given node. The last one defines the relationship between achieved on the test variable space and potential one, which forms the functional coverage of graph node state $Q = \mathbf{card}S_i^r / \mathbf{card}S_i^p$. In the aggregate all nodes have to be full state coverage space of software variables, which determines the test quality, equal to 100%: $Q = \mathrm{card}\bigcup_{i=1}^{m} S_i^r / \mathrm{card}\bigcup_{i=1}^{m} S_i^p = 1$. Furthermore, the assertion set $<A,S>$ that exists in the graph, allows monitoring arcs (code-coverage) $B = (B_1, B_2, ..., B_i, ..., B_n)$ and nodes (functional coverage) $S = \{S_1, S_2, ..., S_i, ..., S_m\}$. The assertions on arcs $B_i \in B$ are designed for diagnosis of the functional failures in software blocks. The assertions on graph nodes $S_i \in S$ carry information about the quality of test and assertion set for their improvement or complement. The ABC-graph makes possible the following: 1) to estimate the software quality via diagnosability design; 2) to minimize the costs for generating tests, diagnosing and correcting the functional failures by using assertions; 3) to optimize test synthesis via coverage all arcs and nodes by a minimum set of activated test paths. For instance, the minimal test for the above mentioned ABC-graph has six segments, which activate all existent arcs and nodes, shown in Fig. 1.

For diagnosing, test segments $T = \{T_1, T_2, ..., T_r, ..., T_k\}$ activate transaction paths in the graph model covered all nodes and arcs. Generally, the testing model is represented by the Cartesian product $M = T \times A \times B$ that accordingly has the dimension $Q = k \times h \times n$. To reduce the amount of diagnosys data, separate monitor or assertion point for visualization functional blocks activation is assigned to each test segment. It makes possible to decrease the matrix dimension to $Q = n \times k$ and retain all features of the triad relationship $M = < T \times A \times B >$. Pair «test – monitor» are represented by three possible forms:

$$< T_i \to A_j >, < \{T_i, T_r\} \to A_j >, < \{T_i\} \to \{A_j, A_s\} >.$$

The method for diagnosis of functional block failure uses pre-built TAB-matrix (table) $M = [M_{ij}]$, where the row is the relation between the test segment and a subset of activated blocks

$$T_i \to A_j \approx (M_{i1}, M_{i2}, ..., M_{ij}, ..., M_{in}), M_{ij} = \{0,1\},$$

observed by the monitor A_j. Column of the table describes the relation between the functional blocks, detected on test segments, relatively monitors $\mathbf{M_j = B_j(T_j, A_j)}$.

For faulty blocks diagnosis at the testing procedure, the real assertion response (vector) $\mathbf{A^* = (A_1^*, A_2^*, ..., A_i^*, ..., A_n^*)}$ on the test pattern T is determined, by forming $\mathbf{A_i^* = f(T_i, B_i)}$. Detecting faulty functional blocks is based on xor-operation between the real assertion response vector and TAB-matrix columns

$$A^* \oplus [M_1(B_1) \vee M_2(B_2) \vee ... \vee M_j(B_j) \vee ... \vee M_n(B_n)].$$

The faulty block is defined by a vector B_j, which gives result with minimal number of 1-unit coordinates:

$$B = \underset{j=1,n}{\min} [B_j = \sum_{i=1}^{h} (B_{ij} \oplus A_i^*)].$$

As an addition to the diagnosis model, necessary to describe the following important features of the TAB-matrix:

$$1)\ M_i = (T_i \times A_j); \quad 2)\ \bigvee_{i=1}^{m} M_{ij} \to \bigvee_{j=1}^{n} M_j = 1;$$
$$3)\ M_{ij} \bigoplus_{j=1}^{n} M_{rj} \neq M_{ij}; \quad 4)\ M_{ij} \bigoplus_{i=1}^{k} M_{ir} \neq M_{ij};$$
$$5)\ \log_2 n \le k \leftrightarrow \log_2 |B| \le |T|$$
$$6)\ B_j = f(T, A) \to B \oplus T \oplus A = 0.$$

The features mean: 1) Each row of the matrix is a subset of the Cartesian product between test and monitor. 2) Disjunction of all matrix rows gives a vector equal to 1-unit over the all coordinates. 3) All matrix rows are distinct, which eliminates the test redundancy. 4) All matrix columns are distinct, which exclude the existence of equivalent faulty blocks. 5) The number of matrix rows must be greater than the binary logarithm of the number of columns that determines the potential diagnosability of every block. 6) The diagnosis function of every block depends on the complete test and monitors, which must be minimized without diagnosability reduction. In accordance with 6 test segments activated the following graph nodes paths relatively assertion point S9:

$$T = S_0S_1S_3S_7S_9 \vee S_0S_1S_4S_8S_9 \vee S_0S_1S_5S_7S_9 \vee$$
$$\vee S_0S_2S_4S_8S_9 \vee S_0S_2S_5S_7S_9 \vee S_0S_2S_6S_8S_9,$$

it will be easy using graph structure to define all functional block paths (oriented arcs) activated by test:

$$B = B_1B_3B_9B_{13} \vee B_2B_7B_{11}B_{13} \vee B_1B_5B_{11}B_{13} \vee$$
$$\vee B_1B_4B_{10}B_{14} \vee B_2B_6B_{10}B_{14} \vee B_2B_8B_{12}B_{14}.$$

The assertion engine can be represented by 3 groups of components, which create logical equations for monitoring software or hardware functionality HDL-code blocks based on visual points $\{A_9 \subseteq S_9, A_3 \subseteq S_3, A_6 \subseteq S_6\}$:

$$A_9 = T_1(B_1B_3B_9B_{13}) \vee T_2(B_2B_7B_{11}B_{13}) \vee$$
$$\vee T_3(B_1B_5B_{11}B_{13}) \vee T_4(B_1B_4B_{10}B_{14}) \vee$$
$$\vee T_5(B_2B_6B_{10}B_{14}) \vee T_6(B_2B_8B_{12}B_{14});$$
$$A_3 = T_1(B_1B_3);\ A_6 = T_6(B_2B_8).$$

The next step allows creating 6 rows of TAB-matrix $M_{ij}(G_1)$ in the form of relations between test segments and blocks activated respectively:

$M_{ij}(G_1)$	B_1	B_2	B_3	B_4	B_5	B_6	B_7	B_8	B_9	B_{10}	B_{11}	B_{12}	B_{13}	B_{14}
$T_1 \to S_9$	1	.	1	.	.	.	.	.	1	.	.	.	1	.
$T_2 \to S_9$	1	.	.	1	.	.	.	.	.	1	.	.	.	1
$T_3 \to S_9$	1	.	.	.	1	.	.	.	.	.	1	.	1	.
$T_4 \to S_9$	.	1	.	.	.	1	.	.	.	1	.	.	.	1
$T_5 \to S_9$	.	1	.	.	.	.	1	.	.	.	1	.	1	.
$T_6 \to S_9$	.	1	.	.	.	.	.	1	.	.	.	1	.	1
$T_1 \to S_3$	1	.	1	.	.	.	.	.	.	.	.	.	.	.
$T_6 \to S_6$	.	1	.	.	.	.	.	1	.	.	.	.	.	.

The TAB-matrix of paths activation shows the existence of equivalent failure blocks 3 and 9, 8 and 12, on 6 test segments with one assertion point in the graph node 9. The columns 3 and 9, 8 and 12 are equivalent. To resolve indistinguishability of two pairs faulty blocks it is necessary to create two additional monitors in the nodes S3 and S6 for test segments T1 and T6 respectively. As a result, three assertions in the nodes $A = (S_9, S_3, S_6)$ allow distinguishing all faulty blocks of software HDL-code. Thus, the graph enables not only to synthesize the optimal test, but also to determine the minimal number of assertion monitors in the nodes to detect faulty blocks with a given diagnosis depth.

Diagnosis procedure by using the created matrix is defined the following equation of vector xor-operation between real 8 assertion values and the B-columns:

$$\{[A_9(T_1, T_2, T_3, T_4, T_5, T_6), A_3(T_1), A_6(T_6)] \oplus B_j = 0\} \to$$
$$\to (B_j - \text{failed}).$$

II. Design for Diagnosability

Diagnosability is the relationship $D = N_d / N$ between the recognized faulty blocks amount N_d, (when there are not equivalent components, or the diagnosis depth is equal to 1), and the total number N of HDL-blocks.

For the expense E evaluation of the TAB-matrix model for detecting functional failures, it can use the pair test-assertions efficiency for a given diagnosis depth. Criterion E functionally depends on the relation between the ideal $]\log_2 N[\times N$ and real $|T| \times |A| \times N$ memory sizes or resources (where $|T|$ – the test length, $|A|$ – a number of assertions) for the corresponding TAB-matrices, which compose the relative expense reduced to 0-1 intervals:

$$E = \frac{]\log_2 N[\times N}{|T| \times |A| \times N} = \frac{]\log_2 N[}{|T| \times |A|}.$$

The general diagnosis quality criterion depends on expense E and diagnosability D:

$$Q = E \times D = \frac{]\log_2 N[}{|T| \times |A|} \times \frac{N_d}{N}.$$

For instance, the diagnosis quality of the TAB-matrix $M_{ij}(G_1)$ before and after adding two rows equal to

$$Q_1[M(6 \times 1 \times 14)] = \frac{]\log_2 14[}{|6| \times |1|} \times \frac{10}{14} = 0{,}47;$$
$$Q_2[M(8 \times 1 \times 14)] = \frac{]\log_2 14[}{|8| \times |1|} \times \frac{14}{14} = 0{,}5.$$

1. It means, the first matrix dimension is a little bit less than the second, but diagnosability is a better in the second variant of matrix, which becomes the winner of the whole. Comparing to the well-known solutions [12], when every cell of a matrix contains all existing assertions $|M_{ij}| = |A|$ the second variant evaluates the following low value:

$$Q_2[M(6 \times 3 \times 14)] = \frac{]\log_2 14[}{|6| \times |3|} \times \frac{14}{14} = 0{,}2.$$

So, the TAB-matrix operating by the selected pair test-assertion concurrently allows having the essential advantages in memory size reducing in $|A| - 1$ times with the same diagnosability value.

The TAB-matrix diagnosis quality is the ratio of the bit number needed for identification (recognition) of all blocks $]\log_2 N[$ related to the real number of code bits, presented by the product of test length and number of assertions $|T| \times |A|$. If the first part E of quality criterion Q is equal to 1 and every block with functional failures is recognized in the field of the rest components $N_d = N$, it means a test and assertions are optimal, that gives the best quality criterion of diagnosis model Q=1.

The purpose of the ABC-graph analysis is structured evaluation of assertion monitor placement, which make possible to obtain maximal diagnosis depth of fault blocks. Diagnosability of the ABC-graph is a function depending on the number N_n of transit not ended nodes where exist only two adjacent arcs, one of which is incoming, other one is outgoing. Such arcs form paths though the node without fan-

in and fan-out branches (N is the total number of arcs in the graph):

$$\mathbf{D} = \frac{\mathbf{N}-\mathbf{N_n}}{\mathbf{N}}.$$

The estimation N_n is the number of unrecognizable or equivalent functional blocks. Potential installation of additional monitors for improving diagnosability of failure blocks is pure transit nodes composed $\mathbf{N_n}$. The diagnosis quality criterion of the ABC-graph takes the form:

$$Q = E \times D = \frac{]\log_2 N[}{|T| \times |A|} \times \frac{N - N_n}{N}.$$

The last expression produce some practical rules for synthesis of diagnosable HDL-code: 1) Test or testbench must create a minimal number of single activation paths, covered all the nodes and arcs in the ABC-graph. 2) The base number of monitors equals to the end node number of the graph with no outgoing arcs. 3) An additional monitor can be placed on each not ended node, which has one incoming and one outgoing arc. 4) Parallel independent code blocks must have n monitors and a single concurrent test, or one integrated monitor and n serial tests. 5) Serially connected blocks have one activation test for serial path and n-1 monitor, or n tests and n monitors. 6) The graph nodes, which have more than 1 number of input and output arcs, create good conditions for the diagnosability of the current section by single path activation tests without installation additional monitors. 7) The test pattern or testbench has to be 100% functional coverage for the nodes of the ABC-graph. 8) Diagnosis quality criterion as a function depending on the graph structure, test and assertion monitors can always be increased close to the 1-value. For this purpose there are two alternative ways. The first one is increasing test segments by activating new paths for recognition equivalent faulty blocks without increasing assertions, if the software graph structure allows the potential links. The second way is adding assertion monitors on transit nodes of the graph. A third so called hybrid variant is possible, based on the joint application of two above-mentioned ways.

III. MULTILEVEL DIAGNOSIS METHOD OF DIGITAL SYSTEM

Multilevel model of the multi-tree B (Fig. 3) is shown, where each node is represented by digital or computer system component, which has a three-dimensional activation TAB-matrix of functional unit subcomponents.

The outcoming from the node arcs are transitioning to a lower detailed level in diagnosing process, when replacing faulty block is too expensive:

$$B = [B_{ij}^{rs}],\ \mathrm{card}B = \sum_{r=1}^{n} \sum_{s=1}^{m_r} \sum_{i=1}^{p_{rs}} \sum_{j=1}^{k_{rs}} B_{ij}^{rs},$$

where n is a number of diagnosis multi-tree levels; m_r is a number of functional units or components at the level r; k_{rs} ($\mathbf{p_{rs}}$) is a number of components (test length) in the table B^{rs}; $B_{ij}^{rs} = \{0,1\}$ is a component of an activation table, which is defined by 1-unit the detected faulty functionality under the test segment $T_{i\text{-}A_i}$ relatively to the observed monitor-assertion A_i. Each node-table has the number of outcoming down arcs equal to the number of functional components, which are represented by activation TAB-matrixes as well.

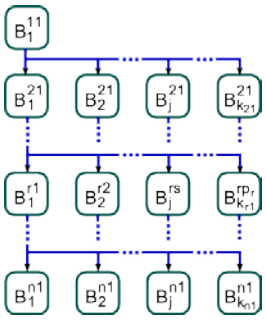

Figure 3. Diagnosis multitree model

Method for faulty blocks diagnosis Hardware-Software HS-system, based on multi-tree model, allows creating the universal engine in form of algorithm (Fig. 4, block 6) for traversal of tree branches on the depth, specified a priory:

$$B_j^{rs} \oplus A^{rs} = \begin{cases} 0 \to \{B_j^{r+1,s}, R\}; \\ 1 \to \{B_{j+1,}^{rs}, T\}. \end{cases}$$

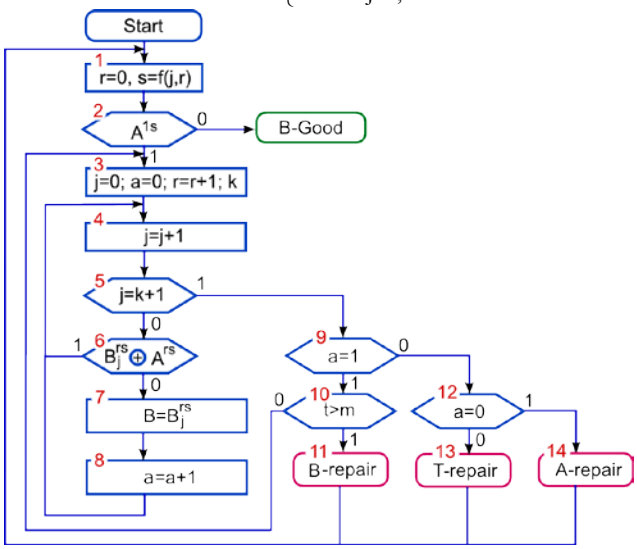

Figure 4. Engine for traversal of diagnosis multitree

Here xor-vector-operation is executing the matrix columns with the assertion (output) response vector A^{rs}, which is determined by the real (m) and gold (g) functionality responses under test patterns based on xor-operation: $A_i^{rs} = m_i^{rs} \oplus g_i^{rs}, i = \overline{1, k_{rs}}$. If all coordinates of vector xor-sum $B_j^{rs} \oplus A^{rs} = 0$ is equal to zero then one of the following action is performed: the transition to the activation

matrix of the lower level $B_j^{r+1,s}$ or repair of the functional block $\mathbf{B} = \mathbf{B}_j^{rs}$.

One of two analysis ways is executed, what is the most important: 1) the time (t>m, block 10) – then repair of faulty block is performed; 2) the money (t<m) – than a transition down is specify more exact fault location, because replacement of smaller block decreases the repair cost. If at least one coordinate of the resulting xor-sum vector is equal to one $B_j^{rs} \oplus A^{rs} = 1$, then transition to the next matrix column is performed. When all coordinates of the assertion vector are equal to zero $\mathbf{A}^{ls} = \mathbf{0}$, fault-free state of a HS-system is defined. If all vector sums by executig TAB-matrix column are not equal to zero $B_j^{rs} \oplus A^{rs} \neq 0$, it means a test, generated for detecting the given component of functionality has to be corrected. If more than one wector sum obtained by executig TAB-matrix column are equal to zero $B_j^{rs} \oplus A^{rs} = 0$, it means an assertion engine, created for detecting the given component of functionality on the represented test has to be supplemented an extra assertion monitors. So, the TAB-engine has four end-nodes, where one of them is B-good which indicates successful finishing of the testing. Anoters three means the intermediate results in the test process, which is nessessary to take into account for the incresing a test quality and diagnosis depth by using extra assertions and/or additional test segments generation.

Thus, the graph shown in the Fig. 3, allows realizing efficient infrastructure IP for the complex technical systems. The advantages of the TAB-engine, which is invariant to the hierarchical levels, are the simplicity of preparation and presentation of diagnostic information in the form of minimized activation table of functional blocks on the test segments.

Technological model of infrastructure for embedded testing, diagnosis and repairing of faulty blocks (Fig. 5) has three components: 1. Block testing (Unit Under Test – UUT) by using a reference gold model (Model Under Test – MUT) for generating the assertion response vector $\mathbf{m_a}$ which dimension corresponds to the number of test patterns. 2. Searching faulty blocks based on analysis of the TAB-matrix. 3. Repairing faulty blocks by replacing the good components from the Spare Primitives.

Process model of embedded IP service operates in real time and allows supporting good state of the HS-system without human actions distantly. The proposed algorithm or TAB-engine for analysis of TAB-matrix, as well as the introduced diagnosis quality criteria allow solving the problems of quasi-optimal coverage for software and hardware blocks by test and assertions. The model shown in Fig. 5 allows effectively servicing complex HS-system. The advantages of this functionality that is invariant to the hierarchical levels, lies in simplification of preparation and presentation of diagnosis information in the form of minimized activation table for functional blocks by using test segments.

In the last case, the effect – time benefits – is obtained via introducing the additional infrastructure to the design, Fig. 6, which allows performing selective testing, diagnosis, and reprogramming some modules in the faulty detected blocks.

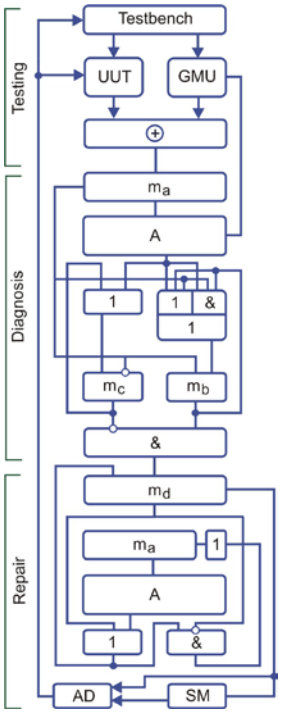

Fig. 5. Model for embedded testing HS-components

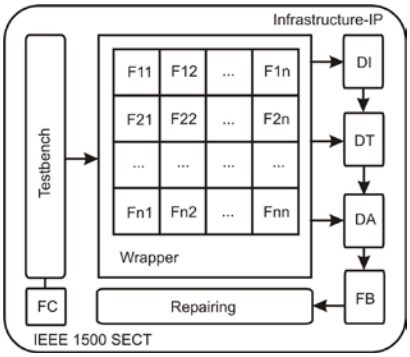

Fig. 6. Infrastructure for testing CS

Here (fig. 5) the blocks are shown: Testbench – tests for functional blocks, FC – functional test coverage, F – functional blocks, DI – diagnosis information in form of faulty blocks detection tables, DT – methods and tools for diagnosing, DA – results of diagnosis analysis, FB – faulty functional modules, Repairing – repair of functional modules. The boundary scan cell, shown in Fig. 7, performs service of a single functional cell.

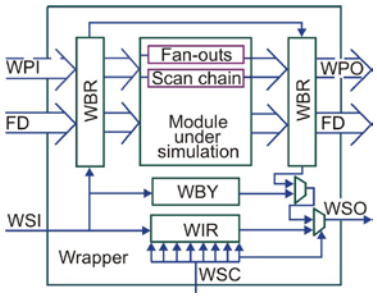

Fig. 7. Boundary scan cell

IV. CASE STUDY FOR DIAGNOSIS

To illustrate the performance of the proposed model and method the functionalities of three modules of the digital filter of Daubechies [11] are considered below.

As a second test case for the practical use of the proposed activation model and xor-method TAB-matrix analysis for searching faulty blocks is further proposed the synthesis of diagnosis matrix for the main graph filter, shown in Fig. 8.

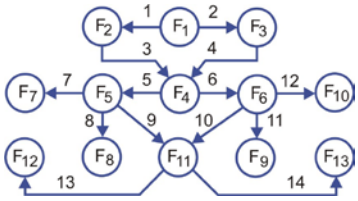

Figure 8. Transaction main-TL graph

The graph is associated with the following diagnosis TAB-matrix, which has 6 activated test segments and 8 assertions:

$M_{ij}(TL)$	B_1	B_2	B_3	B_4	B_5	B_6	B_7	B_8	B_9	B_{10}	B_{11}	B_{12}	B_{13}	B_{14}
$T_1 \to F_7$	1	.	1	.	1	.	1	.	.	.	.	.	.	.
$T_2 \to F_8$	.	1	.	1	1	.	.	1	.	.	.	.	.	.
$T_3 \to F_9$	1	.	1	.	.	1	.	.	.	.	1	.	.	.
$T_4 \to F_{10}$	.	1	.	1	.	1	.	.	.	.	.	1	.	.
$T_5 \to F_{12}$	1	.	1	.	1	.	.	.	1	.	.	.	1	.
$T_6 \to F_{13}$	.	1	.	1	.	1	.	.	.	1	.	.	.	1
$T_1 \to F_2$	1	.	.	.	.	.	.	.	.	.	.	.	.	.
$T_2 \to F_3$	.	1	.	.	.	.	.	.	.	.	.	.	.	.

The system of diagnosis functions for hardware implementation as a part of Infrastructure IP corresponding to the rows or monitors is followed:

$$F_7(T_1) = B_1^1 B_3^1 B_5^1 B_7^1;\ F_8(T_2) = B_2^1 B_4^1 B_5^1 B_8^1;$$

$$F_9(T_3) = B_{11}^1 B_6^1 B_1^1 B_3^1;\ F_{10}(T_4) = B_4^1 B_5^1 B_6^1 B_{12}^1;$$

$$F_{12}(T_5) = B_1^1 B_3^1 B_5^1 B_9^1 B_{13}^1;\ F_{13}(T_6) = B_2^1 B_4^1 B_6^1 B_{10}^1 B_{14}^1;$$

$$F_2(T_1) = B_1^1; F_3(T_2) = B_2^1.$$

Synthesis of the diagnosis matrix for one discrete cosine transform module from the Xilinx library in the form of functional coverage is shown in Listing 1.

Listing 1. Part of functional coverage

```
c0: coverpoint xin {
bins minus_big={[128:235]};
bins minus_sm={[236:255]};
bins plus_big={[21:127]};
bins plus_sm={[1:20]};
bins zero={0}; }
c1: coverpoint dct_2d
{ bins minus_big={[128:235]};
bins minus_sm={[236:255]};
bins plus_big={[21:127]};
bins plus_sm={[1:20]};
bins zero={0};
bins zero2=(0=>0);
}
endgroup
```

The rest 12 modules of the transaction graphs, activation TAB-matrices, and logic functions are developed for testing and fault detection in the discrete cosine transform too.

A fragment of monitor engine is presented by Listing 2.

Listing 2. Code fragment of monitor engine

```
sequence first( reg[7:0] a, reg[7:0]b);
 reg[7:0] d;
 (!RST,d=a)
##7 (b==d);
 endsequence
property f(a,b);
 @(posedge CLK)
 // disable iff(RST||$isunknown(a)) first(a,b);
!RST |=> first(a,b);
endproperty
odin:assert property (f(xin,xa7_in))
 // $display("Very good");
else $error("The end, xin =%b,xa7_in=%b", $past(xin,
7),xa7_in);
```

Testing of discrete cosine transformation in the environment Riviera, Aldec detects incorrectness in seven rows of HDL-models:

```
//add_sub1a <= xa7_reg + xa0_reg;//
```

Subsequent correcting code allowed obtaining the following code (Listing 3).

Listing 3. Corrected code fragment

```
add_sub1a <= ({xa7_reg[8],xa7_reg} + {xa0_reg[8],xa0_reg});
add_sub2a <= ({xa6_reg[8],xa6_reg} +{xa1_reg[8],xa1_reg});
add_sub3a <= ({xa5_reg[8],xa5_reg} +{xa2_reg[8],xa2_reg});
add_sub4a <= ({xa4_reg[8],xa4_reg} + {xa3_reg[8],xa3_reg});
end
else if (toggleA == 1'b0)
begin
add_sub1a <= ({xa7_reg[8],xa7_reg} - {xa0_reg[8],xa0_reg});
add_sub2a <= ({xa6_reg[8],xa6_reg} - {xa1_reg[8],xa1_reg});
add_sub3a <= ({xa5_reg[8],xa5_reg} - {xa2_reg[8],xa2_reg});
add_sub4a <= ({xa4_reg[8],xa4_reg} - {xa3_reg[8],xa3_reg});
```

Practical implementation of models and verification methods is integrated into the simulation environment Riviera of Aldec Inc., Fig. 9. New assertion and diagnosis modules, added into the system, improved the existing

verification process, which allowed 15% reduces the design time of digital product.

Actually, application of assertions makes possible to decrease the length of test-bench code and considerably reduce (x3) the design time (Fig. 10), which is the most expensive. Assertion engine allows increasing the diagnosis depth of functional failures in software blocks up to level 10-20 HDL-code statements.

Due to the interaction of simulation tools and assertion engine, automatically placed inside the HDL-code, an access of diagnosis tools to the values of all internal signals is appeared. This allows quickly identifying the location and type of the functional failure, as well as reducing the time of error detection in the evolution of product with top-down design. Application of assertion for 50 real-life designs (from 5 thousand up to 5 million gates) allowed obtaining hundreds of dedicated solutions, included in the verification template library VTL, which generalizes the most popular on the market EDA (Electronic Design Automation) temporal verification limitations for the broad class of digital products. Software implementation of the proposed system for analyzing assertions and diagnosing HDL-code is part of a multifunctional integrated environment Aldec Riviera for simulation and verification of HDL-models.

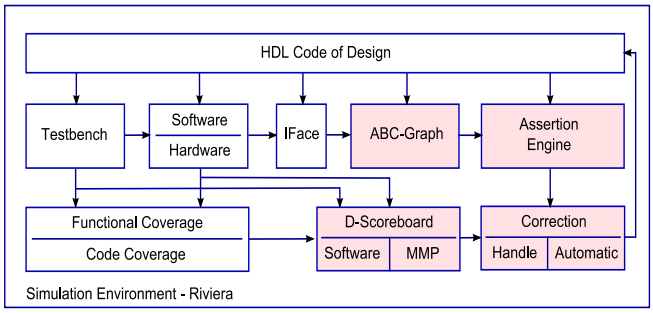

Figure 9. Implementation of results in the system Riviera

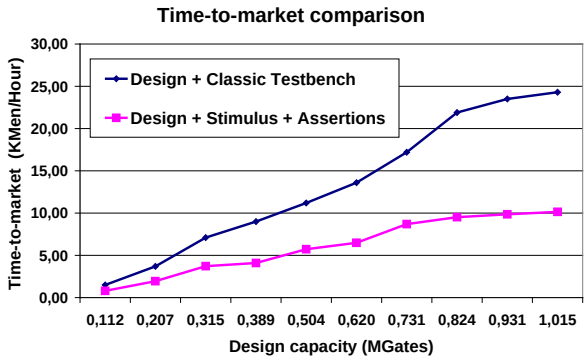

Figure 10. Comparative analysis of verification methods

High performance and technological combination of assertion analysis system and HDL-simulator of Aldec Company is largely achieved through integration with the internal simulator components, including HDL-language compilers. Processing the results of the assertion analysis system is provided by a set of visual tools of the Riviera environment to facilitate the diagnosis and removal of functional failures. The assertion analysis model can also be implemented in hardware with certain constraints on a subset of the supported language structures. Products Riviera including the components of assertion temporal verification, which allow improved the design quality for 3-5%, currently, occupies a leading position in the world IT market with the number of system installations of 5,000 a year in 200 companies and universities in more than 20 countries.

V. CONCLUSION

1. Infrastructure and technology for digital systems analysis are presented. Proposed transactional graph model and method for diagnosis of digital systems-on-chips are focused to considerably reducing the time of faulty blocks detection and memory for storing the diagnosis compact matrix describing ternary relations in format: the monitor-oriented test-segments which detect faulty functional components of the Hardware-Software system.

2. New diagnosis quality criterion as a function depending on the graph structure, test, and assertion monitors is proposed. For this purpose there are two alternative ways. It allows making good choices in diagnosability improving by increasing test segments set for recognition equivalent faulty blocks or adding assertion monitors on transit nodes of the activation HDL-code graph.

3. An improved TAB-engine or algorithm for functional failures detection in software or hardware is proposed. It is characterized by using the xor-operation, which makes possible to improve the diagnosis performance for single and multiple faulty blocks on the basis of parallel analysis of the TAB-matrix, boundary scan standard IEEE 1500, and vector's operations called and, or, xor.

4. A model for diagnosing the functionality of system-on-chip in the form of multi-tree and method for tree traversal, implemented in the engine for detecting faulty blocks with given depth, are developed. They considerably increase the performance of software and hardware Infrastructure IP.

5. Test verification of the diagnosis method is performed by three real case studies, presented by SoC components of a cosine transform filter, which showed the consistency of the results in order to minimize the time of faulty blocks detection and memory for storing diagnosis information, as well as increase the diagnosis depth of digital unit.

REFERENCES

[1] P.P.Parhomenko. Technical diagnosis basics. Moscow: Energy, 1976.

[2] P.P.Parhomenko, and E.S. Sogomonyan, "Technical diagnosis basics (Optimization of diagnosis algorithms, hardware tools)", Moscow: Energy, 1981.

[3] M.F. Bondarenko, O.A. Guz, V.I. Hahanov, and Yu.P. Shabanov-Kushnarenko, "Infrastructure for brain-like computing", Kharkov: Novoye Slovo, 2010.

[4] V.I. Hahanov, I.V. Hahanova, E.I. Litvinova, and O.A. Guz, "Design and Verification of digital systems on chips", Kharkov: Novoye Slovo, 2010.

[5] V.V. Semenets, I.V. Hahanova, and V.I. Hahanov, "Design of digital systems by using VHDL language", Kharkov: KHNURE, 2003.

[6] V.I. Hahanov, and I.V. Hahanova, "VHDL+Verilog = synthesis for minutes", Kharkov: KHNURE, 2006.

[7] IEEE Standard for Reduced-Pin and Enhanced-Functionality Test Access Port and Boundary-Scan Architecture IEEE Std 1149.7-2009.

[8] F. Da Silva, T. McLaurin, and T. Waayers, “The Core Test Wrapper Handbook. Rationale and Application of IEEE Std. 1500™”, Springer, 2006, XXIX.

[9] E.J. Marinissen, and Yervant Zorian, “Guest Editors' Introduction: The Status of IEEE Std 1500’, IEEE Design & Test of Computers, No26(1), pp.6-7, 2009.

[10] A. Benso, S. Di Carlo, P. Prinetto, and Y. Zorian, “IEEE Standard 1500 Compliance Verification for Embedded Cores”, IEEE Trans. VLSI Syst., No 16(4), pp. 397-407, 2008.

[11] V.Hahanov, E.Litvinova, S.Chumachenko, and O. Guz, “Logic associative computer”, Electronic simulation, No 1, pp.73-83, 2011.

[12] Ngene Christopher Umerah, Hahanov V. A diagnostic model for detecting functional violation in HDL-code of SoC // Proc. of IEEE East-West Design and Test Symposium.– Sevastopol, Ukraine.– 19-20 September, pp. 299-302, 2011.

[13] Ubar R., Kostin S., Raik J. Block-Level Fault Model-Free Debug and Diagnosis in Digital Systems. DSD '09. 12th Euromicro Conference 2009, pp. 229 – 232.

[14] Benabboud Y., Bosio A., Girard P., Pravossoudovitch S., Virazel A., Bouzaida L., Izaute I. “A case study on logic diagnosis for System-on-Chip”, Quality of Electronic Design, 2009, pp. 253,259.

[15] Datta K., Das P.P. Assertion based verification using HDVL. Proc. 17th International Conference VLSI Design. 2004, pp. 319 – 32.

Influence of Transport Properties on Energy Resolution of Planar TlBr and CdZnTe Gamma-Ray Detectors: Monte Carlo Investigation

Skrypnyk A.I., Khazhmuradov M.A.

Abstact **- The response of TlBr- and CdZnTe- detectors to gamma-rays was simulated by Monte Carlo method via Geant4 package. We studied the influence of transport parameters of electrons and holes on energy resolution of detectors. The modification of photopeaks with a changing the ratio of the electron and hole mobility-lifetime products was investigated. All results obtained for TlBr detectors were compared with the results for CdZnTe detectors. The efficiency for detecting gamma-quanta in the range of energies from 10 keV to 3 MeV by both kinds of detector was researched.**

I. Introduction

For many years, investigation of wide band-gap semiconductors (CdZnTe, TlBr, HgI_2 and other) is directed to the development of gamma-ray detectors working at room temperatures without additional cooling. However, some features of these semiconductor materials create problems in determining a detector's main operating characteristics. Considerable non-uniformity of electrophysical characteristics of single-crystals is one of the most important factors restraining progress in achieving this goal. The most unstable characteristics include specific resistance of detector and product of mobility μ and mean drift time τ for electrons and holes – $(\mu\tau)_{e,h}$ (transport parameters of charge carriers). Planar gamma-ray detectors based on wide band-gap semiconductors have considerable spread of $(\mu\tau)_{e,h}$ values even if they are produced from one ingot [1]. At the same bias voltage, U_b, the characteristics of such detectors with the same sizes such as sensitivity to the registered radiation δ and charge collection efficiency (*CCE*) will be different. Experiments conducted by Suzuki et al. [1] showed that, for example, in CdZnTe single-crystals, the ratio of charge transport parameters for electrons and holes within the same ingot may vary profoundly from 10 to 100. Furthermore, modification of the ingot's $(\mu\tau)_{e,h}$ product can be due to technological processing of the material during manufacturing into a detector, or may result from the accumulation of defects during growth or operation [2].

For a study of features of room-temperature semiconductor devices which are manufactured for detecting nuclear radiation and measuring the characteristics of the radiation fields Monte Carlo simulation can be used. A computer experiment helps to overcome the difficulties that are present as at the study of features of semiconductors as at the development of detectors based on them. In the present work, we studied the influence of the $(\mu\tau)_{e,h}$ products and $(\mu\tau)_e/(\mu\tau)_h$ ratio on the spectroscopic characteristics of CdZnTe and TlBr- detectors using Geant4 simulation package. The detailed Monte Carlo investigation allowed us to model the response function of planar spectrometers in the gamma-ray energy range to 3 MeV. The dynamics of response function of TlBr-detectors for gamma-ray energies of 122 keV, 136 keV (^{57}Co source) and 661.7 keV (^{137}Cs source) was explored and compared with the dynamics of response function of CdZnTe detectors for the same gamma-ray energies. We presented how change of $(\mu\tau)_e/(\mu\tau)_h$ ratio at constant value of $(\mu\tau)_e$ influences on the high and width of all simulated photopeaks. It was determined and investigated the theoretical energy resolutions of TlBr and CdZnTe detectors.

II. Description of the Model

We simulated the passage of gamma-quanta through the detector by Monte Carlo method via the user program code described detail in [3], embedded in Geant4 package – universal toolkit for the simulating the passage of charged particles, neutrons and gamma-quanta through matter. The simulation procedure is divided into 2 parts. Initially, the program calculates the value of the ionization energy, E_i, transferred to the detector by the absorbed gamma-quantum with the initial energy of E_γ. Then we calculate the value of charge induced on the detector's contacts for every interacted photon. The computer model of the detector is approximated as much as possible to a real spectrometric device. It takes into account the statistical effects of pair generation within the detector's volume and the modification in the amplitude of the output pulse under the influence of the electronic noise and charge-carrier capture [3].

Manuscript received November 12, 2013.

Skrypnyk A.I. is with the National Science Center Kharkov Institute of Physics and Technics. Address: Ukraine, 61108, Kharkov, Academicheskaya Str., 1, tel. (057)335-65-94 (e-mail: belkas@kipt.kharkov.ua).

Khazhmuradov M.A. is with the National Science Center Kharkov Institute of Physics and Technics. Address: Ukraine, 61108, Kharkov, Academicheskaya Str., 1, tel. (057)335-65-94 (e-mail: khazhm@kipt.kharkov.ua)

To verify the described model we applied experimental data from 6×6×3 mm^3 planar $Cd_{0.9}Zn_{0.1}Te$ detectors, equipped with ohmic contacts. The bias voltage, U_b, was 300 V. The electron mobility-lifetime product $(\mu\tau)_e$ was selected as 3×10^{-3} cm^2/V. We specified the total level of noise in the CdZnTe spectrometry systems (Equivalent Noise Charge – *ENC*) at about 300 e^- (electron charge units). The detector's dark current was taken as 3 nA. CdZnTe detector was irradiated by ^{137}Cs. Fig. 1 presents calculated and experimental response functions of CdZnTe detectors from ^{137}Cs source. Overall, it is evident that used model is in good agreement with the experimental measurements.

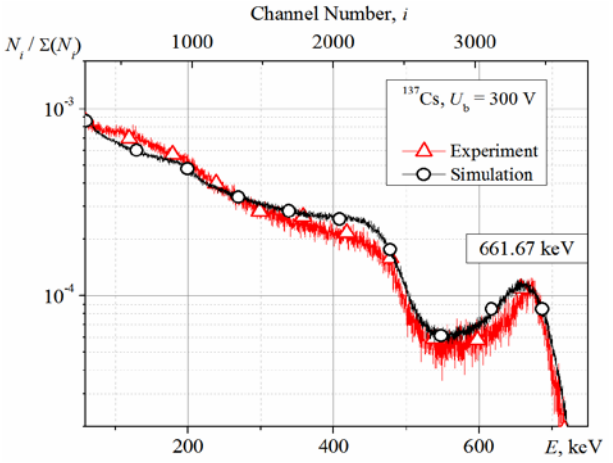

Fig. 1. 661.67-keV photopeak ^{137}Cs spectrum

III. Analysis of Efficiency of Charge Collection

One of the main problems of wide band-gap semiconductor detectors results from considerable spread of $(\mu\tau)$ values for electron and holes. Transport parameters for electrons and holes directly influence on charge collection efficiency. The change in the charge collection efficiency, by turn, leads to distortions to the pulse height spectrum.

Therefore, to interpret correctly the investigated spectra it is necessary to analyze *CCE*. We will consider uniformity of distribution of electric field within detector. In this case, the efficiency of charge collection in the planar detector irradiated by gamma-quanta from the negative contact is described by Hecht model [4]:

$$\eta(z,\mu_e,\tau_e,\mu_h,\tau_h,d,U)=\frac{Q_{ind}}{Q_{gen}}= \\ =\frac{(\mu\tau)_e U_b}{d^2}\left(1-\exp\left(-\frac{(d-z)d}{(\mu\tau)_e U_b}\right)\right)+ \\ +\frac{(\mu\tau)_h U_b}{d^2}\left(1-\exp\left(-\frac{zd}{(\mu\tau)_h U_b}\right)\right) \quad (1)$$

Here, η is the charge-collection efficiency; Q_{ind} is the charge induced on the detector contacts; Q_{gen} is the average charge created at absorption energy E_i, $Q_{gen} = E_i/\varepsilon$; d is the detector's thickness; and z is the depth of the gamma-quantum interaction within the detector's material ($0 < z < d$).

In the following, we suppose that the values of $(\mu\tau)_e$, U_b, and d are constant. We use the notations $\lambda_e = \frac{(\mu\tau)_e U_b}{d}$ corresponding to the electron's mean-free-path which is assumed constant in this analysis, and $\kappa = \frac{(\mu\tau)_h}{(\mu\tau)_e}$, $0 < \kappa < \infty$. Then, equation (1) can be rewritten in the equivalent form [3]:

$$\eta(\kappa,z)=\frac{\lambda_e}{d}\left(1-\exp\left(-\frac{d-z}{\lambda_e}\right)\right)+ \\ +\frac{\kappa\lambda_e}{d}\left(1-\exp\left(-\frac{z}{\kappa\lambda_e}\right)\right) \quad (2)$$

The first derivative of equation (2) $\left.\frac{d\eta(\kappa,z)}{d\kappa}\right|_{z=\text{const}}$ is equal to

$$\left.\frac{d\eta(\kappa,z)}{d\kappa}\right|_{z=const}=\frac{\lambda_e}{d}-\left(\frac{\lambda_e}{d}+\frac{z}{\kappa d}\right)\exp\left(-\frac{z}{\kappa\lambda_e}\right). \quad (3)$$

The first derivative (3) is positive in the whole range, $\frac{z}{\kappa\lambda_e} > 0$, so that the efficiency of charge collection is a monotonically increasing function of the ratio κ and respectively, $(\mu\tau)_h$. It is correct for all z in the range from 0 to d.

In the following section, we check this statement for TlBr and CdZnTe detectors.

IV. Influence of Transport Parameters of TlBr- and CdZnTe- Detector on its Spectroscopic Characteristics

In the present work, we simulated 2.7×2.7×2 mm^3 planar TlBr detectors equipped with ohmic contacts. Given thickness of the TlBr crystal was selected as typical for detectors based on this material. Moreover, TlBr detector with such thickness gives higher efficiency for detecting gamma-quanta with 122-keV and 136-keV energies from ^{57}Co (≈97% and ≈93%, respectively) compared with lower thickness detector (Fig. 2).

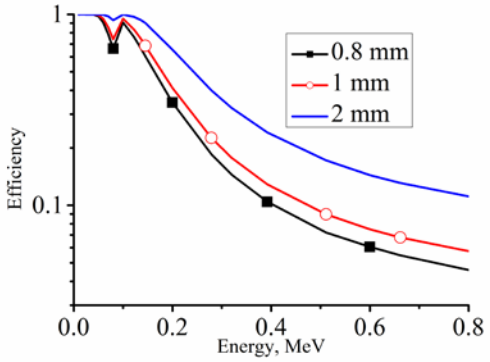

Fig. 2. Efficiency of gamma-ray TlBr-detectors with different thicknesses

In the range of energies of gamma-quanta less than 1 MeV, the gamma ray detector efficiency of 2-mm TlBr detector slightly exceeds this efficiency of 3-mm CdZnTe detector (Fig. 3). Therefore, as evident from Fig. 3, efficiency of detection of 661.7-keV gamma-quanta from ^{137}Cs radioactive source does not exceed 15% for both materials with above mentioned thicknesses.

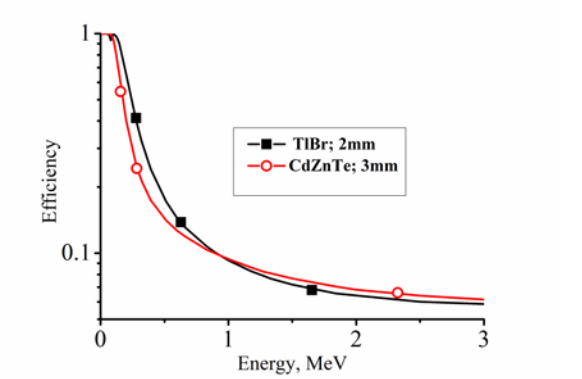

Fig. 3. Comparison of gamma ray detector efficiency for TlBr- and CdZnTe- detectors

Fig. 4 shows the transformation of ^{57}Co spectrum obtained by simulation of TlBr detector with decreasing κ value. The bias voltage, U_b, was 400 V. We specified the total level of noise in the TlBr spectrometry systems at about 400 e^-. It was assumed that the detector's dark current was 3 nA. We considered the material with values of the electron and hole mobility of 30 cm^2/(V·s) and 4 cm^2/(V·s), respectively, which reflect the measured μτ products for electrons and holes.

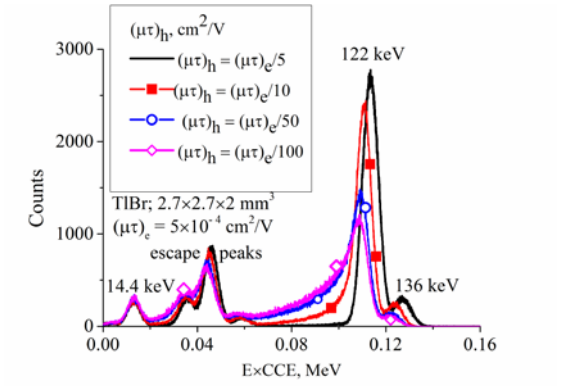

Fig. 4. Transformation of ^{57}Co spectrum obtained by TlBr-detector with decreasing κ value

The electron mobility-lifetime was fixed at 5×10^{-4} cm^2/V. The mobility-lifetime values for holes were varied from 1×10^{-4} [5] to 5×10^{-6} cm^2/V. From Fig. 4, we observe a little shift of the centroids of 122-keV and 136-keV photopeaks in the direction of lower energy with decreasing a value of κ i.e. with decreasing a value of $(\mu\tau)_h$ at const $(\mu\tau)_e$. Moreover, the theoretical energy resolution of the studied TlBr detector for gamma-quantum energy at 122 keV declines from 5.7% to 7.6% with increasing 1/κ value from 5 to 100. 136-keV photopeak tends to full degeneration. 14.4-keV photopeak corresponded to third principal gamma-ray line of ^{57}Co almost does not change.

Spectrum of gamma-quanta from ^{57}Co source obtained by simulation of TlBr-detector was compared with such spectrum received by simulation of CdZnTe detector [3].

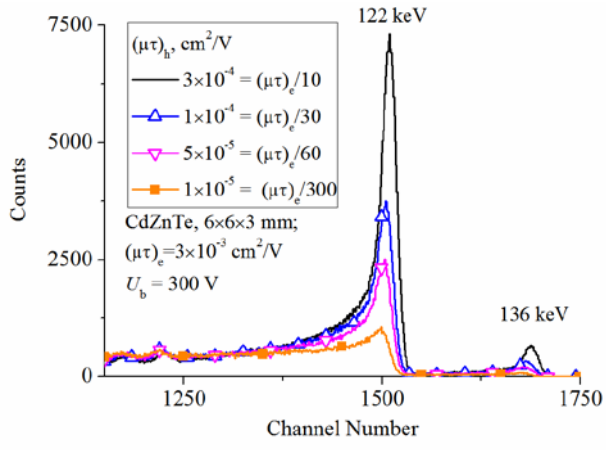

Fig. 5. Transformation of ^{57}Co spectrum obtained by CdZnTe detector with decreasing κ value

From Fig. 4 and 5, it is evident that these spectra of gamma-quanta obtained by both detectors have similar tendency to decreasing and broadening of 122-keV and 136-keV photopeaks and similar shape in this range of energies with decreasing a value of hole mobility-lifetime product. The theoretical energy resolution of CdZnTe detector for gamma-quantum energy at 122 keV drops from 1.8% to 2.3% when the value of 1/κ changes from 10 to 60. The spectrum obtained by CdZnTe also has almost constant 14.4-keV photopeak (it is not shown in Fig. 5). It agrees with the experimental data of Sato et al. [Fig. 6, Ref. 6]. This reflects the fact that the depth of absorption of the main part of the gamma-quanta with 14.4-keV energy in both TlBr- and CdZnTe- materials is near to a hole-drift-length even at the worst $(\mu\tau)_h$ values.

However, irradiation of investigated TlBr detector by gamma-quanta from ^{57}Co source gives high enough peaks in the spectrum in the range between about 30-50 keV in contrast with CdZnTe detector. The centroids of these photopeaks also are shifted in the direction of lower energy with decreasing a value of κ. We suppose that they are escape peaks corresponding to gamma-radiation from *K*-shells of Tl. Our simulation results agree with results of real experiment for TlB-detectors [5].

Consequently, it is evident that for gamma-quantum energies less than 150 keV, planar CdZnTe detectors of 3 mm thickness retain satisfactory spectrometric properties in the ratio range $(\mu\tau)_e/(\mu\tau)_h$ below 30. Energy resolution of the investigated TlBr detectors of 2 mm thickness approximately in two times worse compared with CdZnTe detectors in this range of gamma-quanta energies. It agrees with experimental data for TlBr detectors which are obtained to the present time.

Fig. 6 presents the simulated spectrum of gamma-quanta from ^{137}Cs source obtained for investigated TlBr-detector.

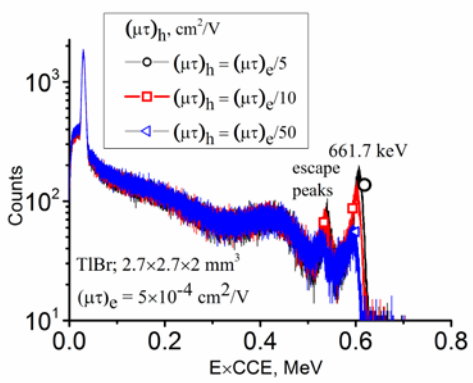

Fig. 6. Transformation of ^{137}Cs spectrum obtained by TlBr detector with decreasing κ value

In this case of investigation, because of low efficiency for detecting the gamma-quantum energy at 661.7 keV we needed to increase the number of simulated gamma-quantum trajectories of ^{137}Cs source compared with ^{57}Co to 10^8 to collect statistics. The theoretical energy resolution of the investigated TlBr-detector at a gamma-ray energy of 661.7 keV drops from 2.6% to 4.8%, when the value of 1/κ changes from 5 to 20.

From Fig. 7 we observe faster degeneration of 661.7-keV photopeak in TlBr compared with 122-keV photopeak. These results agree with results of simulation of CdZnTe detector irradiated by ^{137}Cs source. Fig. 7 shows the changes that occur around the 661.7-keV photopeak with the simulated spectrum of the ^{137}Cs source for a CdZnTe detector [3]. The value of 1/κ = 20 can be considered as the threshold level. The theoretical energy resolution of the investigated CdZnTe detector at 661.7 keV declines from 1.1% to 1.5% in the range of 1/κ values from 10 to 20. The planar CdZnTe detectors with higher value of 1/κ are unsuitable for the spectrometry of high-energy gamma-quanta, because even low accumulation of radiation traps can lead to the disappearance of the photopeak.

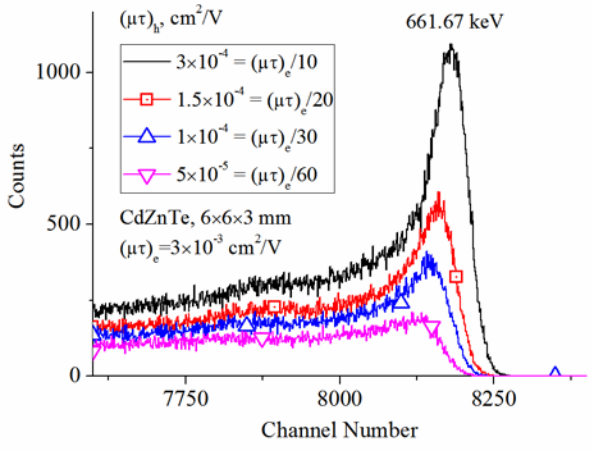

Fig. 7. Transformation of ^{137}Cs spectrum obtained by CdZnTe detector with decreasing κ value

The faster degeneration of the 661.7-keV photopeak in CdZnTe detectors compared with the 122-keV photopeak is connected with the fact that in the simulated detector the interaction of 122-keV gamma-quanta within the detector material mainly occurs in the first one-third of its thickness. Gammas with energy of 661.7 keV uniformly interact with detector throughout its entire thickness. The efficiency of charge collection, Eq. (1), depends on interaction depth. Therefore, decreasing the hole-drift-length relative to the electron-free path more strongly reduces η(κ, *z*) and the pulse amplitude at greater depths. The full absorption cross-section of CdZnTe is small in the energy region E_γ above 100 keV. Therefore, this small total pulse-number from the full absorption of 661.7-keV gamma-quantum is spread therewith over a wider range of amplitudes.

It was determined that planar CdZnTe detectors theoretically can ensure an energy resolution of better than 2% at 661.7 keV provided that the value of 1/κ is less than 20. In the range 1/κ from 20 to 60, the detector's resolution quickly deteriorates to 10-12% after the complete disappearance of the 661.7-keV photopeak.

From simulation of TlBr detectors, we concluded that in the range 1/κ less than 10 we may receive energy resolution better than 3%. At a value of 1/κ more than 45 the 661.7-keV photopeak cannot be observed by TlBr-detector.

V. Conclusion

Basing on the mentioned model, response of semiconductor TlBr-detectors to gamma-quanta from ^{57}Co and ^{137}Cs sources was simulated and then was compared with response of CdZnTe-detectors to gamma-quanta from the same sources. The detection efficiency of both materials was investigated. We conclude that TlBr- and CdZnTe- detectors have the same detection efficiency in the range of energies to 60 keV. At gamma-ray energies of 122 keV and 136 KeV (from ^{57}Co source) TlBr detector has higher detection efficiency compared with CdZnTe detector. For 661.7-keV energy for both investigated detectors the given value does not exceed 15%.

We determined that investigated detectors have similar tendency to broadening of 122-keV, 136-keV and 661.7-keV photopeaks and deterioration of energy resolution with decreasing a value of $(\mu\tau)_h$ at a constant value of $(\mu\tau)_e$. It is concluded that the spectroscopic properties of the both kinds of detector are maintained when the range of the $(\mu\tau)_e/(\mu\tau)_h$ ratio is below 20. For CdZnTe if the $(\mu\tau)_e/(\mu\tau)_h$ ratio is above 60, then the 661.7-keV photopeak cannot be observed for planar detectors, even with very low levels of electronic noise. In the case of TlBr-detectors, complete degeneration of 661.7-keV photopeak is observed at a little less $(\mu\tau)_e/(\mu\tau)_h$ ratio. These criteria establish quality-growth requirements for spectrometric TlBr and CdZnTe materials.

REFERENCES

[1] *Suzuki M., Tashiro M., Sato G., Watanabe S., Nakazawa K., Takahashi T., Okada Y., Takahashi H., Parsons A., Barthelmy S., Cummings J., Gehrels N., Hullinger D., Krimm H., Tueller J.* Hard X-Ray Response of CdZnTe Detectors in the Swift Burst Alert Telescope // IEEE Trans. Nucl. Sci. 52. 2005. P. 1033-1035.

[2] *Cavallini A., Fraboni B., Dusi W., Auricchio N., Chirco P., Zanarini M., Siffert P., Fougeres P.* Radiation effects on II–VI compound-based detectors // Nucl. Instr. and Meth. A 476. 2002. P. 770-778.

[3] *Zakharchenko A., Rybka A., Kutny V., Skrypnyk A., Khazhmuradov M., Fochuk P., Bolotnikov A., James R.* Transport properties and spectrometric performances of CdZnTe gamma-ray detectors // Proc. of SPIE. 2012. V. 8507, P. 85071I-1–7.

[4] *Akutagawa W., Zanio K.* Gamma response of semi-insulating material in the presence of trapping and detrapping // J. Appl. Phys. 40. 1969. P. 3838-3854.

[5] *Shorohov M., Kouznetsov M., Lisitskiy I., Ivanov V., Gostilo V. and Owens A., Member, IEEE.* Recent Results in TlBr Detector Crystals Performance // IEEE Transactions on Nuclear Science. 2009. Vol. 56, No 4, P. 1855-1858.

[6] *Sato G., Parsons A., Hullinger D., Suzuki M., Takahashi T. et al.* Development of a spectral model based on charge transport for the Swift/BAT 32K CdZnTe detector array // Nucl. Instr. and Meth. A 541. 2005. P. 372-384.

Computer System User's Competency Influence on Reliability Factor

G. Krivoulya, A. Shkil, D. Kucherenko, I. Filippenko, Y. Syrevitch
Kharkov National University of Radioelectronics, Kharkov, Ukraine

***Abstract* – Integral reliability characteristics of the monoergative computer system, one of the basic components of which is a human-operator, are examined. Mathematical models and analytical dependences of the restorable system dependability on the numeral values of the user's competency are received. These dependences allow to define necessary expense on the improvement of the operator's learning level, depending on the state of his current competence as an user of the technical system.**

***Index Terms* – competency, operator, reliability factor, repairable system.**

I. INTRODUCTION

The appearance of the complex organic ergative systems (ES) is associated with the rapid development of the computer information technology and the necessity for operators' work with a control interface of the modern technical complexes, such as objects in the space and aviation engineering, power plants, process control systems, networks, internet, etc. ES found application in those objects where the intervention of an operator in the object operation is currently the requirement for error-free performance of these objects.

In most cases, ES is a complex computer-aided control system (CCS), a major component of which is a human-operator or group of operators, and depending on the number of operating staff the monoergative (one operator) and poliergative (several people) system are distinguished. By the operators hierarchy ES can be the first, second and higher order. For example, the second-order system has two levels of control, on the first of which an operator works with a technical device and on the second – the operator in addition to the work with a technical device to provide guidance of the first operator [1]. The research related to the development and improvement of the ES can be described by three stages. At the first stage, the goal of the ES improvement was a human adaptation to the technical device, at the second stage – the technical device to a human: his psychological, physiological, anthropometric and other characteristics. The third stage is characterized by a human factors analysis together with the characteristics of the technical object as a total integral character of the ES. But it isn't a man is considered as an average link included to the technical system, but a technical device – as a tool included to the activity of a human-operator. That human generates and implements the goals of the ES operation by technical devices [2].

The mandatory components of the ES besides operating staff involved in control are computer hardware and software tools. The effectiveness of the ES operation considerably depends on the reliability (availability) of all three components. Subject to this the important task is to ensure their trouble-free operation during the operation. This task has three main components – the ES reliability, the availability to the system application and the qualitative characteristics of the service, in particular, the level of the diagnosability provision. These three components assume the diagnosis and elimination of the possible system problems, generated by faults and failures.

II. PROBLEM DEFINITION

The reliability of the technical computer environment has been researched quite extensively and deeply. The reliability of the complex software systems is studied less and the reliability properties of the ES operators, the evaluation of their performance is currently research not well.

A human-operator is the basic link of the modern ES, statistics show that 20-30% of the accidents and disasters, directly or indirectly, related to the human error. Consequently, the overall assessment of the technical systems reliability and their integral characteristics must necessarily include the analysis of the human factor. In this connection, the development of the ES integral characteristics evaluation procedure, taking into account the properties of all three components – the operating staff, hardware and software – is actual task. In the capacity of the basic integral ES characteristics the reliability factor of the restorable technical system taking into account the readiness of the operator based on his competence is proposed to use.

Manuscript received December 07, 2013.

G. Krivoulya is professor of computer aided design department, KhNURE, Kharkov, Ukraine, e-mail: krivoulya@i.ua.

A. Shkil is assistant professor of computer aided design department, KhNURE, Kharkov, Ukraine, e-mail: shkil@opentest.com.ua.

Y. Syrevitch ia assistant professor of electronic computers department, KhNURE, Kharkov, e-mail: syr_jane@mail.ru.

I. Filippenko is assistant professor of computer aided design department, KhNURE, Kharkov Ukraine, e-maill: kiu@kture.kharkov.ua.

D. Kucherenko is postgraduate student of computer aided design department, KhNURE, Kharkov, Ukraine, e-mail: d_zin@ukr.net.

III. ES RELIABILITY SUBJECT TO THE HUMAN-OPERATOR ACTIVITY

Systematic approach of the ES reliability assessment provides the assessment of a human as one of the main components of the system. In the general case, this reliability is defined as the need of the successfully accomplish of the task on given stage of the system operation within a specified period of time under certain requirements to the activity time.

The ES reliability assessment is based on the following assumptions:

- both hardware failures and operator errors are rare, random and independent events;
- an appearance of more than one single-type event during the time of the system operation is almost impossible;
- the ability of the operator to errors compensation and to the error-free operation – are independent properties of the operator.

Error (failure) of the human-operator is defined as the non-execution of the task (or perform forbidden acts) which can lead to violation of the scheduled operations.

The operator error can be divided into three groups:

- the goal of the problem solving can't be achieved due to the erroneous actions of an operator;
- the operator seeks to achieve the erroneous goal;
- the operator is inactive at the moment when his participation is necessary.

The criteria of the performance and reliability are used for evaluation of an operator activity [3].

The performance criterion is problem time, i.e. the time from the moment of an operator reaction on the signal to the moment of the stimulus end: $T_{on} = a + bH = a + H / V_{on}$, where a – a hidden reaction time, i.e. period of the time from the signal appearance to the operator's response on it (0,2 ... 0,5 sec); b – the time of the one information unit processing (0,15–0,35 min); H – the amount of processed information; V_{on} (2 … 4 units/sec), or bandwidth, which characterizes the time during which the operator grasps the meaning of the information.

The reliability of the operator is characterized by his faultlessness, availability, accuracy, recoverability and timeliness. For each of these indicators the analytical dependences can be developed.

Let's consider the case when the compensation of the operator error and hardware failure is impossible [2]. If hardware failure and human error – are independent events, the probability of the failure-free operation is: $P(t_0, t) = Pt(t_0, t)P_0(t)$, where $Pt(t_0, t)$ – the probability of the no-failure operation of the hardware over a period t_0, $t_0 + t$; $P_0(t)$ – the probability of the error-free operator operation over a period t, subject to the hardware trouble-free operation, t_0 – the total time of the system operation, t – the current period of the system operation.

The ES with noncompensible operator errors and hardware failures is occurring in practice relatively rare. The reliability of such systems can be enhanced by the operators' redundancy with periodic diagnosis of their activities results.

The technical systems with failures recovery and operator errors compensation are widespread. The operators can fix (compensate) the part of the admitted errors in proper time. The errors compensation is an important alternate way of the ES reliability improving. Bringing into the technical system the attachments facilitated the error correction, increases the ES reliability significantly.

The system with errors and failures compensation will work without failures during the time t_0, $t_0 + t$ under the following conditions:

1) the technical system didn't fail and the operator didn't make a mistake;
2) the technical system didn't fail and the operator made a mistake, but fixed (compensated) it;
3) the operator didn't make a mistake, the technical system failed, but through the operator intervention a system performed its functions;
4) the operator made a mistake, but fixed (compensated) it, the technical system failed but, trough the operator intervention, system and operator performed their functions.

IV. THE RELIABILITY FACTOR OF THE REPAIRABLE SYSTEM

For an approximate reliability indexed calculation of the repairable ES let's accept the following assumptions. We consider the set of flows occurring in the system in case of the separate elements failure. The analysis of all the situations that lead to the system failure as a whole is conducted. As a result, the intensity of the events' flow of this type and the length of the failed state by each of the reasons is computed. Then the procedure of the flows superposition of those situations, each of which leads to the system failure or flows' depression for those situations that lead to the system failure during simultaneous implementation is consistently applied.

As a result, we obtain the resulting flow with two summary characteristics: average uptime and average recovery time.

Subject to the reliability of the systems uptime, as a rule, will be exponentially distributed, so these two parameters are sufficient for the evaluation of any other reliability indexes [2].

The process of the repairable object operation can be represented as a sequence of alternating periods of availability and recovery (standing idle) (fig. 1).

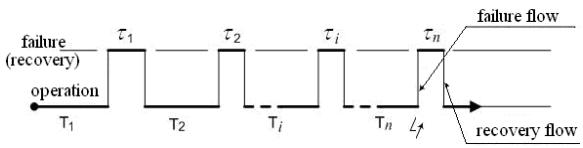

Fig. 1. The repairable object operation, $T_1 \dots T_n$ – the periods of the availability; $\tau_1 \dots \tau_n$ – the periods of the recovery

The reliability factor – is the probability that an object will be in working order at any time, except for the scheduled periods during which intended application of the object isn't provided. This index assesses at the same time the properties of the availability and maintainability of the object.

For restorable object on conditions that there is a simple flow of failures and recoveries the reliability factor equal

$$K = \frac{T}{T+\tau} = \frac{\mu}{\lambda+\mu} = \frac{1}{1+\frac{\lambda}{\mu}} = \frac{1}{1+\frac{\tau}{T}} = \frac{1}{1+\gamma}, \qquad (1)$$

where $\mu = \frac{1}{\tau}$, $\lambda = \frac{1}{T}$ and $\gamma = \frac{\lambda}{\mu} = \frac{\tau}{T}$ – recoverability index.

From the expression (1) it follows that the reliability factor of the object can be increased by increasing of the mean time between failures and reducing of the average time of recovery. On the other hand the reliability factor depends not on the absolute values of the variables T and τ, but of their relations, i.e. on value γ.

Note that for the high-reliability systems $T >> \tau$ or $\gamma =<< 1$.

For high-reliability CCS $0{,}9 < K_R < 0{,}999$, i.e. $0{,}9 < \frac{1}{1+\gamma} < 0{,}999$.

In other words

$$0{,}9(1+\gamma) < 1 < 0{,}999(1+\gamma),$$
$$0{,}9 + 0{,}9\gamma < 1 < 0{,}999 + 0{,}999\gamma.$$

Solving the inequality, we obtain: $0{,}001 < \gamma < 0{,}111$.

For the practical calculations an approximate K calculations is used. For this let's perform the following transformation:

$$K = \frac{1+\gamma-\gamma}{1+\gamma} = 1 - \frac{\gamma}{1+\gamma}.$$

We assume that $\frac{\gamma}{1+\gamma} \approx \gamma$, so the conversion error will be:

$$\Delta = \left| \frac{\gamma}{1+\gamma} - \gamma \right| = \left| \frac{\gamma - \gamma - \gamma^2}{1+\gamma} \right| = \frac{\gamma^2}{1+\gamma},$$

as $\gamma << 1$, $\Delta \approx \gamma^2$.

Thereby, for computing $K \approx 1 - \gamma$.

Together with the rise of the period under review an average reliability factor seeks to the reliability factor as to the limiting value, which with the increase of the interval time, i.e. $K(t) = \lim_{t\to\infty} K(t)$, where $K(t)$ – the probability that at time t the product is up (in certain initial conditions at $t = 0$), i.e. $K(t) = \frac{1}{T+\tau}\int_0^\infty P(t)dt$, $K(t)$ – the probability of the failure-free operation. For an exponential distribution T and τ the dependency diagrams of the basic values $K_R(t) = K_R + ke^{-(\lambda+\mu)t}$ and the time for the corresponding values γ are showed on figure 2.

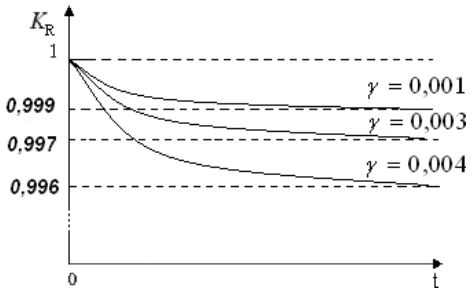

Fig. 2. Dependency diagrams K_R

V. THE RELATIONSHIP OF THE RELIABILITY FACTOR AND USER COMPETENCY

The high-reliability CCS is a set of the technical tools, dataware and software (SW), as well as operating staff that combined to perform control functions. It is assumed that failing of any three components leads to the system failing, which have to operate continuously over a preset time [3].

To simplify further discussion let's introduce the following restrictions, which, in toto, don't affect the calculation nature of the reliability factor:

– mean-time-between-failures T and recovery time τ are random variables that obey an exponential distribution;

– CSS technical parameters which determine the value T and τ, don't change over time;

– T and τ correlation doesn't change over time (stationary process);

– staff qualification (training) affects the changes of the T and τ as well.

The evaluation model of the human-operator activity in the capacity of the CCS component was proposed in [4]. The availability conservation property of the operator under appropriate functional activities on the assumption of training is represented by double exponential model:

$$P_3(t,\tau) = e^{-\lambda t_3 e^{-\nu\tau}}, \qquad (2)$$

where t_3 – the operator's time which required to perform task in the information system; λ – the error intensity during work performance, τ – learning time, ν – the error intensity during learning time.

A consequence of (2) is a formula of the conditional intensity of the operator failure (error) on the assumption of pretraining:

$$\Lambda(t) = P(t)\lambda(t), \qquad (3)$$

where $P(t)$ – the conditional probability of the successful CCS operator activity under availability resource consumption which accumulated during training period,

$\lambda(t)$ – unconditional failure (errors) intensity of the operator. From (3) follows that the conditional failure intensity $\Lambda(t)$ comes to the minimization of the unconditional failure (errors) intensity $\lambda(t)$ in P time. As applied to systems with recovery, where $\lambda = \frac{1}{T}$, it can be assumed that the mean time to failure T_y increases in P_1 time, i.e. $T_y = T \cdot P_1$ (actually, conditional mean time to failure decreases as $0 \le P_1 \le 1$). Applying the similar reasoning to the restorations intensity $\mu = \frac{1}{\tau}$, we can assume that the recovery time τ will decrease in P_2 time, i.e. $\tau_y = \frac{\tau}{P_2}$ (actually, the recovery time will increase, as by-turn $0 \le P_2 \le 1$). On the assumption that the operator learning affect the T and τ as well, let's assume that the conditional probability for them will be identical, i.e. $P_1 = P_2 = P$. For the operating CCS staff let's define the conditional reliability factor: $K_y = \frac{T_y}{T_y + \tau_y}$, that can also be referred as K_P (operating personnel).

Taking into account $T_y = T \cdot P$ and $\tau_y = \frac{\tau}{P}$, we obtain:

$$K_p = \frac{T \cdot P}{T \cdot P + \frac{\tau}{P}} = \frac{T \cdot P}{\frac{T \cdot P^2 + \tau}{P}} = \frac{T \cdot P^2}{T \cdot P^2 + \tau} = \frac{P^2}{P^2 + \frac{\tau}{P}} = \frac{P^2}{P^2 + \gamma} = \frac{1}{1 + \frac{\gamma}{P^2}}. \quad (4)$$

If we accept that $\gamma = 0{,}01$, we will get $K_p = \frac{P^2}{P^2 + 0{,}01} = \frac{1}{1 + \frac{0{,}01}{P^2}}$.

The dependency diagram of the conditional reliability factor K_P on the conditional probability in the range from 0 to 1 when $\gamma = 0{,}01$ is showed on figure 3.

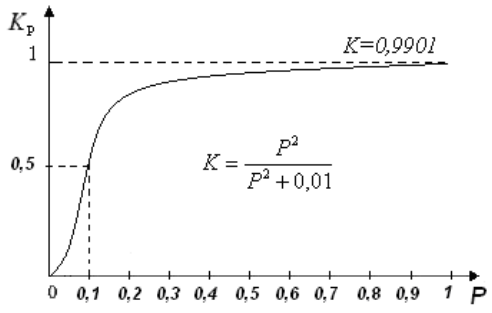

Fig.3. The dependency diagram K_P

For approximate determination of the K_P let's define tolerance range for P:

$$K = 1 - \gamma = 1 - \frac{\tau}{T} = 1 - \frac{\frac{\tau}{P}}{T \cdot P} = 1 - \frac{\tau}{T \cdot P^2} = 1 - \frac{\gamma}{P^2}. \quad (5)$$

On the basis of $K = 1 - \frac{\gamma}{P^2} > 0$, we obtain $\frac{\gamma}{P^2} < 1$ or $P^2 > \gamma$, i.e.

$$P > \sqrt{\gamma}. \quad (6)$$

The dependence P on K_P will be: $\gamma = (1 - K) \cdot P^2$; $P^2 = \frac{\gamma}{1 - K}$; $P = \sqrt{\frac{\gamma}{1 - K}}$, which makes it possible to calculate the increment ΔP depending on ΔK:

$$P + \Delta P = \sqrt{\frac{\gamma}{1 - (K + \Delta K)}}$$

$$\Delta P = \sqrt{\frac{\gamma}{1 - (K + \Delta K)}} - P. \quad (7)$$

VI. THE MODEL OF THE OPERATOR LEARNING

Operator learning C let's define as the frequency of the correct task performance of the operating activities (learning outcome). At the same time $(C - 1)$ – the frequency of the incorrect task performance.

Then $C = \frac{R}{N}$, where R – the number of correct actions of the operator in unit time, N – the total number of operations per unit time.

In terms of (2) and (3) the probability of failure-free operation is $P(t) = e^{-\nu}$, where ν – the operator error intensity during learning time t. If we abstract from the random nature of the human error during the training period and from the learning time t, and consider only the training outcome C, then the operator error intensity during learning time can be replaced by the number of errors during learning time $(C - 1)$:

$$P = e^{-(1-C)} = e^{(C-1)}. \quad (8)$$

For the transition from the conditional probability P to learning C let's find the logarithm:

$$\ln P = C - 1; \quad C = \ln P + 1.$$

Let's define the tolerance range for P on the basis of $0 \le C \le 1$:

$$0 \le \ln P + 1 \le 1, -1 \le \ln P \le 0,$$

$$e^{-1} \le P \le e^{0}, 0.368 \le P \le 1. \quad \textbf{(9)}$$

Thus, then $\gamma = 0.01$ the turndown K_P will be $0{,}932 \le K_P \le 0{,}9901$.

Based on a comparison of (6) and (9), we can conclude that to compute the conditional reliability factor of the personnel K_P it's more than enough to use only approximate formula (5).

Let's consider the extreme case. With the highest level of learning $C = 1$, $P = e^{0} = 1$ as well as K_P is equal to the maximum value of the unconditional reliability factor, which corresponds to the objective nature of the learning process.

With minimal learning level $C = 0$, $P = e^{0-1} = e^{-1} = 0.37$, as well $K_P = 0.932$. This value of the minimum K_P due to the fact that the two-level exponential model takes into account other factors except the personnel learning, for example, learning time, ways of the personnel restorative function and others.

The dependency diagram of the conditional reliability factor K_P on the personnel learning level C with $\gamma = 0.01$ is showed on figure 4.

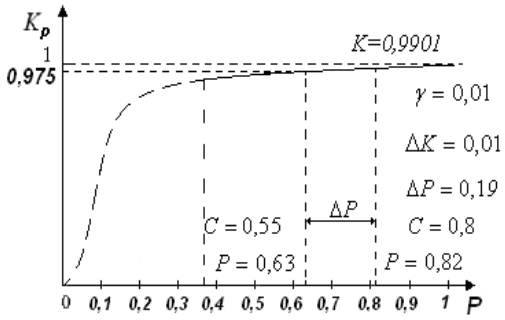

Fig. 4. The dependency diagram K_P on P

Let's show an example of the personnel learning level calculating in assumption of the reliability factor changes. Let's suppose that there is a CCS with recoverability indices $\gamma = 0{,}01$. The analysis results of the staff's skill level showed that the learning level (competency) is equal to $C = 0{,}55$. We have to determine how much personnel learning have to increase for the conditional reliability factor K_P rose to 0.01 ($\Delta K_P = 0{,}01$).

Using (7) $P = e^{(C-1)}$, let's calculate the conditional probability $P = e^{0{,}55-1} = e^{-0{,}45} = 0{,}63$, and base on it – the conditional reliability factor.

On the basis of (6) let's calculate $\Delta P = \sqrt{\dfrac{0{,}01}{1-(0{,}975+0{,}01)}} - 0{,}63 = 0{,}19$.

With reverse transition to the learning index (competency) C on the basis $C = \ln P + 1$ we will get: $C = \ln 0{,}82 + 1 = 0{,}801$.

Thus, the conditional reliability factor or staff reliability factor can be increased by increasing of the personnel learning level (competency) C, on $\Delta K = 0{,}01$ in assumption of $\Delta P = 0{,}19$, but the competency level has to be raised to $C = 0{,}8$ (i.e. $\Delta C = 0{,}25$). For the competency assessment of the ES user we can use the method given in [5].

VII. Conclusion

The analysis of the integral reliability characteristics of the monoergative computer system showed that the availability of the repairable system appreciably depends on the functional availability level of the technical system user, which is determined by his learning (competency) as an operator. The received mathematical models and analytic dependences between system reliability factor and numerical values of user competency make possible to determine improvement costs of the operator learning level according to the state of his current competency.

References

[1] The reliability of technical systems: a guide / J. K. Belyaev, V. A. Bogatyrev, V. V. Bolotin et al. / By ed. I. A. Ushakov. – M.: Radio and Communication, 1985. – 608 p.

[2] The telecommunications infrastructure of data centers [electronic resource] / Document SP-3-0092: (Standard TIA-942, Revision 7.0, February 2005). – Mode of the access: http://www.ups-info.ru/etc/tia_russkii.pdf. – 15.06.2011. – The title from the screen.

[3] Smagin V. A. Technical synergy. Issue 1. Probabilistic models of the complex systems elements / V. A. Smagin. – St. Petersburg: Military-Engineering Space University, 2003. – 66 p.

[4] Smagin V. A. The reliability model of a living organism (the operator). [Electronic resource]. – Mode of the access: http://sir35.narod.ru/Cmagin/index.htm. – 10.12.2010. – The title from the screen.

[5] Krivoulya G. F. Diagnosis of computer systems users competence / G. F. Krivoulya, A. S. Shkil, D. E. Kucherenko, E. V. Garkusha // ACS and automation devices. – 2010. – Issue 150. – p. 125-133.

SSBDDs and Double Topology for Multiple Fault Reasoning

Raimund Ubar, Sergei Kostin, Jaan Raik
Department of Computer Engineering
Tallinn University of Technology

Abstract — **The paper presents a novel view on the Structurally Synthesized BDDs (SSBDD) as a model with inherent double topology for compact modeling of single faults and efficient reasoning of multiple faults. The nodes of SSBDDs represent lower level signal path topology in the original circuit, and the paths of SSBDD represent higher level topology of conditions to be processed during fault reasoning. The double topological view on SSBDDs allows to give easy explanation of the limitations of existing methods of multiple fault testing, and shows the ways how to avoid fault masking. A generalization of the test pair approach in a form of the concept of test groups is introduced for testing multiple faults.**

Keywords: combinational circuits, binary decision diagrams, multiple fault testing, fault masking.

I. INTRODUCTION

Within the last two decades BDDs [1-3] have become state-of-the-art data structure in VLSI CAD for representation and manipulation of Boolean functions. Overviews about different types of BDDs can be found for example in [4,5].

Traditional use of BDDs has been functional, i.e the target has been to represent and manipulate the Boolean functions by BDDs as efficiently as possible. Less attention has been devoted to representing by BDDs the structural properties of logic circuits in form of mapping between the BDD nodes and the circuit implementation. This aspect was introduced in [6,7], where one-to-one mapping between the nodes of BDDs and signal paths in the circuit was introduced. These BDDs were initially called as alternative graphs [6,7], and later as structurally synthesized BDDs (SSBDD) [8]. The name SSBDD stresses the way how the BDDs are created from the gate-level network structure of logic circuits.

The mapping between the SSBDD nodes and the structure of the circuit can be regarded as the *first level diagnostic topology* inherent in SSBDDs, namely the topology of fault propagation paths in the circuit. Each node of SSBDD models different aspects related to a particular signal path in the original circuit, such as propagated signal waveforms, subsets of activated faults, timing characteristics like signal delays. These issues cannot be simulated explicitly with „classical“ BDDs, since the nodes of BDDs have only functional meaning and represent only the primary input variables [8,9].

Manuscript received July 27, 2012.

Raimund Ubar is with the Tallinn University of Technology, Department of Computer Engineering, Estonia, e-mail: raiub@ati.ttu.ee

Sergei Kostin is with the Tallinn University of Technology, Department of Computer Engineering, Estonia, e-mail: skostin@ati.ttu.ee

Jaan Raik is with the Tallinn University of Technology, Department of Computer Engineering, Estonia, e-mail: jaan.raik@ati.ttu.ee

A problem that is still not solved in the field of test and fault diagnosis is how to manage fault masking and generate tests for multiple faults which may mask each other.

The graphical representation of SSBDDs can be regarded as the *second level diagnostic topology*, since each path in the SSBDD may model not only fault activation conditions for test generation purposes, but also potential masking conditions between the multiple faults in the circuit.

The double topology inherent in SSBDDs which is represented first, by the set of nodes, and second, by the set of paths in SSBDDs, allows to create efficient algorithms for multiple fault analysis, test generation and fault diagnosis, because of the straightforward and easily computable representation of very complex fault relationships.

In this paper we consider the use of SSBDDs for analyzing multiple suck-at faults (MSAF) considering in fact only single stuck-at-faults (SSAF). Most approaches to multiple fault test have tried to reduce the complexity of handling MSAF [10-12]. A totally different idea, which is based directly on the SSAF model only, involves two-pattern test approach [13-14] where test pairs were proposed to identify fault-free lines. In [15], the insufficiency of test pairs was shown to guarantee the detection of multiple faults. To overcome the deficiency of test pairs, a new method of test groups was elaborated [16-17]. The idea of test groups for identifying fault-free subcircuits in the circuit under test was introduced the first time in [16]. In [17], it was proven that a test group is robust regarding multiple faults, and is sufficient for detecting any non-redundant multiple fault in a combinational circuit.

In this paper we show the limitations of both, test pairs and the test groups, and show how to overcome these limitations by using the topology inherent in the nodes and paths of SSBDDs.

The rest of the paper is organized as follows. Section 2 explains the concept of SSBDD. In Section 3 we discuss the method of test pairs, and provide a counterexample to show the limits of this approach. Section 4 discusses the fault masking issues, and Section 5 presents the concept of test groups. In Section 6 we show the sufficiency of test groups for detecting multiple faults of any multiplicity using the topological view on SSBDDs. Section 7 provides some experimental results, and Section 8 concludes the paper.

II. STRUCTURALLY SYNTHESIZED BINARY DECISION DIAGRAMS

Let us have a gate level combinational circuit with fan-outs only at inputs. Consider the maximum *fan-out free*

region (FFR) of the circuit with inputs at the fan-out branches and fan-out free inputs. Let the number of the inputs of FFR be *n*. For such a *tree-like sub-circuit* we can create an SSBDD with *n* nodes by *superposition* of BDDs of gates in the circuit [6-9].

Example 1. In Fig. 1 we have a circuit with a FFR-module which can be represented by a Boolean expression:

$$y = x_{11}(x_{21}x_3 \vee x_{41}x_5)(x_{61} \vee x_7) \vee$$
$$\vee\, x_{22}(x_{12}x_8 \vee x_{62}x_9)(x_{42} \vee \overline{x}_7)$$

and as SSBDD in Fig.2. The literals with two indexes in the formula and in the SSBDD denote the branches of fan-out stems, and represent *signal paths* in the circuit. In this example, there are only two branches for each fan-out, the second index 1 is for the upper branch in the circuit in Fig.1, and the second index 2 is for the lower branch. For instance, the bold signal path in Fig.1 is represented by the literal x_{12} in the formula and by the node x_{12} in the SSBDD in Fig.2.

y

Fig. 1. Combinational circuit with four faults

Fig. 2. SSBDD for the circuit in Fig.1 with four faults

Every combinational circuit can be regarded as a network of modules, where each module represents an FFR of maximum size. This way of modeling of the circuit by SSBDDs allows to keep the complexity of the model (the total number of nodes in all graphs) linear to the number of gates in the circuit.

Definition 1. SSBDD model for a given circuit is a subset of SSBDDs, where each of them represents an FFR, and another subset of SSBDDs, where each of them contains a single node representing a primary fan-out input.

As a side effect of the synthesis of SSBDDs, we build up a strict *one-to-one relationship* between the nodes in SSBDDs and the signal paths in the modules (FFRs) of the circuit. Direct relation of nodes to signal paths allows to handle with SSBDDs easily such problems like fault modeling, fault collapsing, and fault masking.

Definition 2. Let us call the one-to-one mapping between the SSBDD nodes and the topology of signal paths in the original circuit as the *first level diagnostic topological property* of SSBDDs.

The first level topological property of SSBDDs allows a compact representation of a set of properties inherent to the circuit signal paths by a single property of the related SSBDD node. For example, all the 10 SAF along the signal path from x_{12} to y in the circuit in Fig.1 are represented by only 2 SAF of the SSBDD node x_{12} in Fig.2.

The variables in the nodes of SSBDD, in general, may be inverted. They are inverted when the number of invertors on the corresponding signal path in the circuit is odd. The two terminal nodes of the SSBDD are labeled by Boolean constants #1 (truth) and #0 (false).

Logic simulation with SSBDDs. Tracing paths on an SSBDD can be interpreted as a procedure of calculating the value of the output variable y for the given input pattern. The procedure is carried out by traversing the nodes in SSBDD, depending on the values of the node variables at the given pattern. By convention, the value 1 of the node variable means the direction to the right from the node, and the value 0 of the node variable means the direction down. Calculation begins in the root node, and the procedure will terminate in one of the terminal nodes #1 or #0. The value of y will be determined by the constant in the terminal node where the procedure stops for the given input pattern.

Example 2. Consider again the circuit and SSBDD in Fig.1, and Fig.2. For the pattern 100111010 (123456789), a path (x_{11}, x_{21}, x_{41}, x_5, x_{61}, #1) in the SSBDD is traced (shown by bold lines in Fig. 2), which produces the output value y =1 for the given pattern.

III. TOPOLOGICAL DIAGNOSTIC MODELING WITH SSBDD

Let have an FFR-module of a circuit which implements a function $y = f(X)$ where X is the set of input variables of the module, and is represented by SSBDD with a set of nodes M. Let $x(m) \in X$ be the variable at the node $m \in M$, and let m^0 and m^1 be the neighbors of the node m for the assignments $x(m) = 0$ and $x(m) = 1$, respectively.

Activation of SSBDD paths. Let T_t be a pattern applied at the moment t on the inputs X of the module. The edge (m,m^e) in SSBDD, where $e \in \{0,1\}$, is called *activated* by T_t if $x(m) = e$. A path (m, n) is called activated by T_t if all the edges which form the path are activated.

To activate a path (m, n) means to assign by T_t the node variables along this path the proper values. Path activation can be interpreted as a reverse task to SSBDD simulation.

Definition 3. Let us call the mapping between the paths $(m_0,\#e)$ in SSBDD from the root node m_0 to one of the terminal nodes $\#e$, where $e \in \{0,1\}$, and the set of input patterns which activate the path $(m_0,\#e)$, as the *second level diagnostic topological property* of SSBDDs.

The second level topological property of SSBDDs allows not only a compact representation of the truth table

of the circuit, but also efficient test generation, fault simulation and straightforward reasoning of complex fault relationships like multiple fault masking.

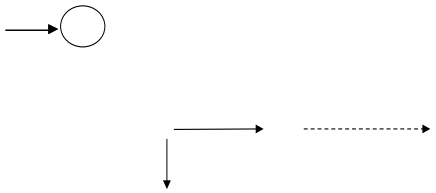

Fig. 3. Topological view on testing of nodes on the SSBDD

Test generation. A test pattern T_t will detect a *single stuck-at-fault* (SSAF) $x(m) \equiv e$, $e \in \{0,1\}$, if it activates in the SSBDD three paths: a path (m_0,m) from the root node to the node under test, two paths $(m^0, \#0)$, $(m^1, \#1)$ for fault-free and faulty cases, and satisfies the fault activation condition $x(m) = e \oplus 1$.

Assume $e = 1$. To simulate the test experiment for T_t, generated for the fault $x(m) \equiv 1$, first, the path (m_0,m) will be traced up to the node m which will "serve as a switch". If the fault is missing, the path $(m^0, \#0)$ will be traced, and if the fault is present, the path $(m^1, \#1)$ will be traced.

Note, that a test pattern T_t for a node fault $x(m) \equiv e$ detects single SAFs on all the lines of the signal path in the circuit, which is represented by the node m in SSBDD.

Example 3. Consider the fault $x_{11} \equiv 1$ in the circuit of Fig.1, represented by the fault $x(m) = x_{11} \equiv 1$ in the SSBDD in Fig.1. Since the node under test m and the root node are the same, $m = m_0$, the first path (m_0,m) is collapsed, and need not activation. To generate a test pattern T_t for $x_{11} \equiv 1$, we have to activate two paths: $(m^0, \#0)$ and $(m^1, \#1)$, like $(x_{22}=0, \#0)$, and $(x_{21}=0, x_{41}=1, x_5=1, x_{61}=1, \#1)$, respectively. For the node under test we take $x_{11} = 0$ which means that the expected value will be $y = 0$. Since the fault $x_{11} \equiv 1$ is present, the path $(x_{11},x_{21},x_{41},x_5, x_{61},\#1)$ will be traced when simulating the test experiment, and the value #1 in the terminal node will indicate the presence of fault.

Fault simulation of a test pattern T_t on the SSBDD is carried out by the following procedure:

(1) The path $(m_0,\#e)$ where $e \in \{0,1\}$, activated by the test pattern T_t will be determined.

(2) For each node $m \in (m_0,\#e)$, its successor $m^* \notin (m_0,\#e)$, is determined, and the path $(m^*,\#e^*)$ from m^* to a terminal $\#e^*$ will be simulated; if $e \neq e^*$ then the fault of the node m is detectable by T_t, otherwise not.

Example 4. Consider the SSBDD in Fig.2. For the input pattern T_t = 100111010 (123456789), a path (x_{11}, x_{21}, x_{41}, x_5, x_{61}, #1) in the SSBDD is activated, which produces $e = 1$. According to Step 2 we find that the nodes x_{11}, x_{41}, and x_5 have all the same successor x_{22}, and by simulation the path $(x_{22},\#e^*)$ we find that $e^* = 0$, which means that the test pattern is able to detect the faults $x_{11} \equiv 0$, $x_{41} \equiv 0$, and $x_5 \equiv 0$, since $e \neq e^*$. The fault $x_{61} \equiv 0$ is as well detectable, since the activated path (x_7, x_{22}, $\#e^*$) gives as well $e^* = 0$. It is easy to see that the fault $x_{21} \equiv 1$ is not detectable since the activated path (x_3, x_{41}, x_5, x_{61}, $\#e^*$) produces the same result $e^* = 1$ as in the case when the node x_{21} is correct.

Fault diagnosis. Let a test pattern T_t is carried out during diagnosis experiment. First, we relate to the test pattern T_t the set of faults $R(T_t) = \{x_{11} \equiv 0, x_{41} \equiv 0, x_5 \equiv 0, x_{61} \equiv 0\}$ detectable by T_t. This set of faults was calculated by fault simulation. We have now two possibilities:

(1) If the pattern T_t fails, we will suspect all the faults of $R(T_t)$ as faulty. To have a better diagnostic resolution we have to carry out additional test patterns to prune the set of candidate faults as much as possible.

(2) If the pattern T_t passes, it would be logical to conclude that the faults of $R(T_t)$ are not present. However, it is correct only in the case when it is assumed that the circuit may consist always only a single fault.

Example 5. Consider the circuit and SSBDD in Fig.1. Assume that the circuit contains four faults: $R = \{x_{11} \equiv 1, x_{22} \equiv 1, x_{42} \equiv 0, x_{61} \equiv 0\}$. Let us apply again to this faulty circuit the test pattern T_t = 100111010 (123456789). Since $(x_{61} \equiv 0) \in R(T_t)$, we should expect that the test pattern will fail. However, the test will pass because the detectable fault $(x_{61} \equiv 0) \in R(T_t) \cap R$, is masked by the fault $(x_{22} \equiv 1) \in R$.

To manage potential fault masking during the test experiments, more advanced methods for test pattern generation and fault diagnosis should be used.

IV. Fault Masking in Digital Circuits

Consider again the combinational circuit in Fig.1 which contains four stuck-at faults: $x_{11} \equiv 1$, $x_{22} \equiv 1$, $x_{42} \equiv 0$, and $x_{61} \equiv 0$. All the faults are depicted also in SSBDD in Fig.2.

Example 6. Table I contains four test patterns targeting these faults ("target faults" in column 11) as single faults. All the four test patterns will pass and not detect the target faults because of circular masking by another fault (Fig.4).

TABLE I
TEST PATTERNS FOR SELECTED FAULTS IN FIG.1

t	Test patterns T_t									Target faults	Mask faults
	x_1	x_2	x_3	x_4	x_5	x_6	x_7	x_8	x_9		
1	0	0	-	1	1	1	0	1	0	$x_{11} \equiv 1$	$x_{61} \equiv 0$
2	1	0	-	1	1	1	0	0	1	$x_{61} \equiv 0$	$x_{22} \equiv 1$
3	0	0	1	1	0	1	1	-	1	$x_{22} \equiv 1$	$x_{42} \equiv 0$
4	0	1	0	1	1	1	1	-	1	$x_{42} \equiv 0$	$x_{11} \equiv 1$
5	1	0	-	1	1	0	0	1	0	$x_{22} \equiv 1$	∅

T_2

Fig. 4. Four faults masking each other in a cycle

There exists however another test pattern T_5 (in Table I and Fig. 4) which would be able to "*break the masking cycle*" by detecting the fault $x_{22} \equiv 1$, one of the targeted four faults. The problem is how to find this pattern, or in general, how to find a test pattern for a given fault, which would be immune against masking by any possible combination of multiple faults.

To avoid fault masking, a method was proposed to use two patterns (test pairs) where the first pattern has the task to test the target fault, and the second pattern has the role of testing the possible masking faults [13,14]. The main idea of this concept is to conclude from the passed test pair the correctness of the wire x_i under test, i.e. the absence of the both faults $x_i \equiv 0$ and $x_i \equiv 1$. Unfortunately, not always the test pairs are working as expected [15,16].

TABLE II

TEST PAIRS FOR TESTING 4 PATHS IN THE CIRCUIT IN FIG.1

t	Test pairs $TP_t = \{T_t, T_{t+1}\}$									Target faults	Test wires
	x_1	x_2	x_3	x_4	x_5	x_6	x_7	x_8	x_9		
1	0	0	-	1	1	1	0	1	0	**$x_{11} \equiv 1$**	**x_{11}**
2	1	0	-	1	1	1	0	1	0	$x_{61} \equiv 0$	
3	1	0	-	1	1	1	0	0	1	**$x_{61} \equiv 0$**	**x_{61}**
4	1	0	-	1	1	0	0	0	1	$x_{22} \equiv 1$	
5	0	0	1	1	0	1	1	-	1	**$x_{22} \equiv 1$**	**x_{22}**
6	0	1	1	1	0	1	1	-	1	$x_{42} \equiv 0$	
7	0	1	0	1	1	1	1	-	1	**$x_{42} \equiv 0$**	**x_{42}**
8	0	1	0	0	1	1	1	-	1	$x_{11} \equiv 1$	
9	1	0	-	1	1	1	0	1	0	$x_{61} \equiv 0$	**x_{61}**
10	1	0	-	1	1	0	0	1	0	$x_{22} \equiv 1$	

Example 7. Table II contains four test pairs targeting the same four faults as shown in Fig.1 ("target faults" in column 11) by testing the corresponding wires x_{11}, x_{22}, x_{42}, and x_{61} for both faults SAF-1 and SAF-0. None of the test pairs will detect any of the four faults (see Fig. 5), all 8 patterns will pass returning the message that all four wires are working correctly, which however is not the case. The first test pair $TP_1(T_1,T_2)$ consisting of test patterns T_1 and T_2 is not able to prove the correctness of the wire x_{11}: the first pattern T_1 targeting the fault $x_{11} \equiv 1$ will pass because of the masking fault $x_{61} \equiv 0$ whereas the second pattern T_2 which targets the masking fault $x_{61} \equiv 0$ will pass because of another masking fault $x_{22} \equiv 1$. The test pair fails to prove the correctness of the wire under test.

In a similar way the test pair TP_3 (T_3,T_4) will fail in testing the wire x_{61}, the test pair TP_5 (T_5,T_6) will fail in testing the wire x_{22}, and the test pair TP_7 (T_7,T_8) will fail in testing the wire x_{42}. The cycle of masking closes.

There is however a test pair TP_9 (T_9,T_{10}) shown in Table II and in Fig. 5, which would be able to "break the masking cycle" by testing the wire x_{22}, and detecting the fault $x_{22} \equiv 1$, one of the four faults in Fig.1. Note, the test pattern T_{10} is the same as the test pattern T_5 in Table I. The problem is how to find the test pair TP_9 involving the pattern T_{10}, or in general, how to find a test pair for a given wire, which would be immune against masking by any possible combination of multiple faults.

V. THE TEST GROUP CONCEPT

The answer lays in a solution based on constructing of test groups instead of test pairs [16,17]. A possible solution for this example is presented in Table III as a set of three test patterns which are targeting to test the wires x_{11} and x_{61}, being immune to the masking fault $x_{22} \equiv 1$. The first pattern T_0 will pass and not detect the fault $x_{61} \equiv 0$, because of the masking fault $x_{22} \equiv 1$. The second pattern T_1 will fail as well in detecting the fault $x_{11} \equiv 1$ because of the masking fault $x_{61} \equiv 0$. However, the third pattern T3 will detect $x_{22} \equiv 1$ and break in this way the cycle of masking.

Fig. 5. Breaking the fault masking cycle

TABLE III

A TEST GROUP WHICH DETECTS ALL THE FOUR FAULTS IN FIG.1

t	Test group $TG = \{T_t, T_{t+1}, T_{t+2}\}$									Test faults	Mask faults
	x_1	x_2	x_3	x_4	x_5	x_6	x_7	x_8	x_9		
0	1	0	1	1	1	1	0	1	0	$\equiv 0$	$x_{22} \equiv 1$
1	0	0	1	1	1	1	0	1	0	$x_{11} \equiv 1$	$x_{61} \equiv 0$
2	1	0	1	1	1	0	0	1	0	$x_{61} \equiv 1$	$\varnothing$

Let us describe shortly the main idea of test groups [14].

Definition 4. Let us introduce the terms: *test group* $TG = \{T_0,T_1...,T_k\}$, *main pattern* $T_0 \in TG$ of the test group, and subset of *co-patterns* $TG^* = \{T_1...,T_k\} \subset TG$ of the test group. The main pattern T_0 activates a *main path* $L_0 = (m_0, \#e)$ in a SSBDD from the root node m_0 to one of the terminal nodes $\#e$, $e \in \{0,1\}$, and each co-pattern T_i activates a *co-path* $L_i = (m_0, \#(\neg e))$ through the node $m_i \in L_0$, so that all T_i will differ from T_0 only in the value of $x(m_i)$.

The test group TG has the target to test a subset of nodes $M_{TG} = \{m_1,...,m_k\} \subseteq L_0$, where at T_0 , for all $i = 1,...,k$: $x(m_i) = e$. T_0 has the target to test all the faults $x(m_i) \equiv \neg e$, $m_i \in M_{TG}$, and each co-pattern T_i has the target to test the fault $x(m_i) \equiv e$. The main condition of TG is that all the variables which do not belong to $M_{TG} = \{m_1,...,m_k\} \subseteq L_0$ should keep the same value for all the patterns in TG.

Example 8. In Table III, a test group $TG = (T_0,T_1,T_2)$ is depicted. Let $D0111D010$ (123456789) be a symbolic representation of the test group where $D = 1$ in T_0, and for other T_t, only one of the D-s is equal to 0.

The main pattern T_0 activates the main path $L_0 = (x_{11},x_{21},x_{41}, x_5,x_{61},\#1)$ shown by bold edges in Fig.2. TG has the target to test the subset of nodes $M_{TG} = \{x_{11},x_{61}\}$ in the SSBDD, particularly, $x_{11} \equiv 0$, and $x_{61} \equiv 0$ by T_0 , $x_{11} \equiv 1$ by T_1, and $x_{61} \equiv 1$ by T_2. Note, the values of the other

variables x_2, x_3, x_4, x_5, x_7, x_8, and x_9, not belonging to the main path L_0, remain unchanged for *TG*.

According to the definition of SSBDD, this test group tests all the SSAF on the signal paths starting on the inputs of the FFR x_{11} and x_{61} up to the output y of the circuit. This conclusion results from the first level diagnostic topology inherent in SSBDDs

It is easy to realize that the test pair is a special case of the test group, where $| M_{TG} | = 1$.

The problem is how to generate test groups to avoid any fault masking in the circuit for arbitrary case of multiple faults. To answer this question, let us discuss the role and meaning of the second level diagnostic topology represented by the paths structures in SSBDDs.

VI. TOPOLOGICAL VIEW ON FAULT MASKING

Definition 5. Introduce a term *activated masking path*. Note that the role of each co-pattern $T_i \in TG$ of the test group *TG* is to keep the masking paths, which may corrupt the result of the main pattern T_0, activated. Activation of the masking path is the necessary and sufficient condition for detecting the faults targeted by the test group.

Consider a skeleton of SSBDD in Fig.6a with highlighted root node m_0, two terminal nodes #0, #1, and two faulty nodes $a \equiv 0$, $c \equiv 1$. The dotted lines represent activated paths during a test pair $TP = \{T_0,T_1\}$which has the goal to test the correctness of the node a. T_0 is for activating the correct path $L_1 = (m_0, a, \#1)$ to detect the fault $a \equiv 0$ with expected test result #1. If the fault is present, then instead of L_1, a "faulty" path $L_0 = (a \equiv 0, c, \#0)$ should be activated with faulty result #0.

In case of another fault $c \equiv 1$ on L_0, a masking path $L_M = (a, c, \#1)$ will be activated, and $a \equiv 0$ will be not detected by T_0. However, at T_1 the masking path L_M remains activated because of the fault $c \equiv 1$, and the wrong test result #1 will indicate the presence of a masking fault in the circuit. It means that the multiple fault $\{a \equiv 0, c \equiv 1\}$ will be detected.

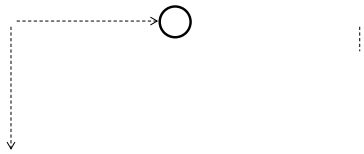

Fig. 6. Comparison of a test pair with a test group

Both patterns of $TP = \{T_0,T_1\}$ will pass and not detect this multiple fault if the masking path L_M will contain a node labeled by the same variable as the tested node. For example, in Fig.6b, both L_1 and L_M contain a node with the same variable a, which is the reason why the test pair is not sufficient for detecting the multiple fault $\{a \equiv 0, c \equiv 1\}$. In this case the co-pattern T_1 of the test pair *TP* is not able to keep the masking path activated.

To overcome the problem, it would be necessary and also sufficient to include into the set of nodes to be tested by a test group at least one node which is labeled by a variable not labeling any node on L_M. For example, in Fig.6b, it would be sufficient for detecting the multiple fault $\{a \equiv 0, c \equiv 1\}$ to generate a test group for testing the nodes {a,b}.

Theorem. A test group *TG* for a subset of nodes M_{TG} is robust with respect to any multiple stuck-at-faults in the circuit if for each possible masking path L_M, there exists a node $m \in M_{TG}$, so that no node on the L_M will have the same variable $x(m)$.

Proof. Suppose, the main test pattern $T_0 \in TG'$ does not detect a fault A because another fault B activates a masking path L_M. According to definition of test groups, each co-pattern $T_i \in TG'$ differs from T_0 in a value of a single variable $x(m_i)$ where $m_i \in M_{TG}$. Suppose T_i is testing the node m_i labeled by the variable $x(m_i)$, and the masking path L_M does not contain a node labeled by the same variable $x(m)$. In this case, L_M remains activated during T_i and hence, provides the same result for T_i as it was for T_0. This means that the pattern T_i will detect the masking fault B. The same considerations hold for every possible masking path. ■

From Theorem, a straightforward algorithm results for tracing all the possible masking paths for the given test group to check if the conditions of Theorem are satisfied. If a path will be found where the conditions are not satisfied, the test group should be extended by additional variable which corresponds to the definition of the test group and satisfies the conditions of Theorem. If the needed extension will be not possible, the masking path is redundant [17], and the corresponding MSAF is redundant as well.

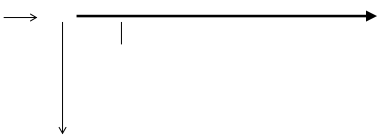

Fig. 7. Topological view on the fault masking mechanism

Example 9. In Fig.7, a topological view is presented, based on a skeleton of SSBDD, on different possibilities of fault masking. L_0 represent a main path as the basis of a test group construction. Let the test group *TG* targets the nodes $M_{TG} = \{a,b,c\}$. $T_0 \in TG$ will not detect the fault $a \equiv 0$ because of another SAF-1 fault. There may be arbitrary combinations of masking faults in the circuit denoted by $\equiv 1$. By dotted lines, possible masking paths are depicted. As we see, for each such a path L_M, there exists always a node $m \in M_{TG}$ with a variable $x(m)$ which is missing on the particular L_M. Hence, the test group satisfies the conditions of Theorem

The concept of test groups was discussed here for single-SSBDD models. In case of a system of more than one SSBDD, we have to either reduce the model by superposition of SSBDDs [8] to the single-SSBDD case

for each output of the circuit, or to use a hierarchical approach to handle the whole system of SSBDDs.

The main goal of test groups is to identify or prove the correctness of a subset of nodes in SSBDD. The knowledge about the nodes identified already as correct allows to generate smaller partial test groups to ease test generation, and the known correct nodes can be dropped from analysis. The method allows creating a sequential procedure of fault diagnosis by extending step by step the fault free core in the circuit at any present multiple fault.

VII. EXPERIMENTAL DATA

In Table IV, experimental data of extending a given SSAF test to MSAF test are presented for ISCAS'85 circuits. Only the test groups with the length of three were considered.

From the SSAF test, all the main patterns were extracted and extended by two co-patterns if they were missing in the original test set. The group cover shows the percentage of main patterns successfully extended up to the test groups. On one hand, the cover demonstrates the level of feasibility of test group generation. On the other hand, it characterizes the robustness of the MSAF test regarding the multiple faults. The columns 3 and 4 show the number of patterns in the SSAF test and in the test set which was composed from the test pattern groups, respectively. The fair comparison between SSAF and MSAF test lengths could not be done in the present research, since the test groups for different outputs were not merged.

TABLE IV
EXPERIMENTAL DATA OF GENERATING TEST GROUPS

Circ.	Gates	SSAF test #	MSAF test #	Group cover%
c432	275	53	314	82,91
c499	683	86	482	67,2
c880	429	84	546	99,8
c1355	579	86	514	65,6
c1908	776	123	621	96,3
c2670	1192	103	820	76,3
c3540	1514	148	995	80,3
c5315	2240	104	1523	91,8
c6288	2480	22	465	98,1
c7552	3163	202	1863	87,8

VIII. CONCLUSIONS

In this paper we presented a novel fault diagnosis oriented view on the SSBDD model as the double topology inherent in SSBDDs. The first level topology refers to signal paths in the original circuit which are mapped to the nodes of SSBDDs, and the second level topology is related to the SSBDD paths structure and refers to the conditions to be processed during fault simulation, test generation and managing fault masking issues.

We presented the idea of generating test groups for testing multiple faults, based on the topological concept of SSBDDs. Differently from the known approaches, we don't target the faults as test objectives. Instead of that, the goal is to verify by test groups the correctness of a selected part of a circuit, represented by a group of nodes in SSBDD.

The main power of the method is to facilitate fault diagnosis in the presence of multiple faults. The knowledge about identified correct parts of the circuit allows to extend step by step the core of the circuit proved as correct.

Experimental results showed high feasibility of generating test groups by achieved high percentages of the group coverage. The coverage can be further increased by using the knowledge about the correct parts of the circuit during testing.

Acknowledgement: The work has been supported by the project FP7-ICT-2009-4-248613 DIAMOND and by EU through the European Regional Development Fund.

REFERENCES

[1] C.Y. Lee. Representation of Switching Circuits by Binary Decision Programs. The Bell System Technical Journal, 1959, pp.985-999.

[2] S.B. Akers. Functional Testing with Binary Decision Diagrams. J. of Design Automat. and Fault-Tolerant Computing,Vol.2,1978,pp.311-331.

[3] R.E. Bryant. Graph-based algorithms for Boolean function manipu-lation, IEEE Trans. on Comp., Vol.C-35, No 8, 1986, pp.667-690.

[4] T. Sasao, M. Fujita (eds.). Representations of Discrete Functions, Kluwer Acad. Publ., 1996.

[5] R. Drechsler, B. Becker: Binary Decision Diagrams, Kluwer Academic Publishers, 1998.

[6] R. Ubar. Test Generation for Digital Circuits with Alternative Graphs. Proceedings of TU Tallinn, No 409, 1976, pp.75-81 (in Russian).

[7] R. Ubar: Test Synthesis with Alternative Graphs, IEEE Design & Test of Computers, Spring, 1996, pp.48-57.

[8] R.Ubar. Multi-Valued Simulation of Digital Circuits with Structurally Synthesized Binary Decision Diagrams. OPA (Overseas Publishers Assotiation) N.V. Gordon and Breach Publishers, Multiple Valued Logic, Vol.4 pp. 141-157, 1998.

[9] R.Ubar, J.Raik, A.Jutman, M.Jenihhin. Diagnostic Modeling of Digital Systems with Multi-Level DDs, In "Design and Test Technology for Dependable SoC", IGI Global 2011, pp.92-118.

[10] M.Abramovici, M.A.Breuer, "Multiple Fault Diagnosis in Comb. Circuits Based on an Effect-Cause Analysis", IEEE Trans. C-29, 1980, pp. 451-460.

[11] I.Pomeranz, S.M.Reddy, "On Generating Test Sets that Remain Valid in the Presence of Undetected Faults", 7th Great Lakes Symp. on VLSI, 1997, pp. 20-25.

[12] Y.C.Kim, V.D.Agrawal, K.K.Saluja, "Multiple Faults: Modeling, Simu-lation and Test", Proc. VLSID'02, 2002, pp. 1-6.

[13] A.G. Birger, E.T.Gurvitch, S.Kuznetsov. Testing of Multiple Faults in Comb Circuits, Avtomatika i Telemehanika, No8, 1975, pp.113-120 (in Russian).

[14] H.Cox, J.Rajski. A Method of Fault Analysis for Test Generation and Fault Diagnosis, IEEE Trans. on CAD, Vol.7, No.7, 1988, pp.813-833.

[15] I.V.Kogan. Testing of Missing of Faults on the Node of Comb. Circuit, Avtomatika i Vychislitelnaja Tehnika, Automation and Computer Engineering, No 2, 1976, pp.31-37 (in Russian).

[16] R.Ubar. Complete Test Pattern Generation for Combinational Networks, Proc. Estonian Academy of Sciences, Physics and Mathematics, No 4, 1982, pp.418-427 (in Russian).

[17] R.Ubar, S.Kostin, J.Raik. Multiple Stuck-at-Fault Detection Theorem, 15th IEEE Symposium on Design and Diagnostics of Electronic Circuits and Systems - DDECS, Tallinn, Estonia, April 18-20, 2012.

Method of Intensity Lowering for Video Stream in Infocommunication Systems

Barannik V.V., Otman Shadi O.U, Krasnorutskyi A.A.

Abstract — **Relevance of the questions connected with improvement of provision quality of video information services with use of wireless telecommunication technologies is shown. Importance of lowering of network load on the basis of intensity lowering an oblate video stream is justified. The vulnerable sides of functioning of the standardized technologies of basic frames processing is shown. Distinctive stages of basic frames coding technology for lowering of intensity of their code representation are considered. The main evaluation stages of intensity of the flow falling on a basic frame taking into account formation of code constructions of oblate representation of transforms on the basis of diagonal and non-uniform positional coding are explained. Development of a method for an intensity assessment on group of frames and all video stream is carried out taking into account: a differentiated contribution of types of frames to intensity and quality of visual acceptability of the reconstructed video stream; compressions of basic frames on the basis of their transformation and the subsequent diagonal and non-uniform positional coding.**

IndexTerms — **dependence, intensity, infocommunication, lowering, method, video stream.**

I. Introduction

Enhancement of provision sector of video information services with use of wireless telecommunication technologies it is connected to need of lowering of network load [1, 2]. It will inevitably increase quality of the received video information. Therefore reduction of intensity of frames flow in the course of their compression is the actual direction of scientific applied researches [3-5]. Here the key component of flow intensity is defined by intensity of code representation of a basic frame. It is caused by that the basic frame in group creates frames of P-type and B-type [4-6]. For processing of a basic frame essentially new method of intensity lowering of its code description is used. The method is based on diagonal and non-uniform positional coding of transforms in nonequilibrium base of the bases. At the same time for such method there is no appropriate valuation method of intensity. From here the purpose of article consists in development of a method for an assessment of video stream intensity taking into account use of the new codec for basic frames coding.

Manuscript received January 17, 2013.

Barannik V.V. is with the Kharkov University of Air Forces, Kharkov, Ukraine, e-mail: barannik_v_v@mail.ru.

Otman Shadi O.U. is with the Kharkov National University of Radio Electronics, Kharkov, Ukraine.

Krasnorutskyi A.A. is with the Kharkov University of Air Forces, Kharkov, Ukraine.

II. Reasons For Need of Basic Frame Processing

Basic structure unit of a MPEG flow is the group frame (Group of Pictures – GOP). The group frame consists of several frames of different type. Each type of frames is processed with use of methods on JPEG compatible platform. Thus the hierarchy concerning dependence of an order of frames reconstruction in group is considered. Inadequate influence of different types frames on quality of reconstruction of all frames in GOP is as a result set. For JPEG technologies such inadequacy is considered by a choice of the appropriate strategy of a quantization. Here the contribution of intensity of basic frame code representation to summary intensity of a video stream depending on quality of visual reconstruction of frames changes from 50 to 75%, and increases with increase in quality of reconstruction of a video stream. It specifies significant influence of basic frame intensity on summary intensity of a video stream.

III. Assessment of Vulnerabilities of the Existing Technologies of Basic Frame Processing

The standardized technologies of basic frames processing of MPEG technologies are characterized by existence of vulnerabilities, namely:

1) the compression ratio reaches the greatest values for low values of PRSN;

2) in case of need to provide PRSN at the level of 45 dB intensity of code representation it is necessary to lower in addition by 1,5 times.

3) for basic frames with high spatial resolution to provide timely delivery with use of infocommunication systems with throughput of the $U_{п} \geq 100$ Mbit\s, in the presence of distortions at the level of PRSN of 25 - 30 dB value of intensity of an oblate video stream needs to be reduced at least by 1,3 times;

4) for the TCP protocol in case of increase in number of nodes from 1 to the 20th time delay will increase by 8 times, and in case of appearance of packets losses - the

time delay will increase to 20% of their total number by 18 times;

5) in case of use of the UDP protocol the lost or damaged packets during transmission aren't transferred by again transmitting end and thus it is considered that all message is delivered to the finite equipment. The analysis of basic frames processing results depending on quantity of the lost packets allows to conclude that for saturated basic frames value of PRSN decreases on average by 86% in case of 1% of packets losses and for 92% respectively in case of 3% of packets losses.

Therefore it is necessary to create new codecs for basic frames.

IV. Development of technology of basic frame coding

Essentially new codec of a basic frame is based that the compression of a transform is provided as a result of diagonal and non-uniform positional coding. Feature of a method is that:

1) positional numbers are built on the basis of non-uniform diagonals of a transform;

2) the bases of diagonal elements are defined as value of dynamic ranges on the basis of a non-uniform and diagonal method of detection;

3) the first and last diagonals are excluded from base of the bases of NDP of numbers and processed separately. It is caused by that: the first diagonal contains a low frequency component of a transform which has sharply excellent characteristics concerning other components of transforms; the last diagonal for rather wide class of images will contain a component with null value.

V. Assessment of intensity of basic frame code representation

We will carry out at first an intensity I_I assessment for the compact I-type provided frames with use of the developed method.

Here length $\overline{Q}_I^{(n\times n)}$ of code construction of oblate representation of a fragment is determined by a formula

$$\overline{Q}_I^{(n\times n)} = \overline{Q}_n + \overline{Q}_Z + \overline{Q}_R \qquad (1)$$

where $\overline{Q}_n$ – quantity of discharges on submission of the codegram of the transform compression description; $\overline{Q}_Z$ – compact representation of a binary matrix of signs; $\overline{Q}_R$ – number of bits on representation of the quantization R step.

Respectively value $\overline{Q}_n$ is defined as the summary quantity of discharges set by the following formula:

$$\overline{Q}_n = \overline{Q}_{DC} + \overline{Q}_{(n\times n)-2} + \overline{Q}_{v_д}\ (\text{bit}), \qquad (2)$$

where $\overline{Q}_{DC}$ – length of a statistical code of a low frequency DC component; $\overline{Q}_{(n\times n)-2}$ – quantity of discharges on representation of a transform by diagonal and non-uniform positional coding without the first and last diagonals; $\overline{Q}_{v_d}$ – quantity of discharges on representation of the last diagonal of a transform.

Respectively the summary quantity of $\overline{Q}'_{(n\times n)-2}$ discharges will be defined on representation of all code values of diagonal non-uniform positional numbers on the basis of a ratio

$$\overline{Q}_{(n\times n)-2} = \sum_{\xi=2}^{2n-2} \overline{Q}_{\xi,n_\xi} = \sum_{\xi=2}^{2n-2} ([n_\xi \ell og_2 d'_\xi] + 1)\ (\text{bit}). \qquad (3)$$

Having contracted expressions (1) – (3) into one, we will receive a ratio for value $I_I^{(n\times n)}$, namely:

$$I_I^{(n\times n)} = \overline{Q}_{DC} + \sum_{\xi=2}^{2n-2} ([n_\xi \ell og_2 d'_\xi] + 1) + \overline{Q}_{v_d} + \overline{Q}_Z + \overline{Q}_R\ . \qquad (4)$$

On the basis of this expression intensity I_I of the flow falling on one basic frame will be created as the amount of intensity of its fragments, i.e.

$$I_I = \sum_{i=1}^{MN/nn} I_{I,i}^{(n\times n)}\ , \qquad (5)$$

$I_{I,i}^{(n\times n)}$ – intensity of i-th fragment of a basic frame; MN/nn – quantity of fragments with $(n\times n)$ size in a basic frame; MN – size of a basic frame.

VI. Assessment of video stream intensity

We will consider the assessment of intensity of the $I(GOP)'_k$ compressed video stream falling on group of frames, with use of the developed technology of diagonal and non-uniform positional coding now. Here it is taken into consideration that the group of frames consists of 8 frames, and includes one frame of I-type, two frames of P-type and five frames of B-type. Processing of frames is carried out according to a real-time mode. In this case compensating of movement between frames in a flow isn't considered, and it is allowed that the compression ratio for frames of specific type will differ at least, than for 5%. Then taking into account expression for intensity of a basic frame, we will receive the following ratio for an intensity assessment $I(GOP)'_k$:

$$I(GOP)_k = I_I + 2I_P + 5I_B = \sum_{i=1}^{MNnn} I_{I,i}^{(n\times n)} + 2I_P + 5I_B =$$
$$= \sum_{i=1}^{MN/nn} (\overline{Q}_{DC} + \sum_{\xi=2}^{2n-2} ([n_\xi \ell og_2 d'_\xi] + 1 + \overline{Q}_{v_д} + \overline{Q}_Z + \overline{Q}_R)_i + \qquad (6)$$
$$+ 2I_P + 5I_B$$

where I_I, I_P, I_B – values of intensity for the compact provided frames according to I-type, P-type and B-type.

$$I(GOP)_k = I_I + 2I_P + 5I_B = \sum_{i=1}^{MN/nn} I_{I,i}^{(n\times n)} + 2I_P + 5I_B =$$

$$= \sum_{i=1}^{MN/nn} (\bar{Q}_{DC} + \sum_{\xi=2}^{2n-2} ([n_\xi \ell og_2 d'_\xi] + 1 + \bar{Q}_{v_a} + \bar{Q}_Z + \bar{Q}_R)_i + \quad (7)$$

$$+ 2I_P + 5I_B$$

Here value $I(GOP)'_k$ is estimated as the number of bits transferred in time t_{GOP} equal $t_{GOP} = 8/\nu_t$ (sec.)., where ν_t – quantity of frames which is transferred for 1 sec.

Each type of frames is processed with use of methods on JPEG to a compatible platform. Thus the hierarchy concerning dependence of an order of frames reconstruction in group is considered. Inadequate influence of frames of different types on quality of all frames reconstruction in GOP is as a result set.

The assessment of intensity $I(GOP)'_k$ and $I'^{(24)}_k$, falling respectively on group of the frames during time t_{GOP} and on frames t_{GOP} for 1 sec. is considered in Tab. I and on charts of Fig. 1. Here $\nu_t = 24$ to frames. Calculations are carried out on a formula (6). Calculations of the value $\Delta I(GOP)'_k$ estimated as a percentage as the level of lowering of frames group flow intensity due to reduction of basic frame intensity are given in the last line of Tab. I. Obtaining charts in Fig. 1 was carried out for three modes of frames processing taking into account support of the PRSN following levels:

- mode 1, high quality of a basic frame: An I-frame – 42 dB, the P-frame – 28 dB, the B-frame – 22 dB;
- mode 2, high quality of a basic frame: An I-frame – 40 dB, the P-frame – 28 dB, the B-frame – 22 dB;
- mode 2, sufficient quality of a basic frame: An I-frame – 38 dB, the P-frame – 28 dB, the B-frame – 22 dB.

TABLE I
DEPENDENCE OF INTENSITY $I(GOP)'_k$ AND $I'^{(24)}_k$ OF PRSN, MBIT\S

Frame type	h, dB					
I-frame	42	40	40	40	38	38
P-frame	28	28	30	32	28	30
B-frame	22	22	24	24	22	24
$I(GOP)'_k$	2,13	1,76	2,01	2,17	1,24	1,49
$I'^{(24)}_k$	6,3	5,2	6	6,4	3,7	4,3
$\Delta I(GOP)'_k$, %	-11,25	-12	-10,7	-9,6	-11,43	-9,7

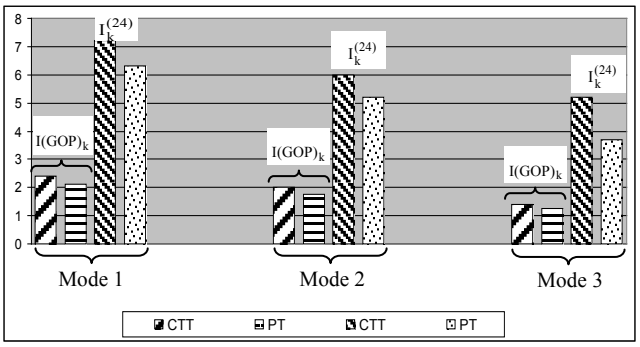

Fig. 1. Values of intensity $I(GOP)'_k$ and $I'^{(24)}_k$ for standardized (CCT) and developed (PT) technology of basic frames processing depending on the video stream PRSN model

By results of researches of data in Tab. I and charts in fig. 1 it is possible to make such inferences:

1. Intensity of frames flow taking into account use for compression of a basic frame of the created technology changes ranging from 3,7 Mbit\s for the mode of sufficient visual quality to 6,3 Mbit\s for the mode of high quality.

2. Due to processing of basic frames on the basis of diagonal and non-uniform positional coding of transforms lowering of video stream summary intensity from 10 to 13% is reached. The greatest lowering of intensity happens in case of the most powerful contribution of basic frames intensity to summary intensity. Such it is watched for the mode of high visual quality of video stream reconstruction.

3. Lowering of intensity of a video stream provides:

- on the one hand use for its transmission of wireless technologies with lower throughput, namely at the level of 4 - 10 Mbit\s;
- on the other hand improvement of quality of video stream visual assessment due to use of the appropriate matrixes of transforms components correction is allowed. First of all there is an opportunity to reduce distortions without increase of intensity of a video stream at the same time for P-frames from level 28db to the level of 32, and for B-type frames from 22 dB to 24 dB.

On materials of researches it is possible to sum up the following:

1) the valuation method of intensity on frames group and all video stream is developed taking into account:

-differentiated contribution of frames types to intensity and quality of visual acceptability of the reconstructed video stream;

- compressions of basic frames on the basis of their transformation and the subsequent diagonal and non-uniform positional coding;

2) lowering of an imbalance between intensity I_k and transmission rate $U_п$ on a network on average for 12% is reached. It allows:

- on the one hand to use for transmission of a video stream IKS technologies with lower throughput, namely at the level of 4 - 10 Mbit\s;

- on the other hand to increase quality of a visual assessment of a video stream due to lowering of distortions without increase of video stream intensity at the same time for P-frames from level 28db to the level of 32 dB, and for B-type frames from 22 dB to 24 dB.

VI. Conclusion

The valuation method of intensity on group of frames and all video streams is developed taking into account: a differentiated contribution of frames types to intensity and quality of visual acceptability of the reconstructed video stream; compressions of basic frames on the basis of their transformation and the subsequent diagonal and non-uniform positional coding.

Lowering of an imbalance between intensity and transmission rate on a network on average for 12% is reached. It allows:

- on the one hand to use for transmission of a video stream IKS technologies with lower throughput, namely at the level of 4 - 10 Mbit\s;

- on the other hand to increase quality of a visual assessment of a video stream due to lowering of distortions without increase of video stream intensity at the same time for P-frames from level 28db to the level of 32 dB, and for B-type frames from 22 dB to 24 dB.

References

[1] Olifer V.G. Komp'juternye seti. Principy, tehnologii, protokoly: Uchebnik dlja vuzov. 3-e izd. / V.G. Olifer, N.A. Olifer. - SPb.: Piter, 2006. 958 p.

[2] Gonzales R.C. Digital image processing / R.C. Gonzales, R.E. Woods. Prentice Inc. Upper Saddle River, New Jersey 2002. 779 p.

[3] Lee S.Y. Temporally coherent video matting / S.Y. Lee, J.C. Yoon, I.K. Lee // Graphical Models 72. 2010. P. 25 – 33.

[4] Krasil'nikov N.N. Cifrovaja obrabotka izobrazhenij. M.: Vuzovskaja kniga, 2011. 320 p.

[5] Barannik V.V. Kodirovanie transformirovannyh izobrazhenij v infokommunikacionnyh sistemah / V.V. Barannik, V.P. Poljakov - H.: HUPS, 2010. 234 p.

[6] Barannik V. Method Of Encoding Transformant Uolsha Is In Systems Air Monitoring Of Earth / V. Barannik, A. Yakovenko, A. Krasnorutkiy // Lviv-Slavsko, Ukraine, Lviv Polytechnic National University, International Conference TCSET'2009, Modern problems of radio engineering, telecommunications and computer science, February 19 – 23, 2009. P. 381-383.

Barannik Vladimir Viktorovich, professor, Doctor in Sciences, chief of department Kharkov university of Air Forces. Scientific interests: telecommunications systems and information technology.

Otman Shadi O.U. aspirant in Kharkiv National University of Radio Electronics. Scientific interests: processing and transmission of information.

Krasnorutskyi Andrew Alexandrovich. Ph.D., professor, chief of department Kharkov university of Air Forces. Scientific interests: telecommunications systems and information technology.

Accessibility Valuation Method for Video Information Resource on Time Recurrent Reconstruction of the Three-Dimensional Data Structures

Barannik V.V., Ryabukha Yu.M.

Abstract — **Contradiction existence between requirements on the one hand concerning safety of obtained information, and on the other side of relatively timeliness of its receiving is shown. It is justified that from position of an assessment of accessibility category of a video information resource is required not only to lower time of its transmission, but also to provide required time delays on processing stages, including reconstruction process. Development the valuation method of accessibility of a video information resource on a temporal time delay on item recurrent three-dimensional polyadic decoding without error introduction is explained.**

Index Terms — **Accessibility, method, reconstruction, restoration, structures, subtraction, three-dimensional.**

I. INTRODUCTION

The last decade is marked by the increased demand for a video conferencing (VC), including in interests of the departmental organizations. Further development of VC systems goes in the direction of use of video streams with the increased resolution capability. However owing to lag of growth rates of productivity of communication systems there is a contradiction between requirements on the one hand concerning safety of obtained information, and on the other side of relatively timeliness of its receiving with use of compression technologies [1]. For these reasons need of further development of technologies of a compression and coding of video information structures [2 – 4] is dictated. In this direction it is required to provide property of accessibility of video data taking into account redundancy abbreviation in three-dimensional data structures. It defines relevance of a scientific and application-oriented perspective of researches.

The effective direction of creation of technologies for three-dimensional coding are the code structures offered in operations [4, 5]. Here code representation is created for three-dimensional polyadic numbers. From a position of an assessment of category of video information resource accessibility is required not only to lower of its transmission time, but also to provide required time delays on processing stages, including reconstruction process. In this connection, it is required to evaluate number of operations on reconstruction of three-dimensional polyadic numbers. Therefore the purpose of researches of article consists in development the valuation method of accessibility of a video information resource on time of recurrent reconstruction of three-dimensional data structures.

Manuscript received January 27, 2013.

Barannik V.V. is with the Kharkov University of Air Forces, Kharkov, Ukraine, e-mail: barannik_v_v@mail.ru.

Barannik V.V. is with the Kharkov University of Air Forces, Kharkov, Ukraine.

II. FEATURES OF IMPLEMENTATION OF RECURRENT DECODING OF THREE-DIMENSIONAL DATA STRUCTURES

For abbreviation of operations number of on processing and lowering of expenses of memory on storage of the intermediate result the recurrent diagram of restoration is used. In this case program implementation of restoration of the three-dimensional polyadic numbers (TDPN) on the universal computing remedies of processing considerably becomes easier. Restoration is organized in the direction on verticals from top to bottom, on columns in depth of a parallelepiped and in the lines from left to right. Sequential restoration of elements of the three-dimensional data structures (TDDS) from a high element, on a position $(j=1; i=1; z=1)$ is set by a formula:

$$a_{111} = [N_v / \omega_{111}] - [N_v / (\psi_{111}\,\omega_{111})]\psi_{111}.$$

According to properties of polyadic numbers for the arbitrary z element of vertical $(j=1; i=1)$, there is performs the inequality

$$N^{(n_{стб}, n_{стр}, n_c - z+1)} < \psi_{11z}\,\omega_{11z}. \qquad (1)$$

Taking into account an inequality (1) restoration of a_{11z} element is based on ratios:

$$a_{11z} = [N^{(n_{стб}, n_{стр}, n_c - z+1)} / V^{(n_{стб}, n_{стр}, n_c - z)}]; \quad (2)$$

$$V^{(n_{стб}, n_{стр}, n_c - z)} = V^{(n_{стб}, n_{стр}, n_c - z+1)} / \psi_{11z}; \quad (3)$$

$$N^{(n_{стб},n_{стр},n_c-z)} = N^{(n_{стб},n_{стр},n_c-z+1)} - a_{11z}V^{(n_{стб},n_{стр},n_c-z)}; \quad (4)$$

where $N^{(n_{стб},n_{стр},n_c-z)}$, $N^{(n_{стб},n_{стр},n_c-z+1)}$ - code values for the three-dimensional polyadic numbers, consisting each of $n_{стр}\times n_{стб}-1$ full verticals on n_c elements and from a vertical with coordinates $(j=1; i=1)$ consisting respectively from $(n_c - z)$ and $(n_c - z+1)$ elements; $V^{(n_{стб},n_{стр},n_c-z)}$, $V^{(n_{стб},n_{стр},n_c-z+1)}$ - values of stored works of the bases ψ_{jiz} for the three-dimensional polyadic numbers, consisting each of $n_{стр}\times n_{стб}-1$ full verticals on n_c elements and from a vertical with coordinates $(j=1; i=1)$ containing respectively $(n_c - z)$ and $(n_c - z+1)$ elements.

On the basis of formulas (2) – (4), intended for receiving the a_{11z} element, a ratio for restoration arbitrary of z element located on a vertical of TSD with coordinates $(j; i)$ will have an appearance:

$$a_{jiz} = [N^{(n_{стб}-j+1,n_{стр}-i+1,n_c-z+1)} / V^{(n_{стб}-j,n_{стр}-i,n_c-z)}]; \quad (5)$$

$$V^{(n_{стб}-j,n_{стр}-i,n_c-z)} = V^{(n_{стб}-j,n_{стр}-i,n_c-z+1)} / \psi_{ijz}; \quad (6)$$

$$N^{(n_{стб}-j,n_{стр}-i,n_c-z)} = N^{(n_{стб}-j+1,n_{стр}-i+1,n_c-z+1)} - a_{jiz}V^{(n_{стб}-j,n_{стр}-i,n_c-z)}, \quad (7)$$

where $N^{(n_{стб}-j,n_{стр}-i,n_c-z)}$, $N^{(n_{стб}-j+1,n_{стр}-i+1,n_c-z+1)}$ - code values for TPC consisting from: $n_{стр}\times(n_{стб}-j)$ full verticals on n_c elements; $(n_{стр}-i)$ verticals on n_c elements and from a vertical with coordinates $(j; i)$ containing respectively $(n_c - z)$ and elements $(n_c - z+1)$; $V^{(n_{стб}-j,n_{стр}-i,n_c-z)}$ - value of weight factor of the a_{jiz} element, equal to value of stored works of the ψ_{jiz} bases for the three-dimensional polyadic numbers having: $n_{стр}\times(n_{стб}-j)$ full verticals on a_{jiz} elements; $(n_{стр}-i)$ verticals on n_c elements and a vertical with coordinates $(j; i)$ consisting from $(n_c - z)$.

Thus, the system of expressions (5) – (7) sets items recurrent restoration of elements of three-dimensional polyadic numbers. For receiving one element it is required to perform only one division operation.

III. Assessment of number of the operations spent for items recurrent restoration of three-dimensional polyadic numbers

Items restoration consists of two main stages.

1. For an exception of overflowing of a machine word it is required to define quantity of r_ν elements of three-dimensional polyadic number (TDPN) for which the N_ν code was created. In this case stored work of the $\psi_{\eta k\gamma}$ bases of the TPC elements is calculated. The checking rule of including the jiz element in group of the elements having one code is set by an inequality

$$\prod_{\gamma=1}^{z}\psi_{ji\gamma}\prod_{k=1}^{i-1}\prod_{\gamma=1}^{n_c}\psi_{jk\gamma}\prod_{\eta=1}^{j-1}\prod_{k=1}^{n_{стр}}\prod_{\gamma=1}^{n_c}\psi_{\eta k\gamma} \le 2^M - 1, \quad (8)$$

where $\prod_{\gamma=1}^{z}\psi_{ji\gamma}\prod_{k=1}^{i-1}\prod_{\gamma=1}^{n_c}\psi_{jk\gamma}\prod_{\eta=1}^{j-1}\prod_{k=1}^{n_{стр}}\prod_{\gamma=1}^{n_c}\psi_{\eta k\gamma}$ - stored work of the $\psi_{\eta k\gamma}$ bases for structural part of TSD consisting of $(n_{стр}(j-1)+(i-1))$ verticals with n_c elements and a vertical with coordinates $(j;i)$, containing z elements.

If the inequality (8) is performed, the element a_{jiz} enters TPC with the general code N_ν and conversely.

2. After the quantity of the TPC elements with the general code is defined restoration of a_{jiz} elements is carried out. This stage consists in N_ν code number decoding.

According to an inequality (8) for restoration of all TPC r_ν elements it is required to perform: multiplication r_ν operations for determination of $\psi_{jiz}\omega_{jiz}$ weight factor; comparing r_ν operations for checking the performing of an inequality (8); division r_ν operations for computation of ω_{jiz} values; division $2r_\nu$ operations of $(N_\nu/(\psi_{jiz}\omega_{jiz}))$ and (N_ν/ω_{jiz}); $2r_\nu$ operations of rounding of results of division $(N_\nu/(\psi_{jiz}\omega_{jiz}))$ and (N_ν/ω_{jiz}); r_ν operations of multiplication of value $([N_\nu/(\psi_{jiz}\omega_{jiz})])$ on the ψ_{jiz} base; value subtraction operations $([N_\nu/(\psi_{jiz}\omega_{jiz})]\psi_{jiz})$ from $([N_\nu/\omega_{jiz}])$ value.

From this it follows that the summary number of $\mu_{d1}^{(r_\nu)}$ operations which is required to be performed for restoration of all r_ν elements of three-dimensional polyadic number on the basis of item diagram, is on a formula:

$$\mu_{d1}^{(r_\nu)} = 2r_\nu \text{ (multiplication)} + 3r_\nu \text{ (dividing)} + 2r_\nu \text{ (rounding)} + r_\nu \text{ (subtraction)} + r_\nu \text{ (comparison)} \quad (9)$$

The maximum quantity of elements with the general code equally to the volume of a three-dimensional data structure,

or $r_\nu = n_{стб}\, n_{стр}\, n_c$. Then the maximum summary number of $\mu_{d1}^{(max)}$ operations will be equal

$\mu_{d1}^{(max)} = 2n_{стб}\, n_{стр}\, n_c$ (multiplication) + $3n_{стб}\, n_{стр}\, n_c$ (dividing) + $2n_{стб}\, n_{стр}\, n_c$ (rounding) + $n_{стб}\, n_{стр}\, n_c$ (subtraction) + $n_{стб}\, n_{стр}\, n_c$ (comparison). (10)

For restoration of the TPC r_ν elements on the basis of items recurrent decoding of a N_ν code by expressions (5) – (7) it is required to expend: r_ν comparing operations for checking of performing of an inequality (8); r_ν operations of multiplication and r_ν division operations for determination of $V^{(n_{стб}-j,\, n_{стр}-i,\, n_c-z+1)}$ and $V^{(n_{стб}-j,\, n_{стр}-i,\, n_c-z)}$ weight factors; r_ν operations of multiplication of values a_{jiz} and $V^{(n_{стб}-j,\, n_{стр}-i,\, n_c-z)}$; r_ν operations of computation of a difference between values $N^{(n_{стб}-j+1,\, n_{стр}-i+1,\, n_c-z+1)}$ and $a_{jiz}V^{(n_{стб}-j,\, n_{стр}-i,\, n_c-z)}$; r_ν arithmetical operations of division $N^{(n_{стб}-j+1,\, n_{стр}-i+1,\, n_c-z+1)}$ on $V^{(n_{стб}-j,\, n_{стр}-i,\, n_c-z)}$; r_ν operations of rounding of division result $N^{(n_{стб}-j+1,\, n_{стр}-i+1,\, n_c-z+1)} / V^{(n_{стб}-j,\, n_{стр}-i,\, n_c-z)}$. The summary number of operations $\mu_{d2}^{(r_\nu)}$ which is required to be performed for restoration of r_ν elements of three-dimensional polyadic number on the basis of the recurrent items diagram means is equal:

$\mu_{d2}^{(r_\nu)} = 2r_\nu$ (multiplication) + $2r_\nu$ (dividing) + r_ν (rounding) + r_ν (subtraction) + r_ν (comparison). (11)

Respectively the maximum number of operations on restoration of $r_\nu = n_{стб}\, n_{стр}\, n_c$ elements is calculated with formula:

$\mu_{d2}^{(max)} = 2n_{стб}\, n_{стр}\, n_c$ (multiplication) + $2n_{стб}\, n_{стр}\, n_c$ (dividing) + $n_{стб}\, n_{стр}\, n_c$ (rounding) + $n_{стб}\, n_{стр}\, n_c$ (subtraction) + $n_{стб}\, n_{стр}\, n_c$ (comparison). (12)

From the comparative analysis of expressions (10) and (11) follows that the number of operations $\mu_{d2}^{(r_\nu)}$ is less, than number of operations $\mu_{d1}^{(r_\nu)}$ on division operations r_ν and on r_ν rounding operations. This results from the fact that for finding of the TPC element on the basis of the recurrent item diagram which set by expression (5), it is required to execute one division operation and rounding. In case of equality of all TSD sizes to a constant n, i.e. the maximum summary number $n_{стб} = n_{стр} = n_c = n$ of operations for item restoration according to a ratio (10) will be equal:

$$\mu_{d1}^{(max)} = n^3\,(8{,}1 + 2{,}7 + 1 + 1{,}5) = 13{,}3\,n^3. \quad (13)$$

Respectively the maximum summary number of operations on recurrent item restoration of TSD is equal

$$\mu_{d2}^{(max)} = n^3\,(5{,}4 + 2{,}7 + 1 + 1{,}5) = 10{,}6\,n^3. \quad (14)$$

With taking into account expressions (13) and (14) time expenditure $t_{d1}^{(max)}$ and $t_{d2}^{(max)}$ on restoration of the TSD elements for item and recurrent item processing are respectively on formulas:

$$t_{d1}^{(max)} = 13{,}3\,n^3 \big/ U_{mp}\,;\; t_{d2}^{(max)} = 10{,}6\,n^3 \big/ U_{mp}\,.$$

Time of recovery of the image with $Z_{row} \times Z_{column}$ sizes respectively for item $T_{d1}^{(max)}$ and recurrent item $T_{d2}^{(max)}$ processing equally:

$$T_{d1}^{(max)} = Z_{row} \times Z_{col}\; t_{d1}^{(max)} \big/ n^3;$$

$$T_{d2}^{(max)} = Z_{row} \times Z_{col}\; t_{d2}^{(max)} \big/ n^3\,.$$

Dependence of values $\mu_{d1}^{(max)}$, $t_{d1}^{(max)}$ и $\mu_{d2}^{(max)}$, $t_{d2}^{(max)}$ from n for $U_{мп} = 10^{-10}$ is provided respectively in Tab. I and II. Dependence of time for recovery of images depending on the size of a frame, volume of TSD and type of item processing is given in Tab. III:

Dependence of number of $\mu_{d1}^{(max)}$ operations of time of restoration $\mu_{d1}^{(max)}$ for item processing of TSD for $n_{col} = n_{row} = n_c = n$ from n

TABLE I
DEPENDENCE OF NUMBER OF $\mu_{d1}^{(max)}$ OPERATIONS OF TIME OF RESTORATION $\mu_{d1}^{(max)}$ FOR ITEM PROCESSING OF TSD FOR $n_{col} = n_{row} = n_c = n$ FROM n

Size TSD	Type of operations: subtraction, 1	multiplication, 1,33	dividing, 2,7	comparison, 1,5	Summary time for restoration, $t_{d1}^{(max)}$
$n = 4$	64	170,24	518,4	96	$8{,}5\times10^{-8}$, sec
$n = 8$	512	1361,92	4147,2	768	$6{,}8\times10^{-7}$, sec
$n = 16$	4096	10895,36	33177,6	6144	$5{,}4\times10^{-6}$, sec

Dependence of number of $\mu_{d_2}^{(max)}$ operations and time of restoration for recurrent item processing of TSD for $n_{стб} = n_{стр} = n_c = n$ from n

TABLE II
DEPENDENCE OF NUMBER OF $\mu_{d_2}^{(max)}$ OPERATIONS AND TIME OF RESTORATION FOR RECURRENT ITEM PROCESSING OF TSD FOR $n_{стб} = n_{стр} = n_c = n$ FROM n

Size TSD	Type of operations: subtraction, 1	multiplication, 1,33	dividing, 2,7	comparison, 1,5	Summary time for restoration, $t_{d_2}^{(max)}$
$n = 4$	64	170,24	345,6	96	$6{,}7\times10^{-8}$, sec
$n = 8$	512	1361,92	2764,8	768	$5{,}4\times10^{-7}$, sec
$n = 16$	4096	10895,36	22118,4	6144	$4{,}3\times10^{-6}$, sec

Dependence of recovery time of the image on the frame size, volume of TSD and type of item processing

TABLE III
DEPENDENCE OF RECOVERY TIME OF THE IMAGE ON THE FRAME SIZE, VOLUME OF TSD AND TYPE OF ITEM PROCESSING

Frame size	Volume of TSD	Type of item restoration: Sequential, $T_{d_1}^{(max)}$	Recurrent, $T_{d_2}^{(max)}$
1024×1024	64	$1{,}4\times10^{-3}$, s.	1×10^{-3}, s
	512	$1{,}4\times10^{-3}$, s.	$1{,}1\times10^{-3}$, s
3000×2000	64	8×10^{-3}, s.	$6{,}3\times10^{-3}$, s
	512	8×10^{-3}, s.	$6{,}31\times10^{-3}$, s
7000×5000	64	$4{,}6\times10^{-2}$, s.	$3{,}66\times10^{-2}$, s
	512	$4{,}6\times10^{-2}$, s.	$3{,}7\times10^{-2}$, s

From the comparative data analysis, given in Tab. I-III follows that: summary time of restoration of a three-dimensional data structure in case of recurrent processing decreases in 1,25 times of rather item processing; the offered recurrent restoration of TSD provides receiving images in real time with a size, equal 1024×1024 elements.

III CONCLUSION

1. The valuation method of accessibility of a video information resource on a temporal time delay on item recurrent three-dimensional polyadic decoding without error introduction is developed. Here it is considered that restoration of elements of three-dimensional polyadic numbers will be organized in the verticals direction from top to bottom, on columns in depth of a parallelepiped and in the lines from left to right. Decoding of a code is carried out with taking into account that the first TPC element is the senior. In difference from sequential items restoration for receiving one element it is required to perform only one division operation. In this case the summary number of operations is reduced on n division operations and on n rounding operations. This result from the fact that for finding of the TPC element on the basis of the recurrent item diagram it is required to perform only one division operation and rounding.

2. Summary time of restoration of a three-dimensional data structure in case of recurrent processing decreases in 1,25 times of rather item processing. The offered recurrent restoration of TSD provides receiving images in real time with a size, 1024×1024 equal elements.

REFERENCES

[1] Gonsales R. Cifrovaya obrabotka izobrazhenij/ R. Gonsales, R. Vuds.- M.: Technosgera, 2005.-1072 c.

[2] Beljaev E.A. Szhatie videoinformacii na osnove trehmernogo diskretnogo psevdo-kosinusnogo preobrazovanija dlja energoffektivnyh sistem videonabljudenija / E.A. Belyaev, T.M. Suhov, N.N. Shostackij // Komp'juternaja optika, tom 34, 2, S. 260 – 272, 2010.

[3] B. Furht, Ken Gustafson, Hesong Huang and Oge Marques, An Adaptive Three-Dimensional DCT Compression Based on Motion Analysis // Proceedings of the 2003 ACM symposium on Applied computing, 2003.

[4] Barannik V.V. Method of the 3-D Image Processing / V.V. Barannik, S.V. Karpenko // Modern problems of Radio Engineering, Telecommunications and Computer Science. Proceedings of the International Conference TCSET'2008, Lviv-Slavsko, Ukraine, February 20 – 24, 2008. – P. 115 – 117.

[5] Barannik V.V. Trehmernoe poliadicheskoe kodirovanie v napravlenii, nachinaja s mladshih elementov / V.V.Barannik, J.N. Rjabuha // Suchasna special'na tehnika. – 2013. - №3. – S. 15 – 20.

Barannik Vladimir Viktorovich, professor, Doctor in Sciences, chief of department Kharkov university of Air Forces. Scientific interests: telecommunications systems and information technology.

Ryabukha Yuriy Nikolayevich, PhD, Kharkov university of Air Forces. Scientific interests: telecommunications systems and security information.

Adaptation of the FPGA to Logic Failures

Tyurin S.F., Grekov A.V., Gromov O.A.

Abstract – **The paper proposes the restoration of logic programmable logic integrated circuits such as FPGA (field-programmable gate array) for critical applications by adapting to failures of logic elements. The principle of adaptation FPGA is to switch to the remaining functionality of the LUT (Look Up Table), with the possibility of hardware and software they use in the event of hardware failure after massive failures. Asked to ensure the preservation of the basis in the sense of Post logic functions that allow you to calculate the input for a longer time at a given failure model.**

I. Introduction

Modern FPGA, containing several billion of transistors [1], provide wide opportunities for logic reconfiguration, but do not use them to adapt to failures. Thus, one of the leading experts in FPGA area Yervant Zorian said: "Now the main problem of system on a chip repair is development of embedded technologies and methods of the logic repair that occupies no more than 10% of chip area" [2].

To solve this problem we may provide retaining of basic in the terms of Post theorem [3] logic functions that allow to calculate the input for a longer time at a given pattern of failures, that is - the reservation bases elements, the use of elements with an excess basis [4, 5]. In case of failures it is possible to calculate the initial logic functions – all or only critical parts of the residual bases of all or a subset of items with the possible use of software and hardware implementation. [6] With that the scheme is adapted to the conditions of a fault with the appropriate reconfiguration.

Contemporary programmable logic – FPGA (field-programmable gate array) provide wide opportunities of logic reconfiguration, but do not use them to adapt to the failures and logic recovery [13].

Let us consider the proposed principle and characteristics of recovery logic FPGA for critical applications by adapting to failures of logic elements.

Manuscript received September 10, 2013.

Tyurin S.F. is with the Perm National Research Politechnical University, Russia, e-mail: tyurinsergfeo@yandex.ru

Grekov A.V. is with the Perm Military Institute of Internal Troops of the Ministry of Internal Affairs of the Russian Federation, e-mail: grekartemvl@mail.ru

Gromov O.A. is with the Perm National Research Politechnical University, Russia, e-mail: ogromov@inbox.ru

II. The Principle of Adaptation to Failure of 8-1 Multiplexer

Let us consider the gate FPGA - multiplexer with three address inputs x_1, x_2, x_3 – 8 channels a, b, c, d, e, f, g, h, (8-1), consisting of seven elementary multiplexers 2-1 (Fig. 1).

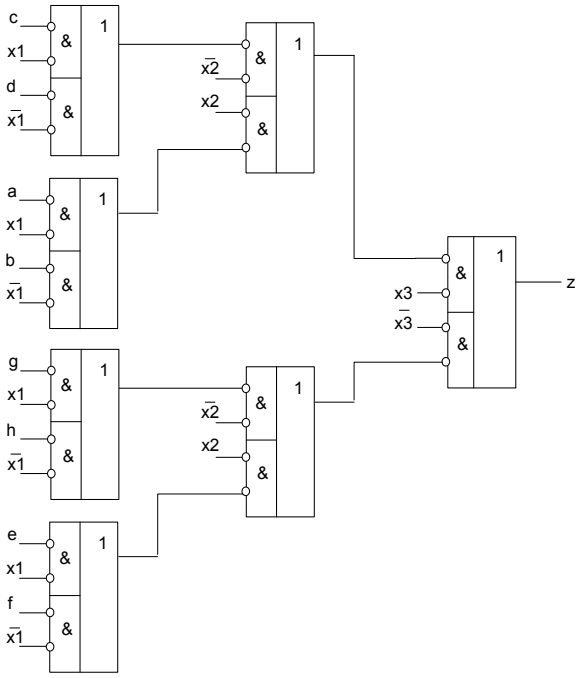

Fig. 1. The 8-1 multiplexer (eight channels), consisting of seven elementary multiplexers

On the assumption that there is not a single failure data inputs a, b, c, d, e, f, g, h, or not more than one failure in seven elementary multiplexers 2-1 propose the switch to the "half" of the scheme.

Let there be a failure in the element, which is connected to the input channels c, d. Then it is necessary to do after finding out the transition to the second half of the scheme – channels e, f, g, h. And the failures may occur on the input – but not of the last element.

When a fault is detected, for example, by external means, it is necessary to perform two tests – on the one and the other half. But this is allowed only in case of failure of elements and data inputs (one failure).

If there is half the items (allow refusal on the inputs of all the elements and even by choice but out on the exit of the last element), for example, the older variable is equal to zero:

$$z = \overline{\bar{0}\ \overline{x_2(cx_1 \vee dx_1)} \vee \bar{x}_2(ax_1 \vee bx_1)} \vee \overline{\bar{0}\ \overline{x_2(gx_1 \vee hx_1)} \vee \bar{x}_2(ex_1 \vee fx_1)} \quad (1)$$

Then we get:

$$z = \overline{\bar{0}\ \overline{x_2(cx_1 \vee dx_1)} \vee \bar{x}_2(ax_1 \vee bx_1)} \quad (2)$$

or

$$z_1 = \overline{x_2(cx_1 \vee dx_1)} \vee \bar{x}_2(ax_1 \vee bx_1) \quad (3).$$

The second half of channels will be implemented similarly:

$$z_2 = \overline{x_2(gx_1 \vee hx_1)} \vee \bar{x}_2(ex_1 \vee fx_1) \quad (4).$$

That is, to restore one eight-channel multiplexer of the three "half" of the four channels is necessary, so that the third multiplexer plug on the leading variable either one or the other half, that is operated in a two-channel multiplexer.

Therefore, to set up the third component is necessary to:

$$z_3 = \bar{x}_3(\overline{\bar{z}_1\bar{0} \vee \bar{1}\bar{0}}) \vee x_3(\overline{\bar{z}_2\bar{0} \vee \bar{1}\bar{0}}), \quad (5)$$

which corresponds to the two-channel multiplexer functions

$$z_3 = z_1\bar{x}_3 \vee z_2 x_3 \ . \quad (6)$$

If there is a failure (one-time constant) to the address inputs – everything is much more complicated.

Table I shows how to rewire channels to counter such denial. Accordingly, the process of failure detecting is getting slow.

TABLE I

REQUIRED RECONNECT CHANNELS WITH CONSTANT DENIALS EIGHT-CHANNEL MULTIPLEXER ADDRESS INPUTS

x_2	x_1	x_0	No fault	Failure					
				x_2^0	x_2^1	x_1^0	x_1^1	x_0^0	x_0^1
0	0	0	0	0	4	0	2	0	1
0	0	1	1	1	5	1	3	0	1
0	1	0	2	2	6	0	2	2	3
0	1	1	3	3	7	1	3	2	3
1	0	0	4	0	4	4	6	4	5
1	0	1	5	1	5	5	7	4	5
1	1	0	6	2	6	4	6	6	6
1	1	1	7	3	7	5	7	6	6

"Half" of the logical elements can be used alone, but to restore a full multiplexer requires three "half" of the multiplexer.

III. FEATURES OF FPGA LOGIC ELEMENTS

Currently, FPGA contain configurable logic blocks (CLB) [1, 7], consisting of the logic elements, programmable local and global matrix connections MC – Fig. 2.

Logic gate FPGA - is a super redundant basis, and it is constructed as a read-only memory ROM (LUT - Look Up Table), which is a variable for the four multiplexer 16-1 (tree multiplexers), input data is set up so-called configurable memory cells [1] – Fig. 3.

In Fig. 3 inputs – S_0, S_1, S_2, S_3, the element is set to implement the sum modulo two $S_0 \oplus S_1 \oplus S_2 \oplus S_3$. On a specific set of variables is realized the only way from input to output, for example, from input 14: S3S2S1 (not S_0) [1].

Elementary multiplexers 2-1 is implemented as a switch (this is also a multiplexer) for example, on the basis of two chains of two transmit MOS transistors [1] - Fig. 4.

Memory configuration (configuration data logic elements and matrices compounds) - this is the configurational cells, each of them contains six transistors [1, 8].

IV. FEATURES OF ADAPTATION TO FAILURES OF TRANSISTORS AND INPUTS OF LUT FPGA

Given the great redundancy logic elements on the basis of the conversion tables LUT, it is possible to restore the faulty conversion table. It is obvious that in this case there is a loss of functionality, but even LUT with limited functionality can be used for the synthesis of a large number of Boolean functions.

Let us consider a simple model of single constant failures. And we shall consider themselves as failures based transistors, which are built LUT, and the failure of address inputs.

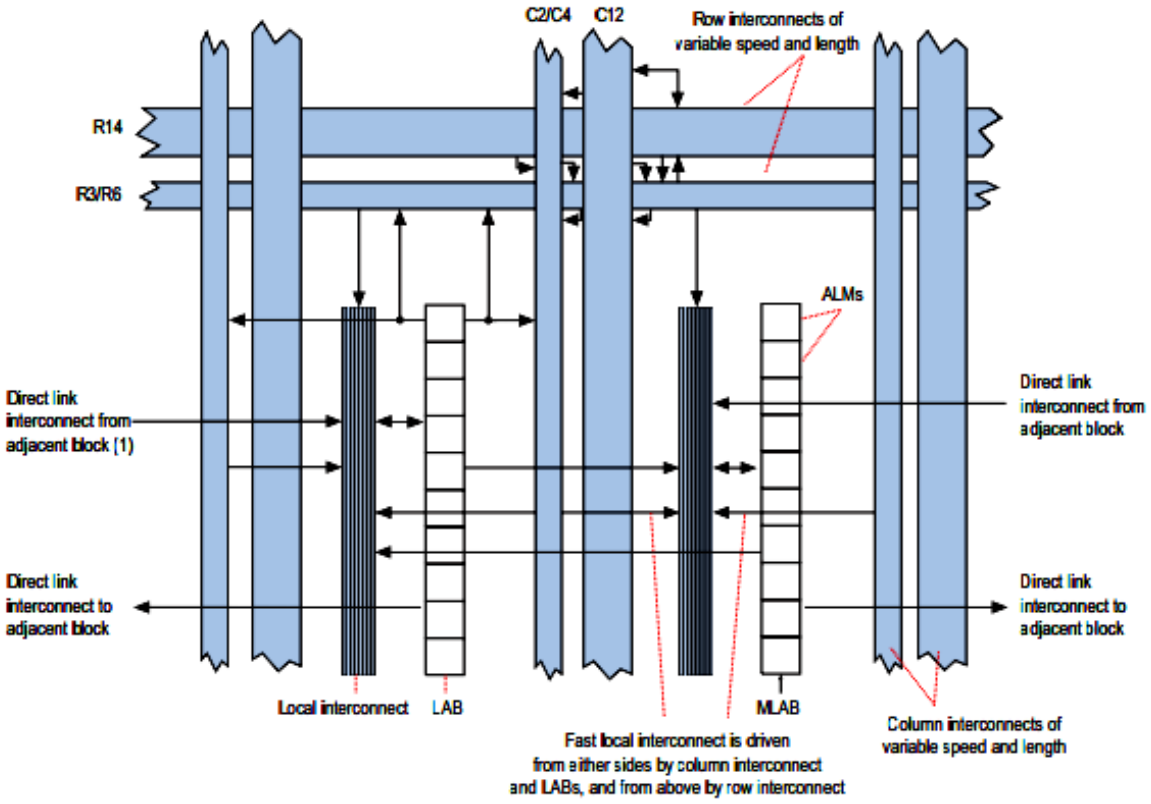

Fig. 2. Configurable logic block of Altera's FPGA

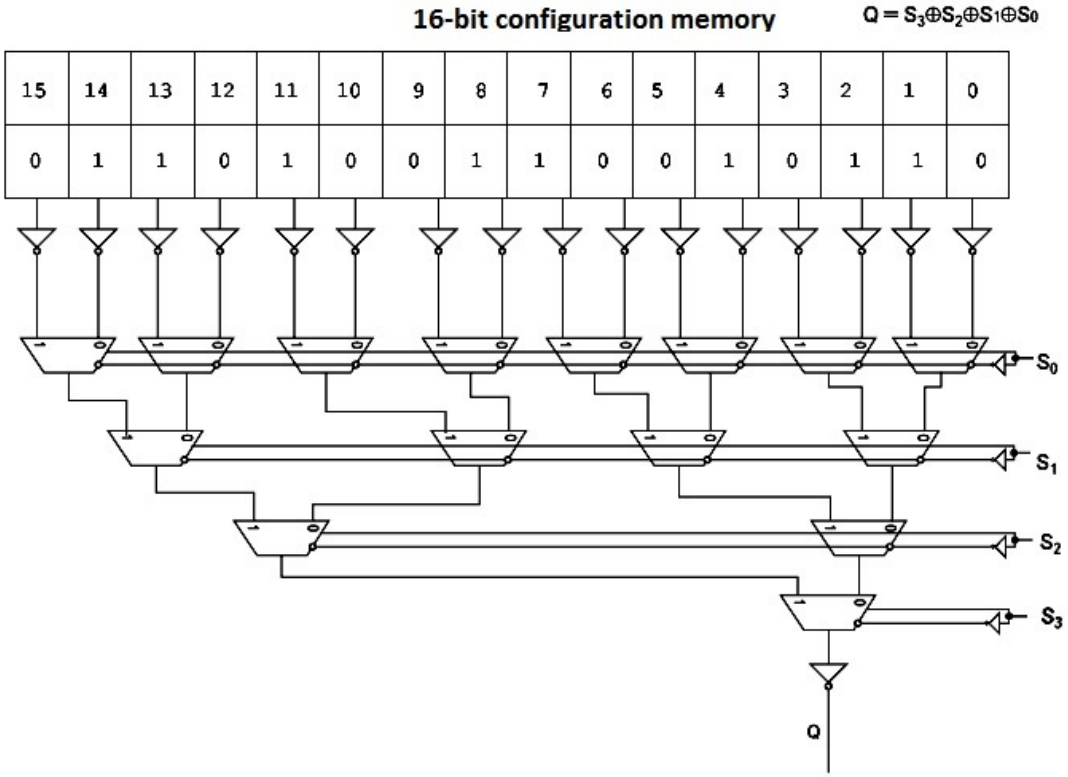

Fig. 3. Conversion table (Look-up Table) of FPGA

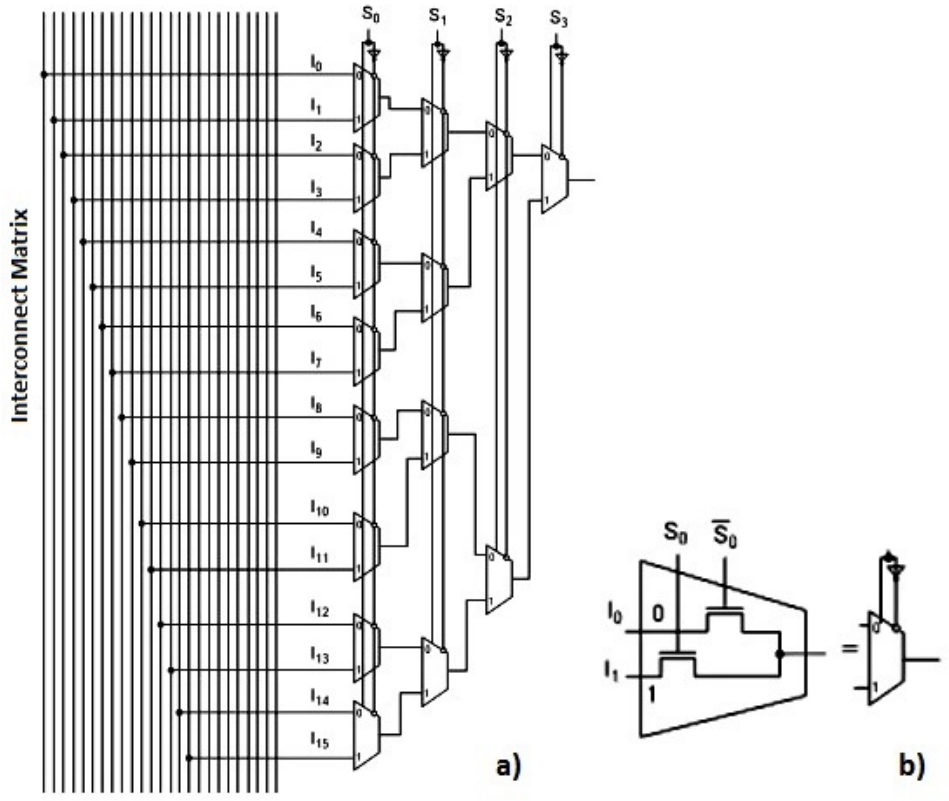

Fig. 4. The switch signals from the local interconnect to the input CLB: multiplexers' tree (a), implementation of the multiplexer transmitting MOSFETs (b)

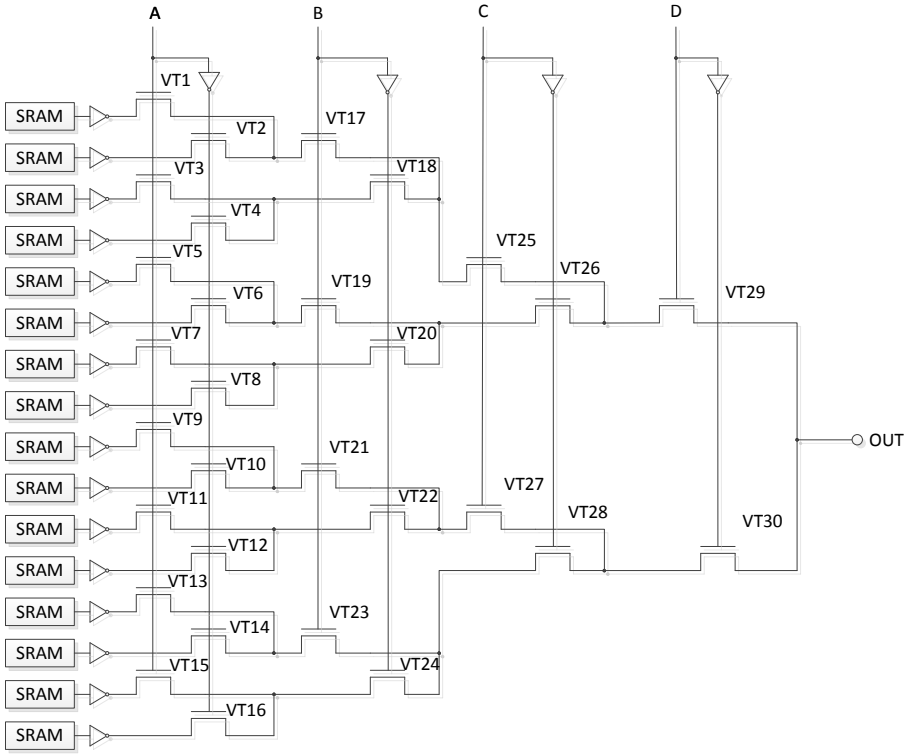

Figure 5. Modeling failure of transistors in LUT

Input failure provides that the address input LUT has fixed logic level "0" and "1." A constant refusal to "1" in the CMOS transistor circuit includes sample source-drain or latching gate. A constant refusal to "0" CMOS transistor – is an open circuit source-drain or open the shutter.

Consider the possible cases of failure of the transistor.

Suppose there was a single constant denial of transistor VT29 (Fig. 5).

If you set a single constant refusal to "0", in this case, the upper part of the network goes down, because the information from the SRAM cells that are connected to transistors VT1-VT8, can not be transferred to the output. But setting D=0, we can always connect the bottom of the exit and realize the function of three variables A, B and C. If you set up once the constant refusal of "1", the top part of the circuit is always connected to the output. In this case, setting D=1, turn off the lower part of the scheme and prevent the occurrence of faults. At the top of the chart can also be synthesized function of three variables A, B, C.

Consider the failures in transistors connected to the line C. Suppose there was a single constant refusal to "0" in the transistor VT27. This means that the information from the SRAM cells that are connected to the transistors VT9-VT11, will never be passed on to the input. However, you can set C=0 and for all open transistors VT28 and VT26. Then we can implement the function of three variables A, B and D. In the event of a "1" on the transistor VT27, can not turn this thread from the transistor VT30. But setting C=1, we will close the transistors VT26 and VT28. Here again we can implement arbitrary functions of three variables A, B and D.

Consider the failures in transistors, which are connected to the line B. Let there was a failure to "0" in the transistor VT19. This means that the transistors and VT5 VT6, can never be switched to the input of the transistor VT26. Filed B=0 we open transistor VT18, VT20, VT22 and VT24. In this case the cells 1,2,5,6,9,10,13,14 will not be used when using LUT. However, in the remaining 8 SRAM can build the function of 3 variables A, C, and D. In the event of a "1" in the transistor VT19, is served B=1 and also implement a function of three variables A, C, and D from the remaining cells and SRAM transistors.

Suppose there was a failure in the transistor of the first stage, for example, not "0" in the transistor VT7. In this case, we can work with even the SRAM cell, it needs to set A=0. In this case, we can construct a function of the variables B, C and D. In case of refusal to "1" in the transistor VT7, similarly set A=1 and work with odd SRAM cells. Here, again, the remaining elements can be synthesized function of three variables B, C and D.

It is obvious that a similar situation will occur during the failure of the other transistors. Thus, a single failure in any transistor reduces the functionality of the item, however, due to the large redundancy is still possible to build a function of three input variables.

At single constant failures of the inputs LUT actually enforce the same situation arises that in case of failure of transistors. That is forcibly turned off one half of the LUT and a conversion table is converted from the multiplexer 16 to 1 in 8 to 1 multiplexer. But in this case it is also possible to synthesize a function of three variables.

V. Conclusion

Thus, this article presents an approach for FPGA logic partial recovery for critical applications by adapting to failures of logic elements based on the Look Up Table. The principle and the example of recovery of the LUT in single constant failures of transistors and inputs - go to the "half" or, more precisely, a "partial" functional. Use classical LUT for 4 variables, however, the same procedure can be applied to a larger number of LUT inputs. This gives rise to new opportunities parry multiple failures in a more complex tree transistors.

In the case of failure of hardware (logic elements) after massive failures, for example, in catastrophic situations, it is also possible software-hardware utilization failed elements.

In the future, should spread this approach, which could be called "partial firmware functionality" in other areas – for the implementation of energy-efficient FPGA.

In addition, it is useful to explore the possibility of using partial functionality for diagnosing FPGA.

References

[1] S. Tsibin. Programmable switching FPGA: a view from the inside. [Electronic resourse]. – Access to: http://www.kit-e.ru/articles/plis/2010_11_56.php – 12.11.2012.

[2] Yervant Z. Gest editors' introduction: Design for Yield and reliability/ Z. Yervant, G. Dmytris // IEEE Design & Test of Computers. - May-June 2004.-P. 177-182.

[3] E. L. Post, The two-valued iterative systems of mathematical logic, Annals of Mathematics studies, no. 5, Princeton University Press, Princeton 1941, 122 pp.

[4] Tyurin S.F. Retention of functional completeness of boolean functions under "failures" of the arguments. Automation and Remote Control. 1999. T. 60. № 9 part 2. P. 1360-1367.

[5] Tyurin S.F., Kharchenko V.S. Redundant Basises for Critical Systems and Infrastructures: General Approach and Variants of ImplementationProceedings of the 1st Intrenational Workshop on Critical Infrastructures Safety and Security, Kirovograd, Ukraine 11-13, May, 2011 / Kharchenko V., Tagarev V. (edits), Vol., 2, P. 300-307.

[6] Tyurin S.F., Kharchenko V.S., Timonkin G.N., Melnikov V.A. The hardware and software implementation of logic algorithms in microprocessor systems / / Foreign electronics. - 1992.- № 2.- P. 24-36.

[7] Look up table implementation of fast carry for adders and counters: US 005274581A, 28.12.1993.

[8] 6T SRAM Cell [Electronic resourse]. – Access to: //http: //www.iue.tuwien.ac.at/ phd/ entner/node34.html – 12.12.2012.

Design of Steganographic System on the Basis of a Code Container in Nonequilibrium Positional Base

Barannik V.V., Bekirov A.E., Hahanova A.V.

Abstract — **In this article the existing methods of direct embedding are analyzed. For elimination of the revealed shortcomings it is offered to use structural redundancy. It is shown that using of nonequilibrium positional base of the bases in case of code container forming for NP number led to appearance of structural redundancy. Use of the revealed potential structural redundancy for information embedding is offered. The steganographic diagram on the basis of code container formation for number without the implanted data is designed.**

Index Terms — **codegram, code container, diagram, method, nonequilibrium, positional base, steganographic.**

I. INTRODUCTION

Owing to wide implementation of the modern special systems of automated management appears need to increase safety of information resources using, both in usual conditions, and in crisis situations.

One of possible methods of the hidden data transfer in the communication links consists in data transfers with use of steganographic technology of embedding. In case of steganographic embedding of data, the fact of presence hidden information in a data stream for malefactor isn't known and the digital container with the built-in confidential message is unknown. Therefore, steganographic algorithms create additional opportunity for avoiding of exception of the hidden information.

At the same time, for detection of the fact of hidden information existence or its destruction in the course of a steganalysis, the opponent can apply passive and active attacks.

One of the most widespread steganographic methods of embedding information in the image container are algorithms of direct embedding in elements of spatial-temporal and spatial-spectral representation of the initial container.

For the existing technologies, process of the direct embedding represents changeover of one bit of the initial element-container by bit of the hidden message. Changeover of bits happens according to some functionality and can be described by expression:

$$A'_2 = \varphi_2(A_2, b_\xi),\ a_i := b_\xi,\ i = \overline{1, n}.$$

Here A'_2 - number-steganogram wich contained ξ-th hidden bit.

Efficiency of direct embedding methods will depend on i-th position of a_i element (bit) of the initial image container which is replaced with an element of the hidden message.

In case of embedding bit of the confidential message in high bit of the initial number increase of resistance of the built-in data to the active attacks is reached, but considerable visual distortions are appeared. On the contrary, embedding in low bit of the confidential message is characterized by low resistance of the built-in data to attacks, but the minimum visual distortions are provided.

In turn for special systems it is necessary to transmit of necessary information volumes. And volumes of operational information which need to be hidden from the opponent permanently increase. But for the existing steganographic system, the increasing volume of embeddable data is followed by growth of quantity of the distorted elements that sharply reduces stability of a steganogram. Therefore there is a need of increase of steganogram resistance to visual attacks at the given volume of embeddable data. From here, the *purpose of researches* of article is designing of steganographic system $F\{A;\ f(A);\ f^{-1}(A');\ B_2\}$ for which it is at the same time reached:

1. Increase of its resistance to passive and active attacks, i.e.

$$\varepsilon(A; A') \to \min \text{ and } P_{iz}(b'_\xi = b_\xi) \to 1$$

2. Support of data embedding, with w_{BCT} volume, not smaller, than the required volume w_{tr}, i.e.

$$w_{vst} \geq w_{tr}.$$

Manuscript received September 17, 2013.

Barannik V.V. is with the Kharkov University of Air Forces, Kharkov, Ukraine, e-mail: barannik_v_v@mail.ru.

Bekirov Ali Enverovich is with the Kharkov National University of Radio Electronics, Kharkov, Ukraine.

Hahanova A.V. is with the Kharkov National University of Radio Electronics, Kharkov, Ukraine, e-mail: anna_hahan@mail.ru.

II. Design of a steganographic system

Shortcomings of the existing methods of direct embedding of the hidden information are caused by that in the course of embedding generally psycho visual regularities (psycho visual redundancy) are considered. Therefore for elimination of the revealed shortcomings it is offered to consider regularities (types of redundancy) which aren't connected with visual apparatus in the course of embedding of the hidden information.

One of such approaches is the approach based on detection of structural regularities (the accounting of structural redundancy).

For design of a steganographic system it is offered to use structural regularities which exist in the image container, caused by existence of restrictions on dynamic range.

Value ψ_i of dynamic range of array line of the image container $A = \{a_{i,j}\}$ is defined as a difference between maximum $a_{i,max}$ and minimum $a_{i,min}$ values of elements in i-th line (fig. 1), i.e.

$$\psi_i = (a_{i,max} - a_{i,min}) + 1 \ .$$

Value ψ_j of dynamic range j-th column of an array of the image container $A = \{a_{i,j}\}$ is defined as a difference between maximum $a_{j,max}$ and $a_{j,min}$ minimum values of j-th column components, i.e.

$$\psi_j = (a_{j,max} - a_{j,min}) + 1 \ .$$

As non-uniformity of dynamic ranges is characteristic both for lines, and for array columns of image container A, the inequality is generally executed:

$$\psi_i \neq \psi_j .$$

Therefore for increase of accuracy of dynamic range determination of $a_{i,j}$ element it is necessary to consider non-uniformity of the ranges in two directions of an array of the image container A. In case of such approach the dynamic range will be equal to value $\psi_{i,j}$, i.e.

$$\psi_{i,j} = \min(\psi_i;\ \psi_j) .$$

Properties to consider restrictions on dynamic range, in the course of representation and coding, nonequilibrium positional (NP) representation is possess. Therefore it is offered to project steganographic system on the basis of a code formation functionality taking into account NP base.

Properties to consider restrictions on dynamic range, in the course of representation and coding, nonequilibrium positional (NP) representation is possess. Therefore it is offered to project steganographic system on the basis of a code formation functionality taking into account NP base.

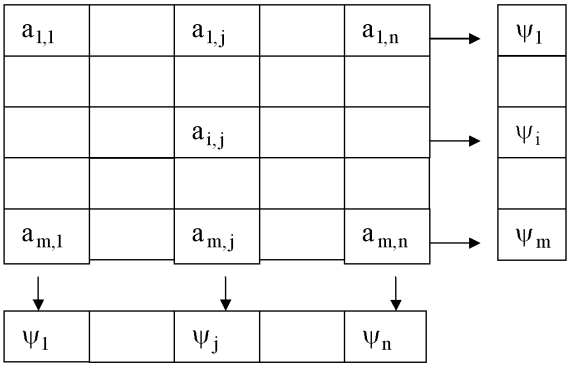

Fig. 1. The diagram of formation of dynamic range base for the image container A

In implementation process of the functional conversion on the basis of nonequilibrium positional coding the area of the source image containing set of video sequences is considered as a set of nonequilibrium positional numbers $\{A(j)\}$. Here the nonequilibrium positional number $A(j)$ without implantation for j-th a column of an array of a video image consists of m elements, i.e.

$$A(j) = \{a_{1,j}; ...; a_{i,j}; ...; a_{m,j}\} .$$

At this stage structural redundancy isn't reduced yet. Elimination of structural redundancy is carried out at the second stage in the course of coding of NP number $A(j)$ without implantation (fig. 2). The rule $f(A(j))$ provides formation of a code container $N(j)$ for nonequilibrium positional number $A(j)$ without implanted element on a formula:

$$N(j) = \sum_{i=1}^{m} a_{i,j} \ V_{i,j} ,$$

where $a_{i,j}$ - the $(i; j)$- th element of NP number $A(j)$ before implantation; $V_{i,j}$ - weight factor of the $a_{i,j}$ element of NP number $A(j)$ without implantation in a code container.

The weight factor $V_{i,j}$ of $a_{i,j}$ element is defined as stored product of elements low bases of NP number, i.e.

$$V_{i,j} = \prod_{\xi=i+1}^{m} \psi_{\xi,j} ,$$

where $\psi_{i,j}$ - $(i; j)$-th element base of nonequilibrium positional number without implantation.

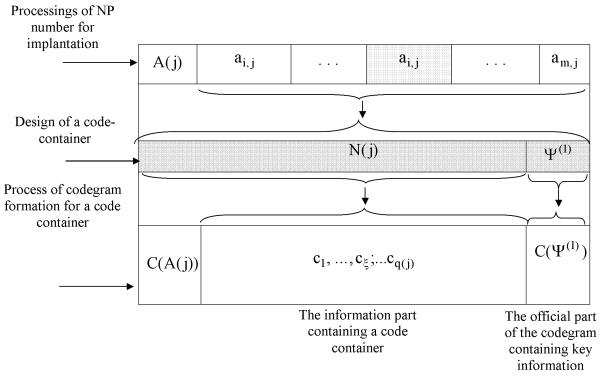

Fig. 2. Design of direct conversion for a steganogramma on the basis of formation of a code container in nonequilibrium positional base

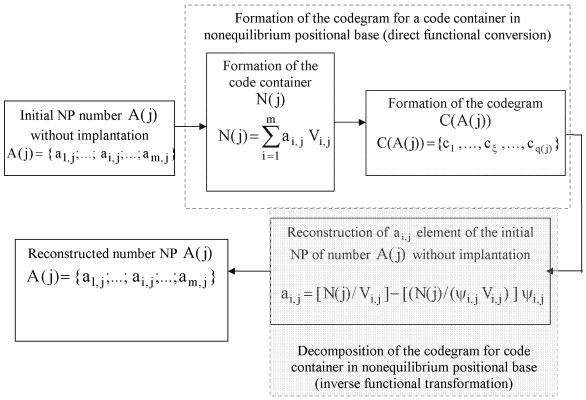

Fig. 3. The diagram of the project for steganographic system on the basis of formation of a code container with nonequilibrium system.

At this stage information embedding process will actually come to an end.

The codegram $C(A(j))$ for a code container $N(j)$ of nonequilibrium positional number $A(j)$ without implantation is created at the third stage by means of the operator of bits allocating $\varphi_c(\bullet)$ be a formula:

$$C(A(j)) = \varphi_c(N(j), \Psi^{(1)}) = \varphi_c(A(j); \Psi^{(1)}; V),$$

where $\Psi^{(1)}$ - the key component containing system of NPN bases; V - values of weight factors of the NPN $A(j)$ elements.

In this case we will receive the following codegram:

$$C(A(j)) = \{c_1, \ldots, c_\xi, \ldots, c_{q(j)}\},$$

where $q(j)$ - is length of the binary codegram $C(A(j))$; c_ξ - ξ - th binary place of the codegram $C(A(j))$.

Process of reconstruction of $a_{i,j}$ element for nonequilibrium positional number $A(j)$ without the built-in information on the basis of a code container $N(j)$ is executed on a formula:

$$a_{i,j} = [N(j)/V_{i,j}] - [(N(j)/(\psi_{i,j} V_{i,j}))] \psi_{i,j}$$

or

$$a_{i,j} = [\sum_{i=1}^{m} a_{i,j} V_{i,j} / V_{i,j}] - [\sum_{i=1}^{m} a_{i,j} V_{i,j} / (\psi_{i,j} V_{i,j})] \psi_{i,j}.$$

Such conversion is carried out without introduction of distortions.

In Fig. 3 stages of formation of the codegram $C(A(j))$ for the number NP code container $N(j)$ of NP number (direct nonequilibrium positional conversion) and its decomposition (inverse nonequilibrium positional transformation) are graphically displayed.

The key component $\Psi^{(1)}$ includes information about system of the bases $\Psi^{(1)} = \{\psi_{i,j}\}$ of nonequilibrium positional number without implantation. The base $\psi_{i,j}$ is defined as the minimum value from two dynamic ranges of a line ψ_i and a column ψ_j on which intersection it is located, i.e.

$$\psi_{i,j} = \min(\psi_i; \psi_j).$$

In design process of steganographic system on the basis of the selected base for NP number without implantation the codegram $C(A(j))$ for code container $N(j)$ of number $A(j)$ is created. In the computing plan the operator of bits allocating $\varphi_c(\bullet)$, considering expression (1), represents stratification of bit sequences.

Determination. Bit sequences which contained information about $a_{i,j} V_{i,j}$ values in the course of code container formation we will call as a bit planes $C_{i,j}$, i.e.

$$C_{i,j} = [a_{i,j} V_{i,j}]_2.$$

Here $[a_{i,j} V_{i,j}]_2$ - means binary notation of $a_{i,j} V_{i,j}$ which contains in i-th bit plane. The length of bit plane $C_{i,j}$ equals $q_{i,j}$ bit.

In the course of code container formation $N(j)$ the values $a_{i,j} V_{i,j}$ accept different value, namely

$$a_{i,j} V_{i,j} \neq a_{i+1,j} V_{i+1,j}.$$

From here values $a_{i,j} V_{i,j}$, will be nonequilibrium.

The minimum quantity of bits which are necessary on representation of values $a_{i,j} V_{i,j}$ will also be different, i.e.

$$[\log_2 a_{i,j} V_{i,j}] + 1 \neq [\log_2 a_{i+1,j} V_{i+1,j}] + 1.$$

Therefore bit planes $C_{i,j}$ will have different length. In other words, such bit planes will be non-uniform.

It is necessary to consider that value of a code container $N(j)$ of nonequilibrium positional number $A(j)$ registers, as the stored amount of values $a_{i,j} V_{i,j}$, i.e.

$$N(j) = a_{1,j} V_{1,j} + ... + a_{i,j} V_{i,j} + ... + a_{m,j} V_{m,j}.$$

Then process of $C(A(j))$ codegram formation can be considered as nonequilibrium merge of non-uniform bit planes $C_{i,j}$. It is set by the following formula:

$$C(A(j)) = [N(j)]_2 = [a_{1,j} V_{1,j}]_2 + ... + [a_{i,j} V_{i,j}]_2 +$$

$$+ ... + [a_{m,j} V_{m,j}]_2 = \bigcup_{i=1}^{m} C_{i,j},$$

where $[N(j)]_2$ - the binary notation of value of a code container defining contents of the output codegram.

From position of protection for hidden information, process of $C(A(j))$ codegram formation owing to nonequilibrium merge of non-uniform bit planes has advantages in comparison with merge of equilibrium bit planes.

As an example of direct nonequilibrium positional conversion we will consider process of codegram formation of a code container for nonequilibrium positional number $A(j) = (3;5;2;6)$ without the implanted element with system of the bases $\Psi^{(1)} = (7,6,6,8)$. In Tab. II the intermediate values of values which were used for obtaining the $C(A(j))$ codegram are displayed. Value of the codegram is determined by a formula:

$$C(A(j)) = [864]_2 + [240]_2 + [16]_2 + [6]_2 = [1126]_2$$

TABLE I
THE INTERMEDIATE VALUES WHICH ARE USED FOR OBTAINING THE CODEGRAM $C(A(j))$

i	$a_{i,j}$	$V_{i,j}$	$a_{i,j}V_{i,j}$	$C_{i,j}$	$[\log_2 a_{i,j}V_{i,j}]+1$	$C(A(j))$
1	3	288	864	1101100000	10	
2	5	48	240	11110000	8	
3	2	8	16	10000	5	1126
4	6	1	6	110	3	

Value of weight factor $V_{i,j}$ of an element $a_{i,j}$ is in tab. 2 calculates as stored product of elements low bases of NP number $A(j)$ without the implanted element on a formula:

$$V_{i,j} = \prod_{\xi=i+1}^{m} \psi_{\xi,j}.$$

Therefore value of weight factor $V_{i,j}$ of an $a_{i,j}$ element will decrease with increasing of a value of its position in NP number. Such change will be reflected in binary representation of values $a_{i,j}V_{i,j}$ on the basis which the appropriate bit planes of the codegram are created $C(A(j))$.

From here length $q(j)$ of code representation of information part of the nonequilibrium positional number codegram without the implanted element is defined on the basis of the following expression:

$$q(j) = |C(A(j))| = [\ell og_2 \prod_{i=1}^{m} \psi_{i,j}] + 1 = 11 \text{ (bits)}.$$

From this it follows that:

1. In case of the codegram formation on the basis of nonequilibrium base $\Psi^{(1)} = (7,6,6,8)$, the bit planes which create the codegram are inadequate. In other words, in process of $C(A(j))$ codegram formation there is a merge of bit planes $C_{i,j}$. Such approach excludes possibility of obtaining original values of bit planes by the malefactor in the conditions when he didn't have nonequilibrium system of the bases.

2. In process of $C(A(j))$ codegram forming with use of NP base of the bases length $q(j)$ of binary submission $\Psi^{(1)} = (7,6,6,8)$ of the codegram are smaller then length of the codegram created for the fixed system ψ. Reduction of quantity of the bits necessary for displaying of the codegram $C(A(j))$ is caused by elimination of structural redundancy due to detection of non-equilibrium of the bases in the course of code container formation.

It is necessary to estimate value of structural redundancy which potentially can be used for embedding of information in a code container. For this purpose we will compare number of bits $q_{исх}$ necessary for binary representation of number $A(j)$ of the initial video sequence with the fixed dynamic range and number of bits $q(j)$ necessary for submission of the codegram $C(A(j))$.

Values of brightness of an element spatial-temporal submission of the image container in RGB system can accept values $a_{i,j} \in [0;255]$, In other words, for each i-th element of number $A(j) = \{a_{i,j}\}$ of the initial video sequence value of dynamic range will be equal 256. Value $q_{исх}$ will be described by expression:

$$q_{исх} = m \cdot \log_2 256 = 8 \cdot m \text{ (bits)}.$$

We will define quantity $q(j)$ of bits, necessary for representation of $C(A(j))$ codegram, received in the course of $N(j)$ code container formation for NP number $A(j)$. On the basis of nonequilibrium positional numbers $A(j)$ property it is possible to conclude that for the given base $\Psi^{(1)}$ of the bases the greatest possible value of a code container $N(j)$ will be restricted on top of the stored product V_{max} of the NP numbers elements. It is set by the following expression:

$$N(j) \le V_{max} = \prod_{i=1}^{m} \psi_{i,j} - 1 .$$

In other words, value V_{max} defines quantity of different codes containers which can be created for the given system of the bases $\Psi^{(1)}$.

From here, length $q(j)$ of the codegram of code containers $N(j)$ information part is defined on the basis of the following expression:

$$q(j) = |C(A(j))| = [\ell og_2 \prod_{i=1}^{m} \psi_{i,j}] + 1 =$$

$$[\sum_{i=1}^{m} \ell og_2 \psi_{i,j}] + 1 \text{ (bits)}.$$

It is necessary to consider that the base of elements of spatial-temporal representation of the initial video sequence is accepted by values $\psi_{i,j} \in [1;256]$. Then the quantity of bits $q(j)$ which necessary for binary submission of the code container $N(j)$ codegram $C(A(j))$ will accept value:

$$q(j) = C(A(j)) \in [0; 8 \cdot m] \text{ (bits)}.$$

Taking into account that the amount of structural redundancy $R(j)$ is calculated as a difference between quantity $q(j)$ of bits for binary submission of the codegram $C(A(j))$ and quantity $q_{исх}$ of the bits necessary for binary representation of the initial video sequences $A(j)$ and is described by expression: $R(j) = q_{исх} - q(j)$.

Here $R(j)$ - the structural redundancy evolving from code container formation for NP number $A(j)$ in the course of the functional conversion. In other words, it is the redundancy arising in the course of formation of a code container $N(j)$ for NP number $A(j)$ as a result of formation of nonequilibrium base of the bases relative to code representation of the initial video sequence.

III Conclusion

1. Methods of direct embedding which have advantages in comparison with other methods are considered. However there is a contradiction between stability of the embedded data and their volume in case of embedding on different positions of initial container elements.

2. For elimination of this contradiction the approach based on detection of structural regularities (the accounting of structural redundancy) of spatial-temporal representation is offered. For the accounting of structural redundancy, it is offered to synthesize the functionality $f(\bullet)$ which realizes conversion in steganographic system taking into account restrictions on dynamic range. As such functionality considering restrictions on dynamic range in the course of conversion it is offered to use code formation function taking into account nonequilibrium positional base.

3. The steganographic system on the basis of code container formation of a code container for NP number with nonequilibrium base of the bases is designed. In implementation process of the functional conversion, on the basis of the rule $f(A(j))$ the code container $N(j)$ for number $A(j)$ with NP base of the bases $\Psi^{(1)}$ is created. In process of $C(A(j))$ codegram formation concealment of values of bits planes are merges. Such approach excludes possibility of obtaining original values of bit planes by the malefactor in the conditions when he didn't have the nonequilibrium system of the bases and creates potential for the hidden embedding of information. Detection of non-equilibrium of the bases due to restrictions on dynamic range in the course of formation of the codegram carries to elimination of structural redundancy of code representation of number $A(j)$.

Scientific novelty. The steganographic code container on the basis of direct embedding of an element in the container is first designed. In difference from other systems, the code container as a result of the functional conversion for nonequilibrium positional number is created. It provides potential opportunity for embedding information in the course of coding on the basis of the structural redundancy accounting of the image.

4. Reconstruction of the NP initial elements of number $A(j)$ without implantation happens without introduction of errors and distortions. From here, code formation function on the basis of nonequilibrium positional base can be used as the functional conversion for number with the built-in information.

References

[1] Gribunin V.G., Okov I.N., Turincev I.V., Cifrovaja steganografija- M.: Solon-Press, 2002 .- 272 s.

[2] Konahovich G.F., Puzyrenko A.J., Komp'juternaja steganografija. Teorija i praktika.- K.: « MK-Press» 2006. – 288s.

[3] Vladimir Barannik. Quality indicators for steganographic transformations of images/ Vladimir Barannik, Bekirov Ali, Konstantin Tryfonenko// XIIth International Conference ["Modern Problems of Radio Engineering, Telecommunications and Computer Science, TCSET'2014 "], (Lviv-Slavske, Ukraine, February 25 – March 1, 2014) / Lviv-Slavske: 2014. – P. 533.

[4] Barannik V.V. Tehnologija neravnovesnogo pozicionnogo kodirovanija dlja funkcional'nogo preobrazovanija chisel so vstroennoj informacii/ V.V. Barannik, J.N. Rjabuha, A.E. Bekirov.// Radiojelektronnye komp'juternye sistemy-2014- №4. S.23-32.

[5] A.E. Bekirov Puti povyshenija bezopasnosti informacionnyh resursov v sistemah special'nogo naznachenija // Suchasna special'na tehnika. - №1. – 2014. – S. 25 – 33.

[6] Barannik V.V. Metod formuvannja funkcionala steganografichnogo koduvannja stijkogo do stegano-atak / V.V. Barannik, A.E. Bekirov //ASU ta priladi avtomatiki. - 2013. - Vip.165. S. 34 – 43.

Barannik Vladimir Viktorovich, professor, Doctor in Sciences, chief of department Kharkov university of Air Forces. Scientific interests: telecommunications systems and information technology.

Bekirov Ali Enverovich, aspirant in Kharkiv National University of Radio Electronics. Scientific interests: processing and transmission of information.

Anna Vladimirovna Hahanova, Ph.D, Ass. Prof. in Kharkiv National University of Radio Electronics. Scientific interests: telecommunications systems and information technology.

Preparation of Papers for IEEE TRANSACTIONS and JOURNALS

First A. Author, Second B. Author, Jr., and Third C. Author, *Member, IEEE*

***Abstract*—These instructions give you guidelines for preparing papers for IEEE TRANSACTIONS and JOURNALS. Use this document as a template if you are using Microsoft *Word* 6.0 or later. Otherwise, use this document as an instruction set. The electronic file of your paper will be formatted further at IEEE. Define all symbols used in the abstract. Do not cite references in the abstract. Do not delete the blank line immediately above the abstract; it sets the footnote at the bottom of this column.**

***Index Terms*—About four key words or phrases in alphabetical order, separated by commas. For a list of suggested keywords, send a blank e-mail to keywords@ieee.org or visit** http://www.ieee.org/organizations/pubs/ani_prod/keywrd98.txt

I. INTRODUCTION

THIS document is a template for Microsoft *Word* versions 6.0 or later. If you are reading a paper or PDF version of this document, please download the electronic file, TRANS-JOUR.DOC, from the IEEE Web site at http://www.ieee.org/web/publications/authors/transjnl/index.html so you can use it to prepare your manuscript. If you would prefer to use LATEX, download IEEE's LATEX style and sample files from the same Web page. Use these LATEX files for formatting, but please follow the instructions in TRANS-JOUR.DOC or TRANS-JOUR.PDF.

If your paper is intended for a *conference,* please contact your conference editor concerning acceptable word processor formats for your particular conference.

When you open TRANS-JOUR.DOC, select "Page Layout" from the "View" menu in the menu bar (View | Page Layout), which allows you to see the footnotes. Then, type over sections of TRANS-JOUR.DOC or cut and paste from another document and use markup styles. The pull-down style menu is at the left of the Formatting Toolbar at the top of your *Word* window (for example, the style at this point in the document is "Text"). Highlight a section that you want to designate with a certain style, then select the appropriate name on the style menu. The style will adjust your fonts and line spacing. **Do not change the font sizes or line spacing to squeeze more text into a limited number of pages.** Use italics for emphasis; do not underline.

To insert images in *Word,* position the cursor at the insertion point and either use Insert | Picture | From File or copy the image to the Windows clipboard and then Edit | Paste Special | Picture (with "float over text" unchecked).

IEEE will do the final formatting of your paper. If your paper is intended for a conference, please observe the conference page limits.

II. PROCEDURE FOR PAPER SUBMISSION

A. Review Stage

Please check with your editor on whether to submit your manuscript as hard copy or electronically for review. If hard copy, submit photocopies such that only one column appears per page. This will give your referees plenty of room to write comments. Send the number of copies specified by your editor (typically four). If submitted electronically, find out if your editor prefers submissions on disk or as e-mail attachments.

If you want to submit your file with one column electronically, please do the following:

--First, click on the View menu and choose Print Layout.

--Second, place your cursor in the first paragraph. Go to the Format menu, choose Columns, choose one column Layout, and choose "apply to whole document" from the dropdown menu.

--Third, click and drag the right margin bar to just over 4 inches in width.

Manuscript received November 8, 2011. (Write the date on which you submitted your paper for review.) This work was supported in part by the U.S. Department of Commerce under Grant BS123456 (sponsor and financial support acknowledgment goes here). Paper titles should be written in uppercase and lowercase letters, not all uppercase. Avoid writing long formulas with subscripts in the title; short formulas that identify the elements are fine (e.g., "Nd–Fe–B"). Do not write "(Invited)" in the title. Full names of authors are preferred in the author field, but are not required. Put a space between authors' initials.

F. A. Author is with the National Institute of Standards and Technology, Boulder, CO 80305 USA (corresponding author to provide phone: 303-555-5555; fax: 303-555-5555; e-mail: author@ boulder.nist.gov).

S. B. Author, Jr., was with Rice University, Houston, TX 77005 USA. He is now with the Department of Physics, Colorado State University, Fort Collins, CO 80523 USA (e-mail: author@lamar.colostate.edu).

T. C. Author is with the Electrical Engineering Department, University of Colorado, Boulder, CO 80309 USA, on leave from the National Research Institute for Metals, Tsukuba, Japan (e-mail: author@nrim.go.jp).

The graphics will stay in the "second" column, but you can drag them to the first column. Make the graphic wider to push out any text that may try to fill in next to the graphic.

B. Final Stage

When you submit your final version (after your paper has been accepted), print it in two-column format, including figures and tables. You must also send your final manuscript on a disk, via e-mail, or through a Web manuscript submission system as directed by the society contact. You may use *Zip* or CD-ROM disks for large files, or compress files using *Compress, Pkzip, Stuffit,* or *Gzip.*

Also, send a sheet of paper or PDF with complete contact information for all authors. Include full mailing addresses, telephone numbers, fax numbers, and e-mail addresses. This information will be used to send each author a complimentary copy of the journal in which the paper appears. In addition, designate one author as the "corresponding author." This is the author to whom proofs of the paper will be sent. Proofs are sent to the corresponding author only.

C. Figures

Format and save your graphic images using a suitable graphics processing program that will allow you to create the images as PostScript (PS), Encapsulated PostScript (EPS), or Tagged Image File Format (TIFF), sizes them, and adjusts the resolution settings. If you created your source files in one of the following you will be able to submit the graphics without converting to a PS, EPS, or TIFF file: Microsoft Word, Microsoft PowerPoint, Microsoft Excel, or Portable Document Format (PDF).

D. Electronic Image Files (Optional)

Import your source files in one of the following: Microsoft Word, Microsoft PowerPoint, Microsoft Excel, or Portable Document Format (PDF); you will be able to submit the graphics without converting to a PS, EPS, or TIFF files. Image quality is very important to how yours graphics will reproduce. Even though we can accept graphics in many formats, we cannot improve your graphics if they are poor quality when we receive them. If your graphic looks low in quality on your printer or monitor, please keep in mind that cannot improve the quality after submission.

If you are importing your graphics into this Word template, please use the following steps:

Under the option EDIT select PASTE SPECIAL. A dialog box will open, select paste picture, then click OK. Your figure should now be in the Word Document.

If you are preparing images in TIFF, EPS, or PS format, note the following. High-contrast line figures and tables should be prepared with 600 dpi resolution and saved with no compression, 1 bit per pixel (monochrome), with file names in the form of "fig3.tif" or "table1.tif."

Photographs and grayscale figures should be prepared with 300 dpi resolution and saved with no compression, 8 bits per pixel (grayscale).

Sizing of Graphics

Most charts graphs and tables are one column wide (3 1/2 inches or 21 picas) or two-column width (7 1/16 inches, 43 picas wide). We recommend that you avoid sizing figures less than one column wide, as extreme enlargements may distort your images and result in poor reproduction. Therefore, it is better if the image is slightly larger, as a minor reduction in size should not have an adverse affect the quality of the image.

Size of Author Photographs

The final printed size of an author photograph is exactly 1 inch wide by 1 1/4 inches long (6 picas × 7 1/2 picas). Please ensure that the author photographs you submit are proportioned similarly. If the author's photograph does not appear at the end of the paper, then please size it so that it is proportional to the standard size of 1 9/16 inches wide by 2 inches long (9 1/2 picas × 12 picas). JPEG files are only accepted for author photos.

How to create a PostScript File

First, download a PostScript printer driver from http://www.adobe.com/support/downloads/pdrvwin.htm (for Windows) or from http://www.adobe.com/support/downloads/ pdrvmac.htm (for Macintosh) and install the "Generic PostScript Printer" definition. In *Word,* paste your figure into a new document. Print to a file using the PostScript printer driver. File names should be of the form "fig5.ps." Use Open Type fonts when creating your figures, if possible. A listing of the acceptable fonts are as follows: Open Type Fonts: Times Roman, Helvetica, Helvetica Narrow, Courier, Symbol, Palatino, Avant Garde, Bookman, Zapf Chancery, Zapf Dingbats, and New Century Schoolbook.

Print Color Graphics Requirements

IEEE accepts color graphics in the following formats: EPS, PS, TIFF, Word, PowerPoint, Excel, and PDF. The resolution of a RGB color TIFF file should be 400 dpi.

When sending color graphics, please supply a high quality hard copy or PDF proof of each image. If we cannot achieve a satisfactory color match using the electronic version of your files, we will have your hard copy scanned. Any of the files types you provide will be converted to RGB color EPS files.

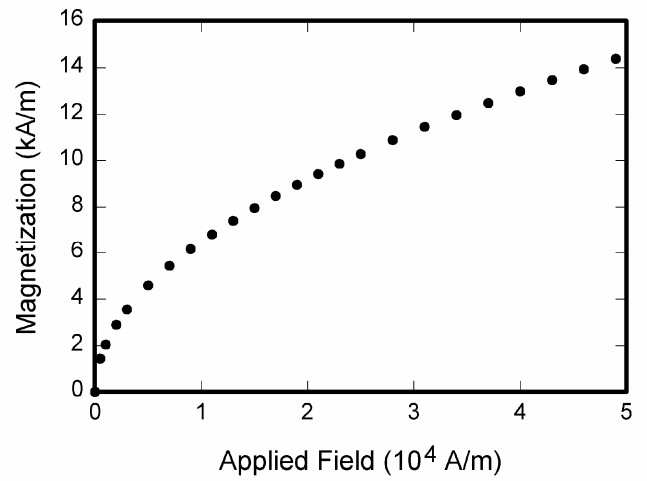

Fig. 1. Magnetization as a function of applied field. Note that "Fig." is abbreviated. There is a period after the figure number, followed by two spaces. It is good practice to explain the significance of the figure in the caption.

Web Color Graphics

IEEE accepts color graphics in the following formats: EPS, PS, TIFF, Word, PowerPoint, Excel, and PDF. The resolution of a RGB color TIFF file should be at least 400 dpi.

Your color graphic will be converted to grayscale if no separate grayscale file is provided. If a graphic is to appear in print as black and white, it should be saved and submitted as a black and white file. If a graphic is to appear in print or on IEEE Xplore in color, it should be submitted as RGB color.

Graphics Checker Tool

The IEEE Graphics Checker Tool enables users to check graphic files. The tool will check journal article graphic files against a set of rules for compliance with IEEE requirements. These requirements are designed to ensure sufficient image quality so they will look acceptable in print. After receiving a graphic or a set of graphics, the tool will check the files against a set of rules. A report will then be e-mailed listing each graphic and whether it met or failed to meet the requirements. If the file fails, a description of why and instructions on how to correct the problem will be sent. The IEEE Graphics Checker Tool is available at http://graphicsqc.ieee.org/

For more Information, contact the IEEE Graphics H-E-L-P Desk by e-mail at graphics@ieee.org. You will then receive an e-mail response and sometimes a request for a sample graphic for us to check.

E. Copyright Form

An IEEE copyright form should accompany your final submission. You can get a .pdf, .html, or .doc version at http://www.ieee.org/copyright. Authors are responsible for obtaining any security clearances.

TABLE I
UNITS FOR MAGNETIC PROPERTIES

Symbol	Quantity	Conversion from Gaussian and CGS EMU to SI [a]
Φ	magnetic flux	1 Mx $\rightarrow 10^{-8}$ Wb = 10^{-8} V·s
B	magnetic flux density, magnetic induction	1 G $\rightarrow 10^{-4}$ T = 10^{-4} Wb/m^2
H	magnetic field strength	1 Oe $\rightarrow 10^3/(4\pi)$ A/m
m	magnetic moment	1 erg/G = 1 emu $\rightarrow 10^{-3}$ A·m^2 = 10^{-3} J/T
M	magnetization	1 erg/(G·cm^3) = 1 emu/cm^3 $\rightarrow 10^3$ A/m
$4\pi M$	magnetization	1 G $\rightarrow 10^3/(4\pi)$ A/m
σ	specific magnetization	1 erg/(G·g) = 1 emu/g $\rightarrow$ 1 A·m^2/kg
j	magnetic dipole moment	1 erg/G = 1 emu $\rightarrow 4\pi \times 10^{-10}$ Wb·m
J	magnetic polarization	1 erg/(G·cm^3) = 1 emu/cm^3 $\rightarrow 4\pi \times 10^{-4}$ T
χ, κ	susceptibility	1 $\rightarrow 4\pi$
χ_ρ	mass susceptibility	1 cm^3/g $\rightarrow 4\pi \times 10^{-3}$ m^3/kg
μ	permeability	1 $\rightarrow 4\pi \times 10^{-7}$ H/m = $4\pi \times 10^{-7}$ Wb/(A·m)
μ_r	relative permeability	$\mu \rightarrow \mu_r$
w, W	energy density	1 erg/cm^3 $\rightarrow 10^{-1}$ J/m^3
N, D	demagnetizing factor	1 $\rightarrow 1/(4\pi)$

Vertical lines are optional in tables. Statements that serve as captions for the entire table do not need footnote letters.

[a]Gaussian units are the same as cgs emu for magnetostatics; Mx = maxwell, G = gauss, Oe = oersted; Wb = weber, V = volt, s = second, T = tesla, m = meter, A = ampere, J = joule, kg = kilogram, H = henry.

III. MATH

If you are using *Word,* use either the Microsoft Equation Editor or the *MathType* add-on (http://www.mathtype.com) for equations in your paper (Insert | Object | Create New | Microsoft Equation *or* MathType Equation). "Float over text" should *not* be selected.

IV. UNITS

Use either SI (MKS) or CGS as primary units. (SI units are strongly encouraged.) English units may be used as secondary units (in parentheses). **This applies to papers in data storage.** For example, write "15 Gb/cm^2 (100 Gb/in^2)." An exception is when English units are used as identifiers in trade, such as "3½-in disk drive." Avoid combining SI and CGS units, such as current in amperes and magnetic field in oersteds. This often leads to confusion because equations do not balance dimensionally. If you must use mixed units, clearly state the units for each quantity in an equation.

The SI unit for magnetic field strength H is A/m. However, if you wish to use units of T, either refer to magnetic flux density B or magnetic field strength symbolized as $\mu_0 H$. Use the center dot to separate compound units, e.g., "A·m^2."

V. Helpful Hints

A. Figures and Tables

Because IEEE will do the final formatting of your paper, you do not need to position figures and tables at the top and bottom of each column. In fact, all figures, figure captions, and tables can be at the end of the paper. Large figures and tables may span both columns. Place figure captions below the figures; place table titles above the tables. If your figure has two parts, include the labels "(a)" and "(b)" as part of the artwork. Please verify that the figures and tables you mention in the text actually exist. **Please do not include captions as part of the figures. Do not put captions in "text boxes" linked to the figures. Do not put borders around the outside of your figures.** Use the abbreviation "Fig." even at the beginning of a sentence. Do not abbreviate "Table." Tables are numbered with Roman numerals.

Color printing of figures is available, but is billed to the authors. Include a note with your final paper indicating that you request and will pay for color printing. Do not use color unless it is necessary for the proper interpretation of your figures. If you want reprints of your color article, the reprint order should be submitted promptly. There is an additional charge for color reprints. **Please note that many IEEE journals now allow an author to publish color figures on Xplore and black and white figures in print. Contact your society representative for specific requirements.**

Figure axis labels are often a source of confusion. Use words rather than symbols. As an example, write the quantity "Magnetization," or "Magnetization *M*," not just "*M*." Put units in parentheses. Do not label axes only with units. As in Fig. 1, for example, write "Magnetization (A/m)" or "Magnetization ($\mathrm{A \cdot m^{-1}}$)," not just "A/m." Do not label axes with a ratio of quantities and units. For example, write "Temperature (K)," not "Temperature/K."

Multipliers can be especially confusing. Write "Magnetization (kA/m)" or "Magnetization (10^3 A/m)." Do not write "Magnetization (A/m) × 1000" because the reader would not know whether the top axis label in Fig. 1 meant 16000 A/m or 0.016 A/m. Figure labels should be legible, approximately 8 to 12 point type.

B. References

Number citations consecutively in square brackets [1]. The sentence punctuation follows the brackets [2]. Multiple references [2], [3] are each numbered with separate brackets [1]–[3]. When citing a section in a book, please give the relevant page numbers [2]. In sentences, refer simply to the reference number, as in [3]. Do not use "Ref. [3]" or "reference [3]" except at the beginning of a sentence: "Reference [3] shows ... ." Please do not use automatic endnotes in *Word*, rather, type the reference list at the end of the paper using the "References" style.

Number footnotes separately in superscripts (Insert | Footnote).[1] Place the actual footnote at the bottom of the column in which it is cited; do not put footnotes in the reference list (endnotes). Use letters for table footnotes (see Table I).

Please note that the references at the end of this document are in the preferred referencing style. Give all authors' names; do not use "*et al*." unless there are six authors or more. Use a space after authors' initials. Papers that have not been published should be cited as "unpublished" [4]. Papers that have been accepted for publication, but not yet specified for an issue should be cited as "to be published" [5]. Papers that have been submitted for publication should be cited as "submitted for publication" [6]. Please give affiliations and addresses for private communications [7].

Capitalize only the first word in a paper title, except for proper nouns and element symbols. For papers published in translation journals, please give the English citation first, followed by the original foreign-language citation [8].

C. Abbreviations and Acronyms

Define abbreviations and acronyms the first time they are used in the text, even after they have already been defined in the abstract. Abbreviations such as IEEE, SI, ac, and dc do not have to be defined. Abbreviations that incorporate periods should not have spaces: write "C.N.R.S.," not "C. N. R. S." Do not use abbreviations in the title unless they are unavoidable (for example, "IEEE" in the title of this article).

D. Equations

Number equations consecutively with equation numbers in parentheses flush with the right margin, as in (1). First use the equation editor to create the equation. Then select the "Equation" markup style. Press the tab key and write the equation number in parentheses. To make your equations more compact, you may use the solidus (/), the exp function, or appropriate exponents. Use parentheses to avoid ambiguities in denominators. Punctuate equations when they are part of a sentence, as in

$$\int_0^{r_2} F(r,\varphi)\, dr\, d\varphi = [\sigma r_2 / (2\mu_0)] \cdot \int_0^{\infty} \exp(-\lambda\,|z_j - z_i|)\, \lambda^{-1} J_1(\lambda r_2)\, J_0(\lambda r_i)\, d\lambda . \tag{1}$$

Be sure that the symbols in your equation have been defined before the equation appears or immediately following. Italicize symbols (*T* might refer to temperature,

[1]It is recommended that footnotes be avoided (except for the unnumbered footnote with the receipt date on the first page). Instead, try to integrate the footnote information into the text.

but T is the unit tesla). Refer to "(1)," not "Eq. (1)" or "equation (1)," except at the beginning of a sentence: "Equation (1) is ... ."

E. Other Recommendations

Use one space after periods and colons. Hyphenate complex modifiers: "zero-field-cooled magnetization." Avoid dangling participles, such as, "Using (1), the potential was calculated." [It is not clear who or what used (1).] Write instead, "The potential was calculated by using (1)," or "Using (1), we calculated the potential."

Use a zero before decimal points: "0.25," not ".25." Use "cm^3," not "cc." Indicate sample dimensions as "0.1 cm × 0.2 cm," not "0.1 × 0.2 cm^2." The abbreviation for "seconds" is "s," not "sec." Do not mix complete spellings and abbreviations of units: use "Wb/m^2" or "webers per square meter," not "webers/m^2." When expressing a range of values, write "7 to 9" or "7-9," not "7~9."

A parenthetical statement at the end of a sentence is punctuated outside of the closing parenthesis (like this). (A parenthetical sentence is punctuated within the parentheses.) In American English, periods and commas are within quotation marks, like "this period." Other punctuation is "outside"! Avoid contractions; for example, write "do not" instead of "don't." The serial comma is preferred: "A, B, and C" instead of "A, B and C."

If you wish, you may write in the first person singular or plural and use the active voice ("I observed that ..." or "We observed that ..." instead of "It was observed that ..."). Remember to check spelling. If your native language is not English, please get a native English-speaking colleague to carefully proofread your paper.

VI. Some Common Mistakes

The word "data" is plural, not singular. The subscript for the permeability of vacuum μ_0 is zero, not a lowercase letter "o." The term for residual magnetization is "remanence"; the adjective is "remanent"; do not write "remnance" or "remnant." Use the word "micrometer" instead of "micron." A graph within a graph is an "inset," not an "insert." The word "alternatively" is preferred to the word "alternately" (unless you really mean something that alternates). Use the word "whereas" instead of "while" (unless you are referring to simultaneous events). Do not use the word "essentially" to mean "approximately" or "effectively." Do not use the word "issue" as a euphemism for "problem." When compositions are not specified, separate chemical symbols by en-dashes; for example, "NiMn" indicates the intermetallic compound $Ni_{0.5}Mn_{0.5}$ whereas "Ni–Mn" indicates an alloy of some composition Ni_xMn_{1-x}.

Be aware of the different meanings of the homophones "affect" (usually a verb) and "effect" (usually a noun), "complement" and "compliment," "discreet" and "discrete," "principal" (e.g., "principal investigator") and "principle" (e.g., "principle of measurement"). Do not confuse "imply" and "infer."

Prefixes such as "non," "sub," "micro," "multi," and "ultra" are not independent words; they should be joined to the words they modify, usually without a hyphen. There is no period after the "et" in the Latin abbreviation "*et al.*" (it is also italicized). The abbreviation "i.e.," means "that is," and the abbreviation "e.g.," means "for example" (these abbreviations are not italicized).

An excellent style manual and source of information for science writers is [9]. A general IEEE style guide and an *Information for Authors* are both available at http://www.ieee.org/web/publications/authors/transjnl/index.html

VII. Editorial Policy

Submission of a manuscript is not required for participation in a conference. Do not submit a reworked version of a paper you have submitted or published elsewhere. Do not publish "preliminary" data or results. The submitting author is responsible for obtaining agreement of all coauthors and any consent required from sponsors before submitting a paper. IEEE Transactions and Journals strongly discourage courtesy authorship. It is the obligation of the authors to cite relevant prior work.

The Transactions and Journals Department does not publish conference records or proceedings. The Transactions does publish papers related to conferences that have been recommended for publication on the basis of peer review. As a matter of convenience and service to the technical community, these topical papers are collected and published in one issue of the Transactions.

At least two reviews are required for every paper submitted. For conference-related papers, the decision to accept or reject a paper is made by the conference editors and publications committee; the recommendations of the referees are advisory only. Undecipherable English is a valid reason for rejection. Authors of rejected papers may revise and resubmit them to the Transactions as regular papers, whereupon they will be reviewed by two new referees.

VIII. Publication Principles

The contents of IEEE Transactions and Journals are peer-reviewed and archival. The Transactions publishes scholarly articles of archival value as well as tutorial expositions and critical reviews of classical subjects and topics of current interest.

Authors should consider the following points:

1) Technical papers submitted for publication must advance the state of knowledge and must cite relevant prior work.
2) The length of a submitted paper should be commensurate with the importance, or appropriate to

the complexity, of the work. For example, an obvious extension of previously published work might not be appropriate for publication or might be adequately treated in just a few pages.

3) Authors must convince both peer reviewers and the editors of the scientific and technical merit of a paper; the standards of proof are higher when extraordinary or unexpected results are reported.
4) Because replication is required for scientific progress, papers submitted for publication must provide sufficient information to allow readers to perform similar experiments or calculations and use the reported results. Although not everything need be disclosed, a paper must contain new, useable, and fully described information. For example, a specimen's chemical composition need not be reported if the main purpose of a paper is to introduce a new measurement technique. Authors should expect to be challenged by reviewers if the results are not supported by adequate data and critical details.
5) Papers that describe ongoing work or announce the latest technical achievement, which are suitable for presentation at a professional conference, may not be appropriate for publication in a TRANSACTIONS or JOURNAL.

IX. CONCLUSION

A conclusion section is not required. Although a conclusion may review the main points of the paper, do not replicate the abstract as the conclusion. A conclusion might elaborate on the importance of the work or suggest applications and extensions.

APPENDIX

Appendixes, if needed, appear before the acknowledgment.

ACKNOWLEDGMENT

The preferred spelling of the word "acknowledgment" in American English is without an "e" after the "g." Use the singular heading even if you have many acknowledgments. Avoid expressions such as "One of us (S.B.A.) would like to thank ... ." Instead, write "F. A. Author thanks ... ." **Sponsor and financial support acknowledgments are placed in the unnumbered footnote on the first page, not here.**

REFERENCES

[1] G. O. Young, "Synthetic structure of industrial plastics (Book style with paper title and editor)," in *Plastics*, 2nd ed. vol. 3, J. Peters, Ed. New York: McGraw-Hill, 1964, pp. 15–64.

[2] W.-K. Chen, *Linear Networks and Systems* (Book style). Belmont, CA: Wadsworth, 1993, pp. 123–135.

[3] H. Poor, *An Introduction to Signal Detection and Estimation*. New York: Springer-Verlag, 1985, ch. 4.

[4] B. Smith, "An approach to graphs of linear forms (Unpublished work style)," unpublished.

[5] E. H. Miller, "A note on reflector arrays (Periodical style—Accepted for publication)," *IEEE Trans. Antennas Propagat.*, to be published.

[6] J. Wang, "Fundamentals of erbium-doped fiber amplifiers arrays (Periodical style—Submitted for publication)," *IEEE J. Quantum Electron.*, submitted for publication.

[7] C. J. Kaufman, Rocky Mountain Research Lab., Boulder, CO, private communication, May 1995.

[8] Y. Yorozu, M. Hirano, K. Oka, and Y. Tagawa, "Electron spectroscopy studies on magneto-optical media and plastic substrate interfaces (Translation Journals style)," *IEEE Transl. J. Magn.Jpn.*, vol. 2, Aug. 1987, pp. 740–741 [*Dig. 9th Annu. Conf. Magnetics* Japan, 1982, p. 301].

[9] M. Young, *The Techincal Writers Handbook.* Mill Valley, CA: University Science, 1989.

[10] J. U. Duncombe, "Infrared navigation—Part I: An assessment of feasibility (Periodical style)," *IEEE Trans. Electron Devices*, vol. ED-11, pp. 34–39, Jan. 1959.

[11] S. Chen, B. Mulgrew, and P. M. Grant, "A clustering technique for digital communications channel equalization using radial basis function networks," *IEEE Trans. Neural Networks*, vol. 4, pp. 570–578, Jul. 1993.

[12] R. W. Lucky, "Automatic equalization for digital communication," *Bell Syst. Tech. J.*, vol. 44, no. 4, pp. 547–588, Apr. 1965.

[13] S. P. Bingulac, "On the compatibility of adaptive controllers (Published Conference Proceedings style)," in *Proc. 4th Annu. Allerton Conf. Circuits and Systems Theory*, New York, 1994, pp. 8–16.

[14] G. R. Faulhaber, "Design of service systems with priority reservation," in *Conf. Rec. 1995 IEEE Int. Conf. Communications,* pp. 3–8.

[15] W. D. Doyle, "Magnetization reversal in films with biaxial anisotropy," in *1987 Proc. INTERMAG Conf.*, pp. 2.2-1–2.2-6.

[16] G. W. Juette and L. E. Zeffanella, "Radio noise currents n short sections on bundle conductors (Presented Conference Paper style)," presented at the IEEE Summer power Meeting, Dallas, TX, Jun. 22–27, 1990, Paper 90 SM 690-0 PWRS.

[17] J. G. Kreifeldt, "An analysis of surface-detected EMG as an amplitude-modulated noise," presented at the 1989 Int. Conf. Medicine and Biological Engineering, Chicago, IL.

[18] J. Williams, "Narrow-band analyzer (Thesis or Dissertation style)," Ph.D. dissertation, Dept. Elect. Eng., Harvard Univ., Cambridge, MA, 1993.

[19] N. Kawasaki, "Parametric study of thermal and chemical nonequilibrium nozzle flow," M.S. thesis, Dept. Electron. Eng., Osaka Univ., Osaka, Japan, 1993.

[20] J. P. Wilkinson, "Nonlinear resonant circuit devices (Patent style)," U.S. Patent 3 624 12, July 16, 1990.

[21] *IEEE Criteria for Class IE Electric Systems* (Standards style), IEEE Standard 308, 1969.

[22] *Letter Symbols for Quantities*, ANSI Standard Y10.5-1968.

[23] R. E. Haskell and C. T. Case, "Transient signal propagation in lossless isotropic plasmas (Report style)," USAF Cambridge Res. Lab., Cambridge, MA Rep. ARCRL-66-234 (II), 1994, vol. 2.

[24] E. E. Reber, R. L. Michell, and C. J. Carter, "Oxygen absorption in the Earth's atmosphere," Aerospace Corp., Los Angeles, CA, Tech. Rep. TR-0200 (420-46)-3, Nov. 1988.

[25] (Handbook style) *Transmission Systems for Communications,* 3rd ed., Western Electric Co., Winston-Salem, NC, 1985, pp. 44–60.

[26] *Motorola Semiconductor Data Manual,* Motorola Semiconductor Products Inc., Phoenix, AZ, 1989.

[27] (Basic Book/Monograph Online Sources) J. K. Author. (year, month, day). *Title* (edition) [Type of medium]. Volume (issue). Available: http://www.(URL)

[28] J. Jones. (1991, May 10). Networks (2nd ed.) [Online]. Available: http://www.atm.com

[29] (Journal Online Sources style) K. Author. (year, month). Title. *Journal* [Type of medium]. Volume(issue), paging if given. Available: http://www.(URL)
[30] R. J. Vidmar. (1992, August). On the use of atmospheric plasmas as electromagnetic reflectors. *IEEE Trans. Plasma Sci.* [Online]. *21(3)*. pp. 876–880. Available: http://www.halcyon.com/pub/journals/21ps03-vidmar

First A. Author (M'76–SM'81–F'87) and the other authors may include biographies at the end of regular papers. Biographies are often not included in conference-related papers. This author became a Member (M) of IEEE in 1976, a Senior Member (SM) in 1981, and a Fellow (F) in 1987. The first paragraph may contain a place and/or date of birth (list place, then date). Next, the author's educational background is listed. The degrees should be listed with type of degree in what field, which institution, city, state, and country, and year degree was earned. The author's major field of study should be lower-cased.

The second paragraph uses the pronoun of the person (he or she) and not the author's last name. It lists military and work experience, including summer and fellowship jobs. Job titles are capitalized. The current job must have a location; previous positions may be listed without one. Information concerning previous publications may be included. Try not to list more than three books or published articles. The format for listing publishers of a book within the biography is: title of book (city, state: publisher name, year) similar to a reference. Current and previous research interests end the paragraph.

The third paragraph begins with the author's title and last name (e.g., Dr. Smith, Prof. Jones, Mr. Kajor, Ms. Hunter). List any memberships in professional societies other than the IEEE. Finally, list any awards and work for IEEE committees and publications. If a photograph is provided, the biography will be indented around it. The photograph is placed at the top left of the biography. Personal hobbies will be deleted from the biography.

Camera-ready was prepared in Kharkov National University of Radio Electronics
Approved for publication: 27.12.2013. Format 60×84 1/8.
Relative printer's sheets: 9,9. Circulation: 300 copies.
Published by SPD FL Stepanov V.V.
Lenin Ave, 14, Kharkov, 61166, Ukraine

Рекомендовано Вченою радою Харківського національного
університету радіоелектроніки (протокол № 4 від 27.12.2013)
Підписано до друку 27.12.2013. Формат 60×841/8.
Умов. друк. арк. 9,9 . Тираж 300 прим. Ціна договірна.
Віддруковано у ФОП Степанов В.В.
61166, Харків, просп. Леніна, 14.